On-Line Monitoring and Diagnostics of the Integrity of Nuclear Plant Steam Generators and Heat Exchangers

Annual Report: Phase-2

Report No. DE-FG07-01ID14114/UTNE-04

NEER Grant Number: DE-FG07-01ID14114

Belle R. Upadhyaya
J. Wesley Hines
(Principal Investigators)

Xuedong Huang
Baofu Lu
Sergio R. Perillo
Rosani L. Penha

The University of Tennessee
Nuclear Engineering Department
209 Pasqua Engineering Building
Knoxville, TN 37996-2300
E-mail: bupadhya@utk.edu

DOE Program Manager for NEER
Nancy A. Elizondo
Idaho Operations Office

June 2003

SUMMARY

The overall objective of this research project is to integrate new, innovative, and existing technologies to develop a fault diagnostics and characterization system for nuclear plant steam generators (SG) and heat exchangers (HX). Issues related to the structural integrity of SG and HX tubing, including the damage caused by tube – tube support interaction, are dominating factors that influence overall plant operation, maintenance, and economic viability of nuclear power systems. The research at The University of Tennessee focuses on the development of a system for monitoring process dynamics and structural integrity of steam generators and heat exchangers. The project includes a task of studying the feasibility of incorporating smartness in tubing structures using embedded piezo-electric devices for continuous on-line monitoring.

The objectives of the project are being accomplished by the completion of the following tasks. Considerable progress has been made in the various technical tasks during ***Phase-2*** (second year) of the project and is described in this report.

- Development of a high-fidelity nodal model of a U-tube steam generator (UTSG) to simulate changes in the heat transfer characteristics and other degradation of the UTSG performance caused by tube fouling, and to generate a database representing normal and degraded process conditions.

- Development of hybrid first principle and data-driven modeling technique for tuning and updating process models.

- Development of a sensor suite using piezo-electric devices for monitoring structural integrity of SG and HX tubing and to build a smart monitoring module; the study of elastic wave propagation of Lamb waves (longitudinal and shear waves) in metallic flat plates and tubing with and without flaws.

- Implementation of short-time Fourier transform (STFT) and wavelet transform techniques for processing high frequency non-stationary acoustic data.

- Development of a laboratory HX test module to simulate tube degradation and monitoring for various conditions.

- Experimental study of tube fouling caused by particulate fouling and comparison with particulate fouling models.

The tasks include both analytical research and experimental studies. The experimental results would help to enhance the robustness of fault monitoring methods and to provide a systematic verification of the analytical results. An extensive bibliographic review has also been performed during this research phase.

TABLE OF CONTENTS

1. INTRODUCTION AND OBJECTIVES

1.1. Background and Objectives

The objective of the research project at The University of Tennessee is to develop a system for *On-line Monitoring and Diagnostics of Integrity of Nuclear Plant Steam Generators and Heat Exchangers.* Both structural and process integrity of these components are considered. Steam generators (SG) and heat exchangers (HX) constitute a significant part of power generation systems, and their reliability and availability influence plant operation, maintenance, and cost control issues. Such issues are especially important for the next generation of reactors, which require remote monitoring for both system integrity and for increasing the maintenance interval necessitated by increased fuel cycle lengths. Furthermore, the incorporation of an on-line monitoring system must be considered during the design phase, thus increasing its effectiveness and avoiding unnecessary retrofitting. The three-year project has been planned to achieve the integration of new, innovative, and existing technologies to develop an automated structural fault diagnostics and characterization system for nuclear plant heat exchangers and steam generators.

The nuclear plant steam generator is one of the most important components of a nuclear power plant. There are thousands of tubes in a typical steam generator. The U-tube steam generator (UTSG) in a typical four-loop, 1,300 MWe pressurized water reactor (PWR), consists of about 3,500-4,000 tubes. Tube degradation can occur due to thermal and mechanical stresses, fouling and deposits, fatigue and creep, wear and fretting, and stress corrosion cracking and intergranular attack. Depending on the nature of plant operating conditions, one or more of the above causes may result in tube damage. The degradation of tubes in a steam generator is the primary cause of its reduced performance and of its structural failure. A remedy often used by the industry is to plug damaged and leaking tubes. This, in turn, results in decreased operational efficiency with time. The cost of replacement of a large UTSG in a 1,300 MWe four-loop PWR is about $150 million. Several operating PWR units in the U.S. have either replaced steam generators or are seriously considering this upgrading. These provide a strong argument for the development of continuous on-line monitoring of their structural integrity and incipient fault detection and isolation.

It is envisioned that the use of a distributed and embedded sensor suite and extracting information from sensor arrays will result in a *smart structure* with self-inspection capability. Since the project emphasizes the application of this technology to next generation reactors, the creation of hybrid database for use in predictive models, will be given high priority. Figure 1.1 is a schematic of the integration of plant monitoring, diagnosis, and prognosis modules. It is anticipated that this system will provide timely decision-making information about the status of plant devices and components to operational personnel.

The results of this project will be disseminated to U.S. vendors and utilities through the Electric Power Research Institute (EPRI) and through direct collaborative effort. The capability and experience of The University of Tennessee in artificial intelligence and new analytical and experimental methods, being developed under this project, are directed towards implementation

in the next generation nuclear power plants. Features such as the use of this technology in the plant design-phase, wireless communication, Internet-based e-maintenance, and other remote technologies are also being considered for plant implementation.

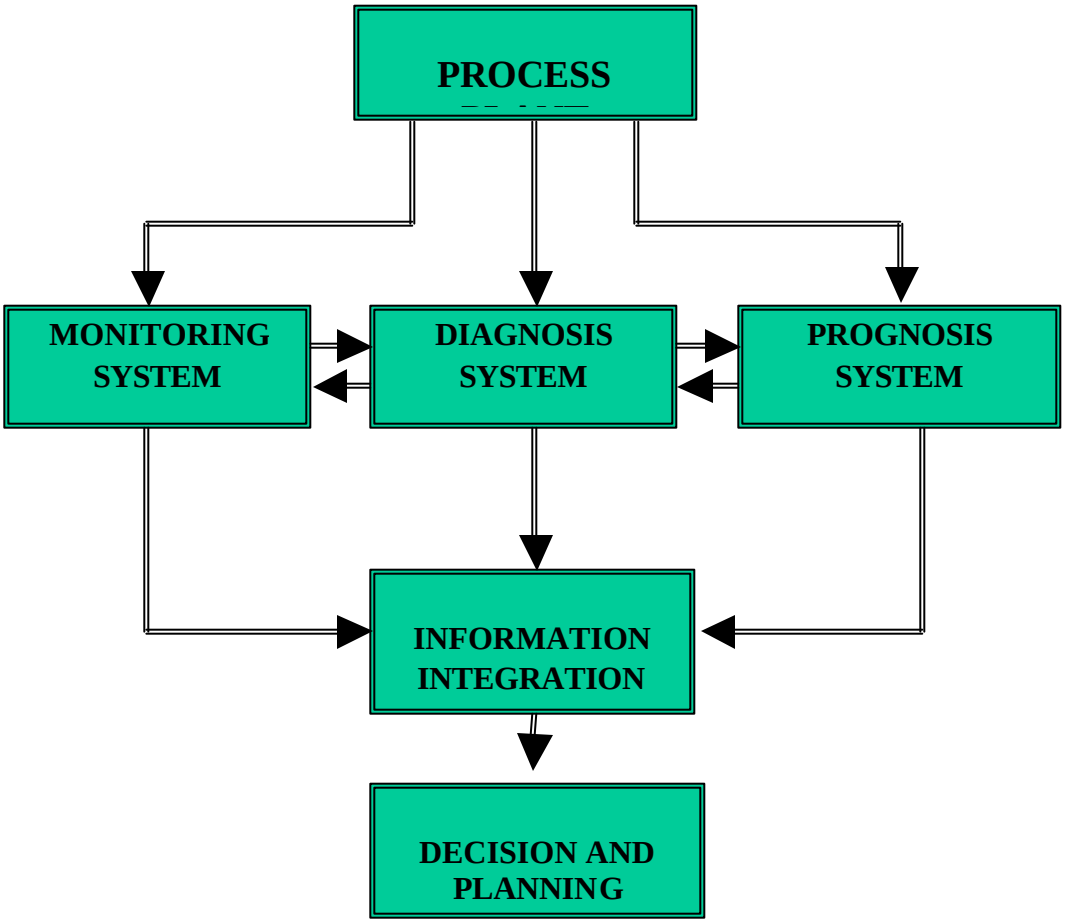

Figure 1.1. Schematic of a plant monitoring, diagnosis, and prognosis system.

1.2. Summary of Progress and Significant Results

The following major tasks have been accomplished during this reporting period:

1. Completion of the MATLAB-Simulink™ code to simulate the dynamic performance of a U-tube steam generator (UTSG) in a typical 1,140 MWe PWR. This multi-nodal model is being used to simulate the effects of tube fouling and tube plugging. The nodal structure has been expanded to account for spatial variations in the physical parameters. For example, the effect of fouling in the sub-cooled region has a higher influence on the steam pressure compared to a similar effect in the boiling region. A detailed model of particulate fouling, with time-dependent variations in the heat transfer coefficient, has been developed.

2. Experimental study of the fouling caused by particulate deposits in a tube-and-shell heat exchanger. The effect of fouling has been clearly demonstrated by the change in the heat transfer resistance, and follows the theoretically formulated characteristics.

3. Completion of a hybrid first principle and data-based model that is used to update and fine-tune the model using process data. Predictive artificial neural network and local regression techniques are used for process monitoring and diagnostics. The hybrid models are classified into serial hybrid and parallel hybrid models. Our studies show that the serial modeling exhibits a better performance in predicting process variables compared to parallel modeling. A simple heat exchanger model is used for this study.

4. This model study is being complimented by the development of a laboratory heat exchanger system that is used to generate normal operation data and data under faulty device operation. This portable test rig is being equipped with flow and pressure transmitters, flow meters, and thermocouples to measure fluid temperatures. An extensive database has been generated for testing the hybrid model approach.

5. Development of a laboratory piezo-device sensor suite for structural monitoring and a data acquisition system for measuring both the input excitation signal and the response signal. Both flat metal plates and tubular specimens are used for this study. The comparison of the input excitation signal (transmitted signal) and the signal received at another location in the plate show excellent frequency response characteristics. The frequency characteristics change when there is a flaw in the plate (or tubing) such as a crack, indentation, or a through hole. This task includes the review of elastic wave propagation in plates under normal and fault conditions. The results to date indicate that the frequency characteristics of the signals change with the presence of a defect in the specimen. These include (a) shift in the energy peaks to lower frequencies, (b) decrease in the overall signal energy, and (c) an increase in the frequency and time spread of signal features.

6. Publications/Presentations of the following papers at the 2002 Americas Nuclear Energy Symposium (ANES 2002), Miami, Florida, October 2002:

(a) *Structural Monitoring of Steam Generators and Heat Exchangers Using Piezoelectric Devices.*
(b) *Application of Hybrid Modeling for Monitoring Heat Exchangers.*

Presentations at MARCON 2003, Knoxville, TN, May 2003.
(a) *Particulate Fouling and its Effects on U-Tube Steam Generator Thermal Performance.*
(b) *Time-Frequency Analysis of Acoustic Signals for Flaw Monitoring in Steam Generator Structures.*

Presentation at the American Nuclear Society Annual Meeting, San Diego, CA, June 2003.
Defect Monitoring in Steam Generator Structures Using Piezoelectric Transducers and Time-Frequency Analysis.

1.3. Project Personnel

Principal Investigator:	B.R. Upadhyaya
Co-Principal Investigator:	J.W. Hines
Graduate Research Assistants	X. Huang B. Lu
Visiting Scholars:	S.R. Perillo (at no cost to the project) R.L. Penha

1.4. Outline of the Annual Report

The review of steam generator and heat exchanger degradation mechanisms (including fouling) and their characterization is presented in Section 2. The development of a simulation model of the UTSG and the results of application to study the effect of fouling on thermal performance are described in Section 3. Section 4 describes the development of a laboratory experiment to study the effect of fouling in a tube-and-shell heat exchanger and the results of this experimental study. Section 5 presents the details of the hybrid modeling approach and results of application to a double tube heat exchanger. The general development of the use of embedded piezo-sensors for monitoring metallic structures is described in Section 6. New results of fault monitoring in flat plate and tubular specimens are presented in Section 7. The experimental data are processed using both short-time Fourier transform (STFT) and Discrete Wavelet Transform (DWT). Concluding remarks and the outline of future work are given in Section 8. The report contains an extensive bibliography (including new citations) of pertinent literature.

2. REVIEW OF STEAM GENERATOR TUBE CORROSION AND WATER CHEMISTRY EFFECTS

2.1. Introduction

Steam generators have long been one of the most troublesome major components in pressurized water reactor (PWR) nuclear power plants. Over the past several years, utilities with PWR plants have experienced degradation in steam generator structural integrity and/or thermal performance. Such degradation can result in costly reductions in the electrical generating capacity of the plant. Even a small 1% decrease in electrical generation corresponds roughly to $2 million of lost revenues per year for a typical PWR.

Numerous causes of SG degradation have been identified, including stress corrosion cracking (SCC), intergranular attack (IGA), denting, pitting, fretting, wear and thinning, high-cycle fatigue and wastage, primary and secondary tube fouling, dryer clogging, flow resistance due to scale, and tube plugging and sleeving, etc. Many of these degradations of steam generator tubing in PWR plants with recirculating steam generators (RSGs) have resulted from a variety of corrosion-related mechanisms that are directly related to secondary system water chemistry. Hence, study of corrosion and water chemistry is very important in ensuring the integrity of steam generators as well as heat exchangers and it directly affects the plant economy and safe operation. (See Annual Report, DE-FG07-011D4114/UTNE-02, June 2002, for more details).

Corrosion problems have appeared both on the primary side and on the secondary side of the SG tubes, though plant operation experiences shows that the secondary side corrosion of SG tubes represents the main degradation of components in operating power plants. See the bibliography on corrosion [98-115].

2.2. Corrosion Mechanisms

According to Kuppan, corrosion is defined as the deterioration of a metal caused by the reaction of the metal with the environment. Though other factors may be also important in certain cases, here the environment include the following primary factors: (1) physical states----gas, liquid or solid; (2) chemical composition----constituents and concentrations; and (3) temperature.

According to electrochemical theory, the combination of anode, cathode, and aqueous solutions constitutes a small galvanic cell (Figure 2.1), and the corrosion reaction proceeds with a flow of current in a way similar to that of the current is generated by chemical action in a primary cell or in a storage battery on discharge. The anode is dissolved because of the electrochemical action. A complete electrical circuit is necessary for a current to flow. In a typical corroding system, as shown in Figure 2.1a, the circuit is comprised of the following four components:

(1) Anode: The anode is the electrode at which the oxidation (corrosion) takes place and current in the form of positively charged metal ions enters the electrolyte. At the anode, the metal atom loses an electron, oxidizing to an ion.

(2) Electrolyte: The electrolyte is the solution or a solid layer e.g. a thick metal oxide scale) that surrounds or covers both the anode and the cathode. The conductivity of this solution is closely related to the corrosion speed. The lower the conductivity, the slower the corrosion reaction; and vice versa. If there is a total absence of an electrolyte, then little or no corrosion will occur.

(3) Cathode: The cathode is the electrode at which reduction takes place and current enters from the electrolyte.

(4) An external circuit: If there are two pieces of metal, they must either be in contact or have an external connection for corrosion to occur. The external circuit is a metallic path between the anode and the cathode that completes the circuit. If the anode and the cathode are on the metal surface, then this metal itself acts as the external circuit.

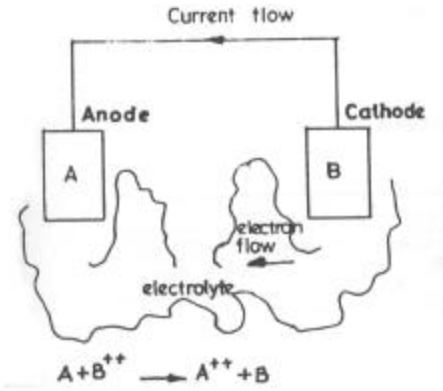

Figure 2.1a. A Basic Corroding System (From Ref. 102).

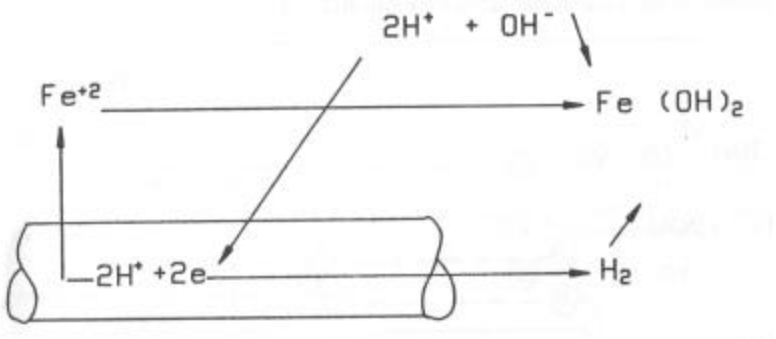

Figure 2.1b. Corrosion of Iron in Water (From Ref. 102).

2.3. Forms of Corrosion

Corrosion attack on the metal surfaces can be either uniform or localized. In the latter, the major part of the metal surfaces remains unaffected but certain localized areas are corroded at a high rate. In contrast, the uniform corrosion occurs when a metal is corroded in an acid or alkali, or when the metal is exposed to natural environment such as air, soil, etc. Generally, uniform

corrosion occurs when the metal and the environment system is homogeneous. When there exist heterogeneities in the metal and/or variations in the environment, corrosion may be localized. For metals and alloys, factors that favor localized corrosion include grain boundaries, inter-metallic phases, inclusions, impurities, regions that differ in their mechanical or thermal treatments, discontinuities on metal surfaces such as cut edges or scratches, discontinuities in oxide or passive films or in applied metallic or nonmetallic coatings, and geometrical factors such as crevices, etc.

More specifically, the most common forms of corrosion include:
(1) Uniform corrosion
(2) Galvanic corrosion
(3) Crevice corrosion
(4) Pitting corrosion
(5) Intergranular corrosion
(6) Stress corrosion cracking
(7) Erosion-corrosion
(8) Dealloying corrosion
(9) Hydrogen damage
(10) Liquid-Metal Embrittlement, etc.

2.4. Effect of Some Important Variables on Corrosion

The pH, electrochemical potential, and impurities in SG are the key factors that affect steam generator tube corrosion.

A. pH

pH is a measure of the concentration of hydrogen ions and indicate whether and how strong the solution is acidic or basic. The stability of the oxide films on metal alloys in SG depends strongly on the pH. For many alloys, either very low (acidic) pH or very high (basic) pH causes unacceptable corrosion. As indicated above, depending on specific conditions, the corrosion can be general (or uniform, e.g. wastage) or localized (e.g. pitting or cracking). The pH of the bulk solution is controlled by the concentration of dissolved species in the solution, while the pH of local areas can be strongly affected by the electrochemical reactions occurring in the area. The stability of the oxide films is strongly affected by the oxygen concentration in the water or steam that the metal alloys are exposed to. The regions of stability depend on pH, electrochemical potential, temperature, other dissolved species, and the oxygen concentration. For high temperature water with very low levels of oxygen, stability of the oxide films on steel is increased as the pH increases, at least up to a pH of around 10. Figure 2.2 presents the corrosion rate versus pH. The general shape of this curve is typical for copper-base alloys. Such curves can be prepared for various metals and alloys and they may have their minima broadened or shortened. And the slopes may vary considerably, depending upon the characteristics of the metal or alloy and the composition of the solution.

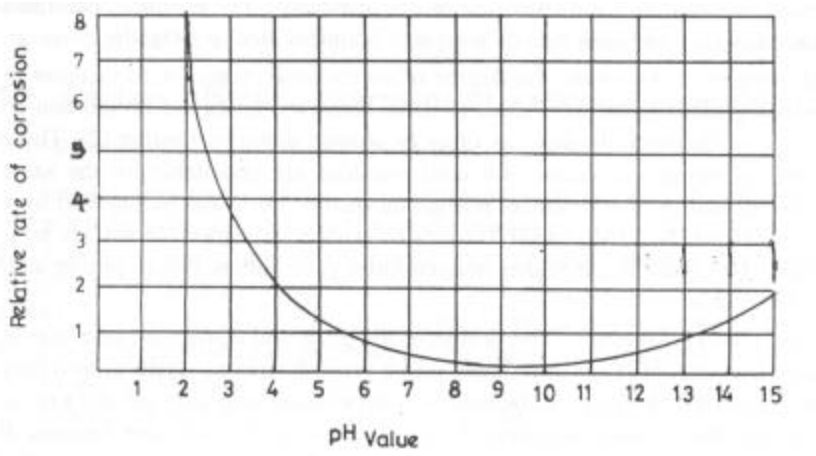

Figure 2.2. Relative Corrosion Rate versus pH (From Reference 5)

B. Electrochemical potential

The electrochemical potential of the surface is a measure of the galvanic force (voltage) available to cause electrochemical reactions to occur. This potential, together with other important variables such as temperature, pH, and the dissolved species, controls the form and extent of corrosion. The electrochemical potential is affected by the bulk and local solution chemistry, temperature, material, etc.

C. Impurities

Many impurities that enter the secondary side of SG can aggravate corrosion of SG materials, especially tubes and tube support plates. The following impurities have been found to be especially harmful to SG integrity:

a. Chloride: Since Inconel 600 is immune to chloride-induced SCC, it is selected and used as SG structural material. Nevertheless, chloride impurities have been found to be important causes for denting and pitting. The main source of chloride is condenser leakage, and the introduction of chloride by impurities in the makeup water.

b. Sulfate: Concentrated sulfates can be aggressive to Inconel 600, and can cause IGA and IGSCC. They can also cause accelerated corrosion of carbon steel and thus lead to denting. The main sources of sulfates are condenser leakage and leakage of chemicals or resin fines from condensate polisher and makeup water demineralizers.

c. Sodium: Concentrated sodium hydroxides are believed to be the major causes of IGA and IGSCC of SG tubes. The main sources of sodium are condenser leakage and leakage from condensate polisher and makeup water demineralizers.

d. Copper: copper and copper oxides, together with other species such as chlorides, severely speed up denting and pitting in SGs and may also aggravate caustic IGSCC. Meanwhile, the copper contributes to the total amount of sludge and deposits in SG. The main source of copper is the corrosion of copper containing alloys in secondary system heat exchanger tubes.

e. Iron: Iron oxide tube deposits and sludge promote local boiling and concentration of impurities, which causes corrosive attack such as IGA, IGSCC, and Pitting of SG tubes. In addition, iron oxide deposits in OTSGs have caused significant increases in pressure drop in the tube bundle and have led to plant power level reductions and extensive cleaning operations, including chemical cleaning.

f. Organics: Organics have not been directly implicated in specific corrosion problems in SGs, but concerns remain because they may be introduced into SGs and then break down into aggressive species. Organics can be introduced by condenser leaks as impurities in the makeup water, resin fines, or lubricating oils.

2.5. Approaches for Corrosion Control

There are various techniques for corrosion control. These include the following.

(1) Proper engineering design
(2) Changing the characteristics of the corrosive environment
(3) Selecting the corrosion-resistant material
(4) Bimetal concept involving cladding and bimetallic tubes
(5) Application of protective coatings and inhibitors
(6) Providing electrochemical protection by cathodic and anodic protection
(7) Passivation.

From the point of view of water chemistry, the following main approaches are used to control corrosion of nuclear power plant materials, including steam generators [105]:

(1) Maintenance of high purity

Since many corrosion processes in high temperature water system are aggravated by the presence of impurities, one of the main approaches to control corrosion is to control impurity concentrations to levels that result in tolerable corrosion during the expected lifetime.

To achieve a desired high purity, a number of requirements must be satisfied. These include use of high integrity condensers, use of makeup systems that can produce water with very low impurity levels, continuous or periodic monitoring of makeup and system water purity, and continuous purification of all or portion of the system flow.

In locations such as crevices, sludge piles, or other occluded areas where boiling occurs, the concentration of impurities can increase by many orders of magnitude. This makes it difficult to prevent corrosion attack in such locations. In fact, corrosion attack at occluded locations continues to occur in the secondary side of many SGs over the past years, though great efforts have been made to reduce the impurity levels in the secondary coolant. Nevertheless, since the rate at which the impurities concentrate in occlude areas is directly proportional to their concentration in the bulk water, thus reduction in impurity concentrations can help to delay or slow down the corrosion attack, if the attack cannot be prevented at all.

(2) Oxygen and pH control

Many materials used in power plants are thermodynamically unstable in high temperature water and tend to oxidize. However, under proper water chemistry conditions, stable thin films of protective oxides form on the metal surfaces and reduce the rate of oxidation to acceptable

levels. Therefore the main objective of water chemistry is to maintain the integrity of these oxide films. Both neutral pH-high oxygen (for BWR) and high pH-low oxygen (for PWR) water treatment schemes have been successfully used for this purpose.

PWRs have used high pH-low oxygen approach for both primary and secondary water chemistries. Low oxygen is achieved on the secondary side by combined use of mechanical deaeration coupled with chemical scavenging using hydrazine; and it is obtained on the primary side by use of a hydrogen overpressure, which result in scavenging of oxygen in the core. The pH is controlled using chemical additives like ammonia or lithium hydroxide.

Maintaining the desired pH value is very difficult in occluded areas due to the presence of concentrated impurities. The concentrated impurities can make the pH change widely. The occluded area pH can range from very low (strongly acidic) to very high (strongly basic), leading to a variety of corrosion problems. Some chemical additives have the potential to minimize these pH swings by a buffering action.

(3) Avoidance of deposits

Prevention of the formation of deposits and sludge piles on or around the heat transfer surfaces is another important aspect of water chemistry and corrosion control. This can minimize interference with heat transfer and avoid development of occluded areas where boiling can concentrate chemicals in the water to levels that can cause corrosive attack. Deposits in the primary system also need to be minimized so as to reduce activation in the core and buildup of plant radiation levels. The following approaches can be used to avoid or reduce the occurrence of deposits:

a. Minimizing the introduction of impurities into the system, e.g. by keeping the condensers leak-tight and controlling the purity of makeup water.

b. Limiting the ingress of corrosion products into the SGs and reactor core by controlling the corrosion rate of system materials.

c. Purification of bleed-off streams (primary coolant letdown and secondary coolant blowdown) to keep the concentrations of impurities and solids in the primary and secondary systems at acceptable levels.

d. Full flow purification of the secondary system water.

2.6. Corrosion Monitoring

There are generally three approaches for corrosion monitoring:

(1) Local approach: This approach involves investigations of corrosion in terms of local conditions.

(2) Component approach: This approach involves investigating plant components and their corrosion phenomena that occur due to the complex environmental and operational conditions.

(3) System approach: This approach considers the plant system as a whole. It deals with interrelations of phenomena occurring in different components of the system.

More specifically, the following techniques, generally classified as online monitoring or offline monitoring, are used in corrosion monitoring:

(1) Online monitoring techniques: Online corrosion monitoring is necessary for assessing the corrosivity of the process stream and for detecting the changes that may occur in operation. Online corrosion data are obtained from probes or sensors inserted into the system at accessible points that reproduce the specific area of interest. Online corrosion techniques include corrosion coupons, electrical resistance principle, pitting potential, linear polarization principle and Tafel plots, hydrogen test probe, galvanic measurements, pH measurements, dimensional changes through online ultrasonic testing, radiography, and acoustic emission technique, etc. [103].

Online monitoring of a cooling water system, including SG or heat exchanger, involves monitoring the calcium hardness, alkalinity, total solids, pH, dissolved oxygen and hydrogen, etc. Automatic analyzers continuously monitor the water and steam purities. Typical parameters monitored by online instruments include:

a. Conductivity, pH (purity and acidity of the water)
b. Ammonia, hydrazine phosphate (control of conditioning)
c. Oxygen and Hydrogen (dissolved gases)
d. Sodium, chloride, silica, etc. (harmful impurities in the system).

(2) Offline monitoring techniques: Offline corrosion monitoring mainly involves various nondestructive examination techniques to determine the thickness and integrity of SG or heat exchanger. The following nondestructive testing techniques are used:

a. Visual examination
b. Eddy current testing
c. Magnetic particle examination
d. Liquid penetrant test
e. Ultrasonic examination
f. Radiography
g. Thermography.

As stated above, corrosion monitoring of condensers is very important. It can be done through systematic examination of the state of the tubes. This involves extracting representative tubes and examining them in the laboratory. The following four aspects should be checked:

a. Microscopic examination of the condition of the tube surfaces
b. Residual wall thickness
c. Weight of the surface layer
d. Composition of the surface layer.

2.7. Steam Generator Program Guidelines

Since it is of great importance to maintain the structural integrity of steam generators, a well-established steam generator program is very important to achieve this goal. Nuclear Energy Institute issued the document NEI 97-06 Steam Generator Program Guidelines, which, along with the referenced EPRI guidelines [108-115], provide very good management guidelines for steam generator and heat exchanger management. This is an industry self-imposed requirement on a number of steam generators, including water chemistry, etc. It establishes a framework for structuring and strengthening existing steam generator programs. It also provides the fundamental elements expected to be included in a steam generator program. These elements

incorporate a balance of prevention, inspection, evaluation, repair and leakage monitoring measures. This guideline refers licensees to EPRI guidelines or other documents that must be conformed with so as to meet the requirements. The intent of this document is to bring consistency in application of industry guidelines relative to managing steam generator programs.

Water chemistry control is one of the important elements in the steam generator program guidelines. In this aspect, EPRI issued the following two important guidelines [110-111]:

- *PWR Secondary Water Chemistry Guidelines*, EPRI Report TR-102134
- *PWR Primary Water Chemistry Guidelines*, EPRI Report TR-105714.

3. FOULING OF UTSG TUBING AND ITS EFFECT ON THERMAL PERFORMANCE

3.1. Modeling of UTSG Particulate Fouling

As we determined from the review in Section 2, there exist various mathematical models for simulation of fouling in simple tubing. However, very few model for steam generator fouling has been developed. Liner et al [116,117] developed a model for simulation of magnetite particulate fouling in nuclear steam generators. This model is presented here as follows.

The deposited mass per unit area is based on Cleaver and Yates' analysis [118] of simultaneous deposition and re-entrainment of particles on a surface and is given by:

$$M = (KCru/(a(U^*)^2))(1-\exp(-a(U^*)^2 t/u)) \tag{3.1}$$

According to Bowen et al [119] and Ruckenstein et al [120], the deposition velocity, K, in the above equation is written as:

$$K = (1/K_t + 1/K_a)^{-1} \tag{3.2}$$

This equation basically means that particle deposition occurs by two steps in series: transport to the surface followed by attachment to the surface.

For a vertical surface (such as that of UTSG tubes), the transport coefficient K_t includes contributions from molecular plus eddy diffusion, inertial transport, thermophoresis and boiling. These transport processes take place in parallel. Hence we have

$$K_t = K_d + K_i + K_{th} + K_b \tag{3.3}$$

The contribution to the particle transport by eddy plus molecular diffusion can be calculated from Cleaver and Yates [121]:

$$K_d = (Sc)^{-2/3} U^*/11.9 \tag{3.4}$$

The inertial contribution to the particle transport velocity is computed by

$$K_i = \frac{1}{500}\frac{U^* t_p^*}{5.23}\frac{r}{r_p}\exp(0.48 t_p^*) \tag{3.5}$$

The dimensionless relaxation time t_p^* is given by

$$t_p^* = \frac{1}{18}\frac{r_p}{r}\left(\frac{U^* d_p}{u}\right)^2 \tag{3.6}$$

The contribution from boiling to the particle transport velocity can be estimated from the data of Asakura et al [122]:

$$K_b = bq/(h_{fg} r) \tag{3.7}$$

The contribution from thermophoresis to the particle transport rate can be computed using the model by McNab and Mewsen [123]:

$$K_{th} = -\frac{0.26 h_c u (T_s - T_b)}{6(2k_f + k_p) T_b} \tag{3.8}$$

The velocity of particle attachment is given by

$$K_a = K_0 \exp(-E_a/(R * T_s)) \tag{3.9}$$

The unit thermal resistance (or fouling factor) caused by fouling is given by [124]

$$R_f = M/(r_f k_f) \tag{3.10}$$

The various symbols are defined as follows:
C: Bulk particle concentration
d_p: Particle diameter
D: Diffusion coefficient
g: Acceleration due to gravity
h_c: Heat transfer coefficient
h_{fg}: Latent heat of vaporization
k_g: Thermal conductivity of liquid
k_p: Thermal conductivity of magnetite particles
k_f: Thermal conductivity of fouling deposit
K: Particle deposition coefficient
K_a: Attachment coefficient
K_b: Boiling deposition coefficient
K_d: Eddy diffusion coefficient
K_i: Inertial coasting coefficient
K_t: Transport coefficient
K_{th}: Thermophoresis coefficient
M: Deposited mass per unit area
q = Heat flux
R: Universal gas constant
Sc: Schmidt number
T_b: Bulk fluid temperature
T_s: Surface temperature
t: time
t_p^*: Dimensionless relaxation time

$U^* = \sqrt{t / r}$

t : Surface shear stress

u : Kinematic viscosity of liquid

R_f = Fouling resistance

Sc = Schmidt number = u /D

r : Mixture density

r_p : Particle density

r_f : Density of fouling deposit

As experience has shown, the secondary side SG fouling is of a major concern [99], hence we have mainly simulated the secondary side SG tube surface fouling using the above mathematical model and related constants. The model has been implemented using MATLAB and simulations have been performed to simulate the progress of the secondary side SG tube surface fouling. The results are given in Figure 3.1 and Figure 3.2. Comparing the results with those from Y. Liner et al [116] and the general magnitude of heat exchanger fouling factor [117], we see that the results are reasonable.

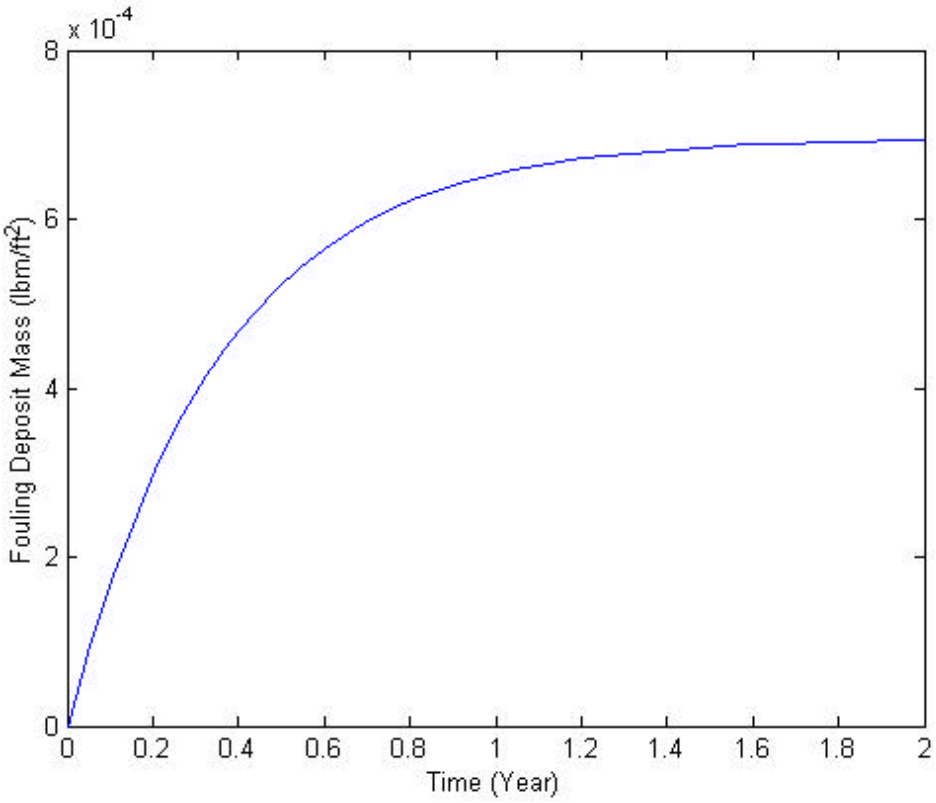

Figure 3.1. Fouling Deposit Mass Variation versus Time.

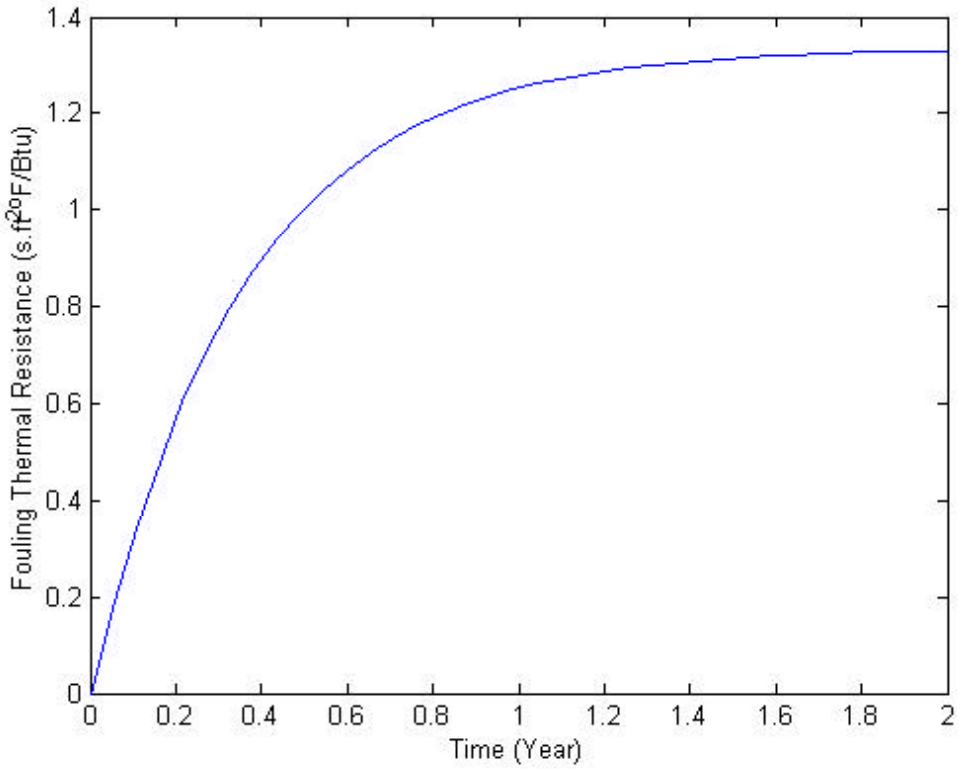

Figure 3.2. Fouling Thermal Resistance versus Time.

3.2. Effect of UTSG Fouling on Thermal Performance

In order to study the effect of secondary side tube fouling on UTSG thermal performance, we use the previously developed multi-node UTSG SIMULINK model for the simulation and use the above results for fouling simulation as part of the inputs. Finally the UTSG thermal performance variations versus time have been obtained.

The following important assumptions are made in the study:

(1) Only secondary side tube fouling on UTSG tubes is simulated
(2) The distribution of fouling deposit along UTSG tube is uniform
(3) The increase in pressure drop across the UTSG tube due to cross-sectional area reduction caused by fouling deposition layer is not considered. This is reasonable since the flow area on the secondary side is relatively larger than on the primary side of UTSG.

Figure 3.3 shows the steam pressure variation versus time. Figure 3.4 presents the average heat flux (on outer tube surface) variation versus time. From the figures, we can see that as the UTSG secondary side tube fouling progresses and the thermal resistance due to fouling increases, both UTSG steam pressure and the average heat flux decreases until the fouling process reaches a balance, that is, the fouling factor, the steam pressure and heat flux all asymptotically remain

constant. From Figure 3.3 and Figure 3.4, we see that as the fouling factor increases and reaches the balanced value of about 1.4 $s \cdot ft^{2} \cdot °F/Btu$

(1) The steam pressure decreases from 875 Psia to 798 Psia, which means a percentage decrease of steam pressure by about 11.4%

(2) The average heat flux on outer tube surface will decrease from 30.3 $Btu/(ft^{2} \cdot s)$ to about 27.7 $Btu/(ft^{2} \cdot s)$, which means a percentage decrease of average heat flux by about 11.7%.

These results show that both the steam pressure and average heat flux have been changed by about the same percentage, more than 11%, due to the secondary side tube fouling. This steam pressure decrease is too large in practical plant operation and means that the plant performance is degraded and cannot produce the required steam for electricity generation. Hence, necessary measures, such as UTSG cleaning or washing, or improvement of the water chemistry, must be taken to recover the plant performance.

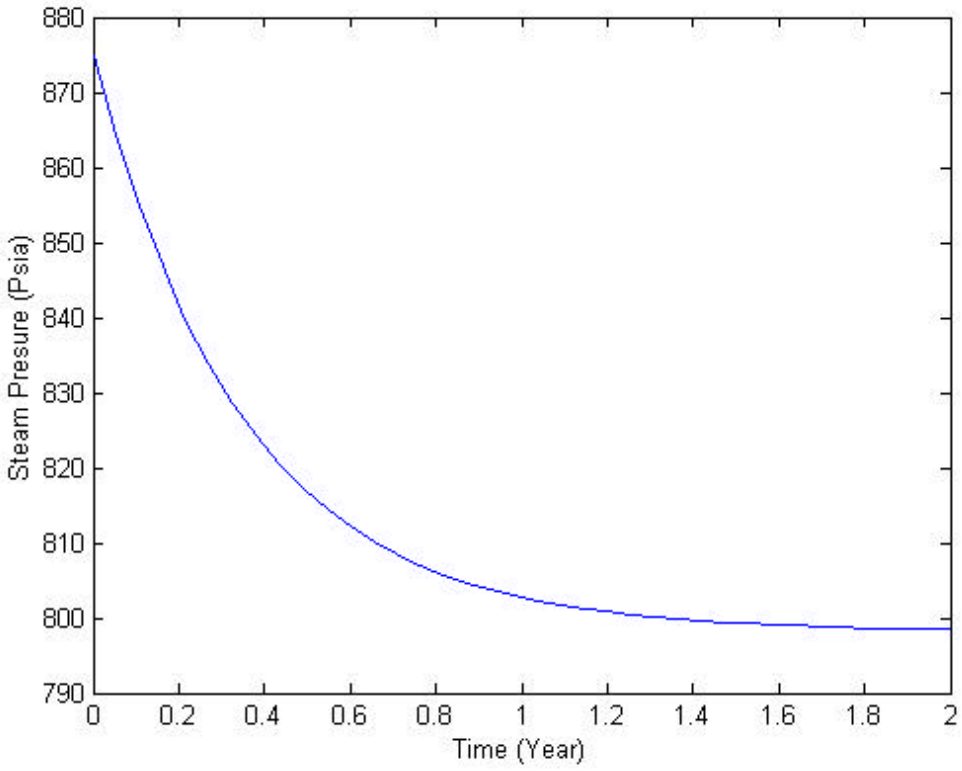

Figure 3.3. Steam Pressure Variation versus Time.

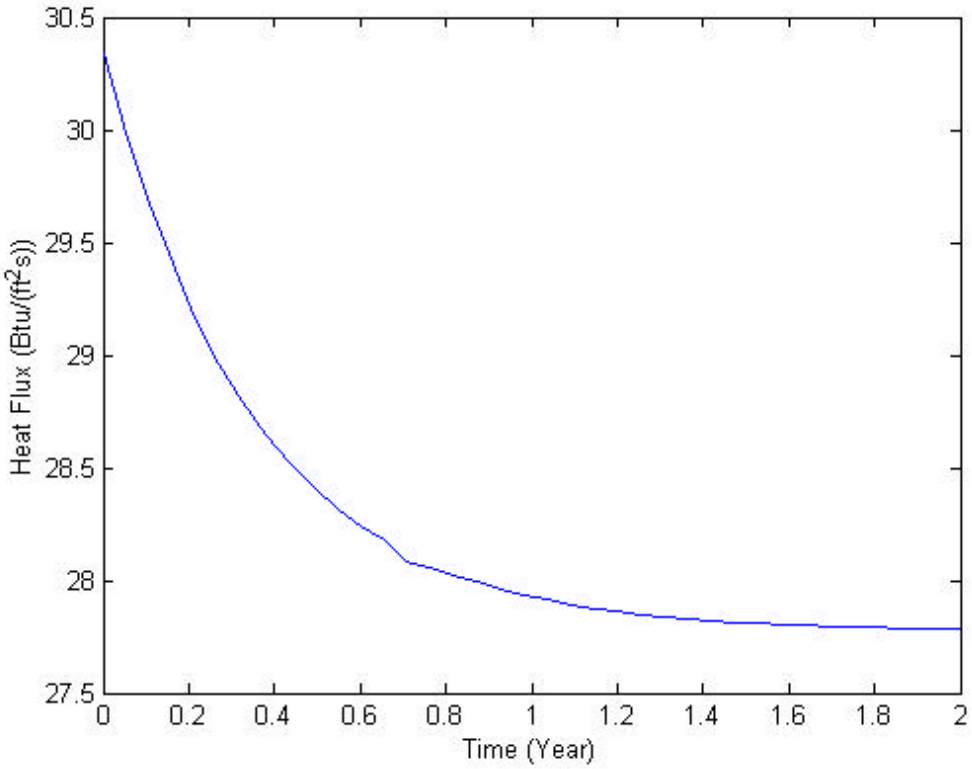

Figure 3.4. Average Heat Flux (on Outer SG Tube Surface) Variation versus Time.

3.3. Remarks

From the above study on simulation of UTSG secondary side fouling and the effects on thermal performance, we can reach the following conclusions:

(1) Since fouling may involve different kinds of mechanisms simultaneously, there does not exist a generally applicable mathematical model for modeling of fouling involving several fouling mechanisms. For example, to simulate fouling due to corrosion products, we have to study the physical process of corrosion. In up-to-date study, we have only simulated the UTSG particulate fouling. The simulation results are reasonable.

(2) The effect of fouling on UTSG thermal performance can be studied using the previously developed multimode SIMULINK model if the fouling process can be appropriately simulated using a proper model. The simulation results can be used for the prediction of UTSG thermal performance and scheduling of the USTG maintenance activities. For example, according to Figure 3.4 we can infer when the steam pressure is supposed to decrease by a certain percentage, for example 5%, and we know proper UTSG maintenance or other actions are needed before a specific time so as to recover the satisfactory UTSG thermal performance.

4. EXPERIMENTAL STUDY OF PARTICULATE FOULING OF HEAT EXCHANGER TUBING

4.1. Introduction

This section provides a review of experimental study of particulate fouling by earlier investigators. In this research we want to verify the particulate fouling model by a laboratory experiment. In order to accomplish this task, we have adapted a previously developed experimental setup to perform experimental studies of particulate fouling in a small-scale heat exchanger. In this section, we present a literature review of experimental studies of particulate fouling, description of our experimental setup, and experimental results.

4.2. Review of Experimental Study of Particulate Fouling in Heat Exchangers

Several researchers have performed experiments to study the particulate fouling. Here we review some representative work from the literature.

L. F. Melo et al. studied particle transport in fouling on copper tubes. They used the material KAOLIN to simulate suspended particles in water. Their fouling tests were performed in an annular heat exchanger consisting of a 2-meter long external Perspex tube and a removable inner copper tube, which was electrically heated. Water-KAOLIN suspensions were circulated through the annular section at different Reynolds numbers. KAOLIN particles were studied with a laser flow granulo-meter and a scanning electron microscope (SEM) and the fouling layer was roughly characterized as a thin disc with 16 *mm* (mean diameter) by 1 *mm* (mean thickness). SEM visualization of the deposits formed on the copper tube surfaces showed that the particles adhere by their larger faces (the bases of the disc). The thermal conductivity, density, final thickness, mass and thermal resistance were measured or estimated. Figures 4.1 and 4.2 show the experimental fouling results obtained at two different axial positions in the heat exchanger (D and E, both in the fully developed flow region), for lower range of Reynolds numbers. From these figures, we see that the fouling data fit well into the asymptotical behavior. Figure 4.3 illustrates the effect of the Reynolds number (Re) on the deposition flux (f_d). These results suggest that mass transfer controls the deposition rate when Re < 3900, and the adhesion dominates the process at higher Re values.

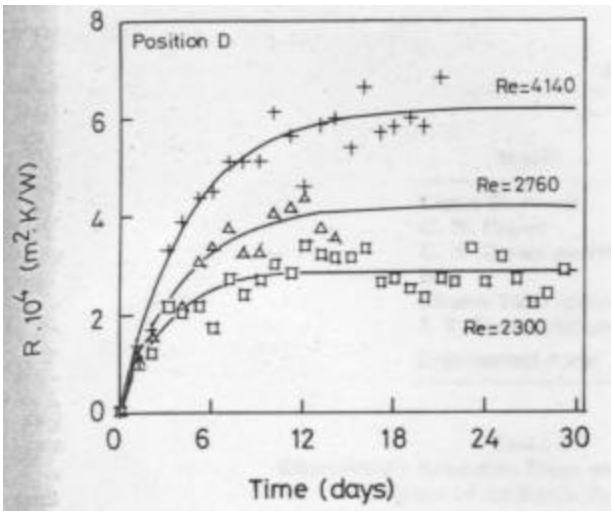

Figure 4.1. Fouling Data in Position D (From Ref. 150).

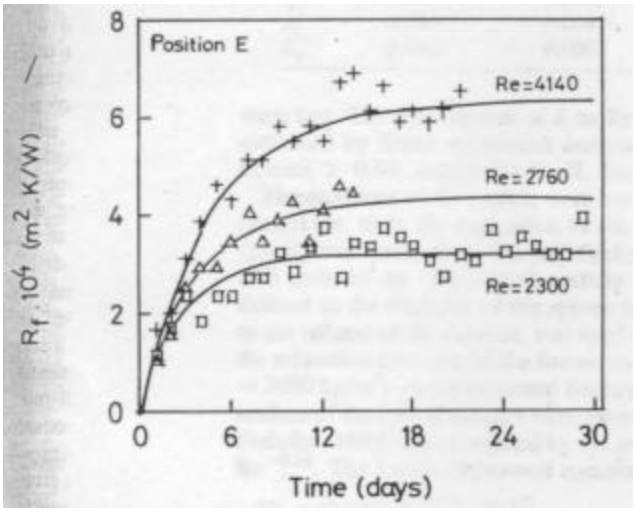

Figure 4.2. Fouling Data in Position E (From Ref. 150).

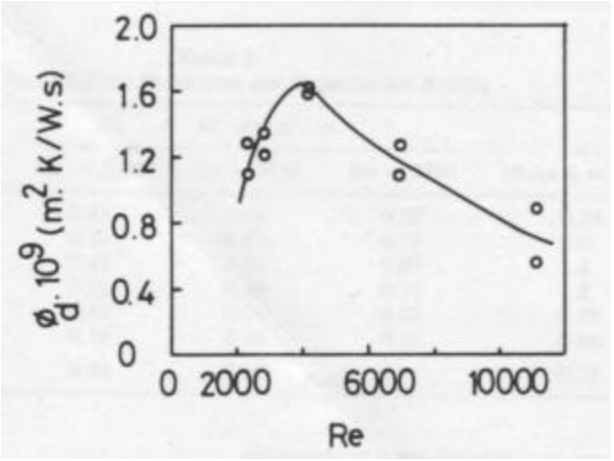

Figure 4.3. Deposition Flux versus Reynolds Number (From Ref. 150).

J. Middis et al. performed experimental study on particulate fouling in heat exchangers with enhanced surfaces. In their study, KAOLIN particles in X-2 were chosen as the fouling suspension. They studied the particulate fouling in a plate heat exchanger and a double pipe heat ecxchanger over a wide range of flow conditions. The typical fouling experimental results are shown in Figure 4.4. Here again we can see that the graph shows the characteristic asymptotic behavior. They also studied the effect of Reynolds number and other factors on the fouling behaviour, and conclusions similar to those in of Melo et al., were reached.

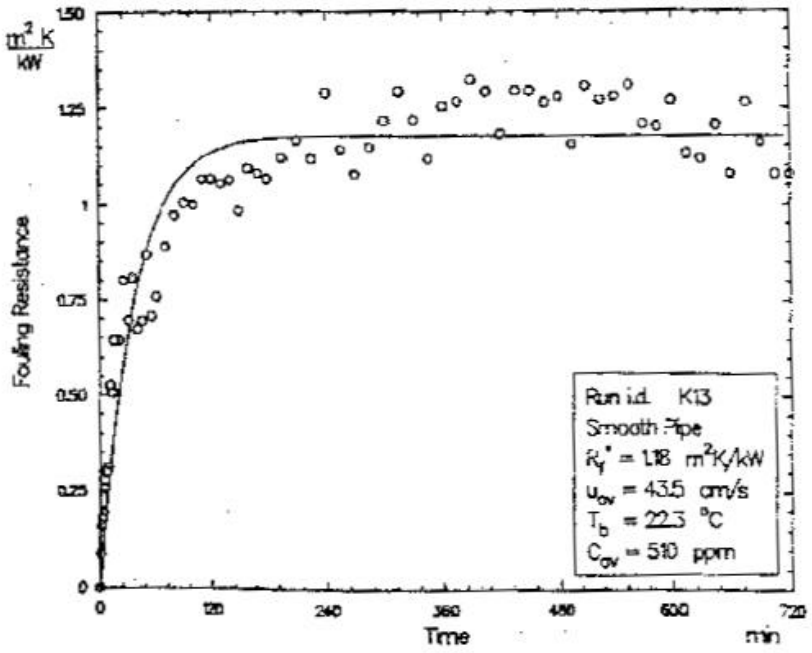

Figure 4.4. Typical Fouling Resistance versus Time Behavior (From Ref. 151).

L. M. Charmra et al. made a study on the effect of particle size and size distribution on particulate fouling in tubes. In their study, the Wieland NW, Wolverine Korodense, and a plain tube were chosen for testing. Two types of foulants, clay and silt, were used in the tests. The fouling tests were conducted for different concentrations, flow rate, foulant type, and particle diameter. Figure 4.5 shows the fouling curves for a 2,000 ppm concentration of 2 mm particle size. This figure shows that the enhanced tubes exhibit higher fouling resistance than the plain tubes. Figure 4.6 shows the fouling curves at 800 ppm. This figure shows that the enhanced and the plain tubes exhibit the same fouling behavior. Figure 4.6 also gives the fouling curves for 4 mm particle diameter at 800 ppm. It shows that the enhanced and the plain tubes did not foul. The asymptotic fouling resistances were very small. In fact Figure 4.7 shows that the rough and plain tubes experienced very little fouling with the 16 mm particles at 1,200 ppm. Figure 4.8 presents the asymptotic fouling resistance, R_f^*, as a function of concentration for the Korodense tube. We can see that the fouling resistance decreases as the concentration decreases for all particle sizes. This is because the deposition rate decreases as the concentration decreases since the deposition rate is proportional to fouling concentration. In addition, as the particle size (diameter) increases, the asymptotic fouling resistance decreases. This is because the particle deposition rate is proportional to $Sc^{-0.57}$. Thus, smaller particles, whose Schmidt numbers are

smaller, should undergo higher deposition rates (fouling resistances) than larger particles. Figure 4.9 shows the asymptotic fouling resistance, R_f^*, as a function of Reynolds number for the Korodense tube. It shows that R_f^* decreases as the Reynolds number increases. This is because the removal rate is directly proportional to the wall shear stress. Therefore, as the Reynolds number increases, the wall shear stress increases, which in turn increases the removal rate, and as a result the fouling resistance decreases. Again, this figure also shows that the fouling resistance decreases as the particle diameter increases. Figure 4.10 shows the asymptotic fouling resistance versus particle diameter for the enhanced and plain tubes. It shows that the fouling resistance increases as the particle size decreases. In fact, the asymptotic fouling resistance for the 16 *mm* particles is significantly smaller than for the 4 *mm* particles except for the plain tube. This is due to the transition from the diffusion dominant regime to the inertia dominant regime. This figure also shows that the enhanced tubes (NW and Korodense tubes) have higher asymptotic fouling resistances than the plain tube.

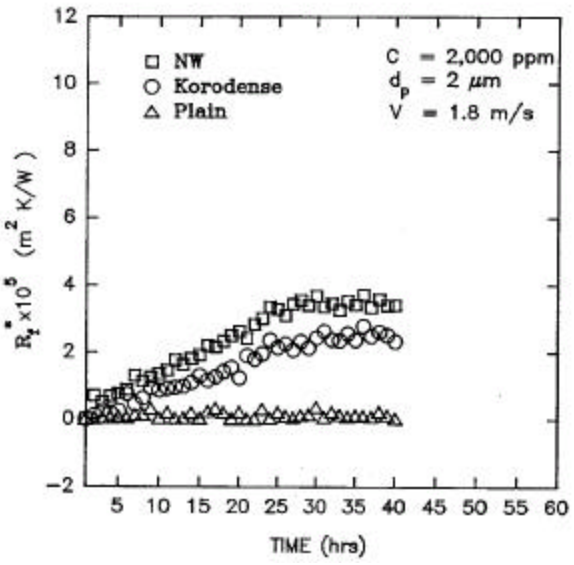

Figure 4.5. Asymptotic Fouling Curves at 1.8 m/s using 2000 ppm of 2 *mm* particles. (From Ref. 152).

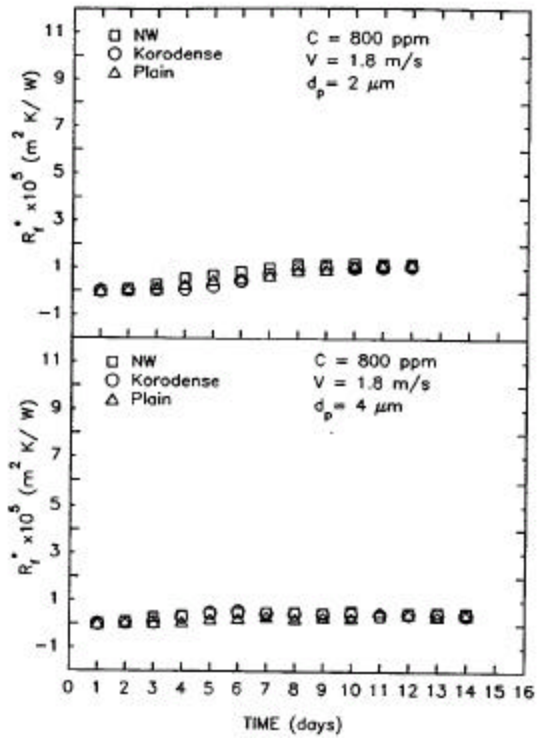

Figure 4.6. Asymptotic Fouling Curves at 1.8 m/s using 800 ppm (From Ref. 152).

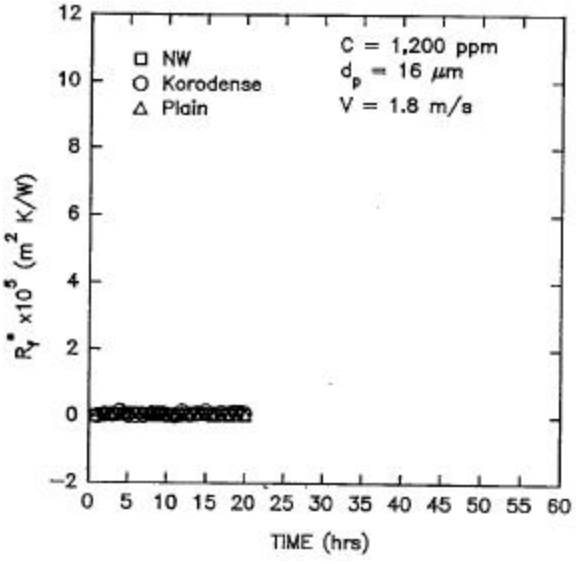

Figure 4.7. Asymptotic Fouling Curves at 1.8 m/s using 1200 ppm of 16 *mm* particles (From Ref. 152).

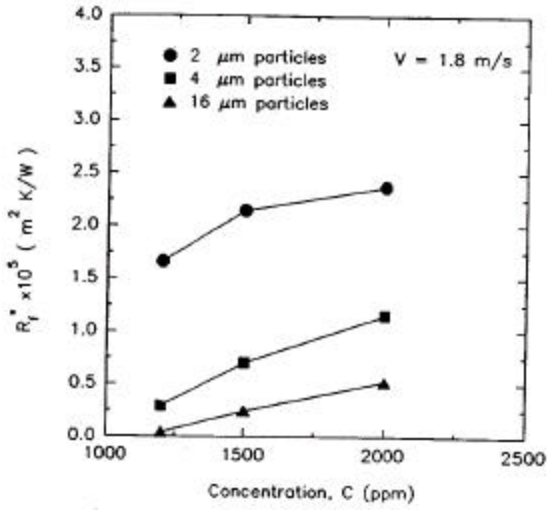

Figure 4.8. Asymptotic Fouling Resistance vs Concentration for the Korodense Tube (From Ref. 152).

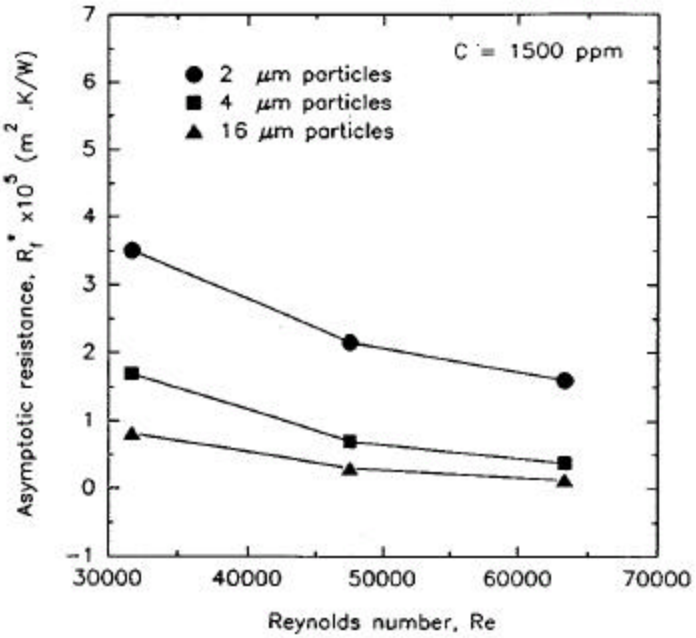

Figure 4.9. Asymptotic Fouling Resistance vs Reynolds Number for the Korodense Tube (From Ref. 152).

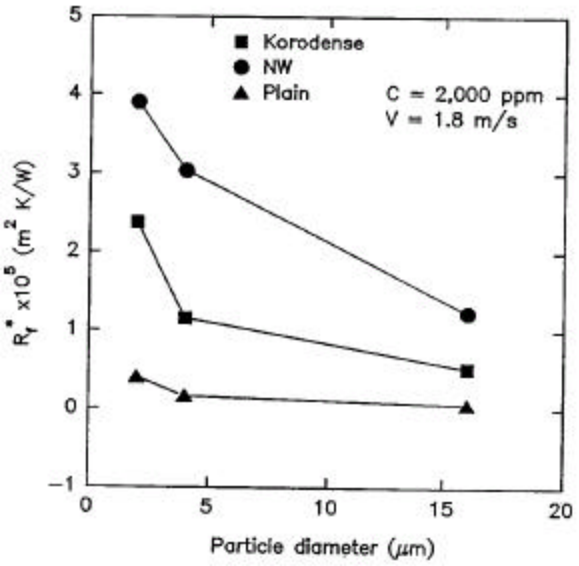

Figure 4.10. Asymptotic Fouling Resistance vs Particle Diameter (From Ref. 152).

There are other researchers who used other types of material to simulate the fouling particles. Among them, Hans Muller-Steigen et al. used the Al_2O_3 particles to study particulate fouling in heat exchangers; Mark Basset et al. used the sol-gel method to synthesize the simulated magnetite particles so as to study the fouling of Alloy-800 heat exchanger surfaces by magnetite particles, etc. It should be noted that most of the above researchers only used a single tube or even a tube section in their experimental study. Hence it is necessary to use a real heat exchanger to study the particulate fouling behavior.

4.3. Current Experimental Setup for Particulate Fouling Tests

As mentioned above, we want to use a real heat exchanger and perform experiments to study the particulate fouling behavior. For this purpose we have designed and adapted an experimental setup. Figure 4.11 presents the configuration of this setup, and Figure 4.12 shows an overview of it. In our experiment, we have use KAOLIN clay suspended in water and a small-scale tube-and-shell heat exchanger. The particulate material is the RC-90 KAOLIN from the Thiele KAOLIN Company. The particle size is < 2 *mm* with a percentage of 98.0%; pH (dry clay tested at 20% solids) is 6.8. The heat exchanger, HT-1-A-CI-2-24, was procured from Mahan's Thermal Products, Inc. It has 31 copper tubes, with shell diameter $2\frac{1}{8}$ inch, tube length 24 inch, and tube outer diameter $1/4^{"}$.

As can be seen from Figures 4.11 and 4.12, the experimental setup consists of a stainless steel water tank, a 2 KW electrical heater, a stainless steel centrifugal pump, a shell-and-tube heat exchanger, two flow-meters measuring the tube-side and shell-side flow rates, four thermocouples measuring the inlet and outlet temperatures of the tube-side and shell-side coolant, and a data acquisition system. The data acquisition system includes two conditioning modules, a connection box, a data acquisition board, and a personal computer, which uses the

LABVIEW to collect, display, and store the experimental data. Water with KAOLIN particles is designed to flow through the tube side of the heat exchanger so that it is convenient to remove or wash off the fouling layer after the experiment is completed.

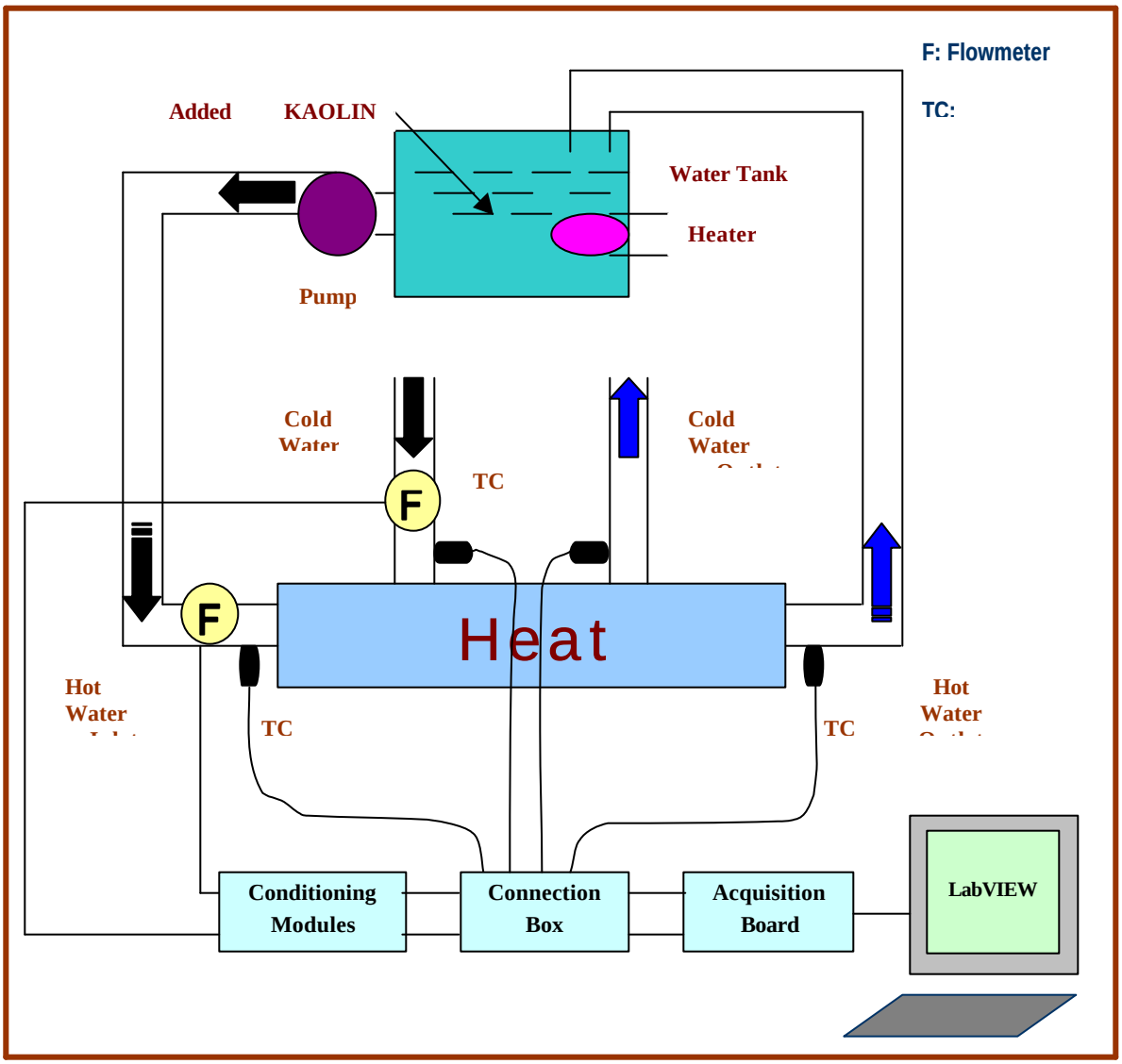

Figure 4.11. Configuration of the Heat Exchanger Experimental Set-up for Particulate Fouling Tests.

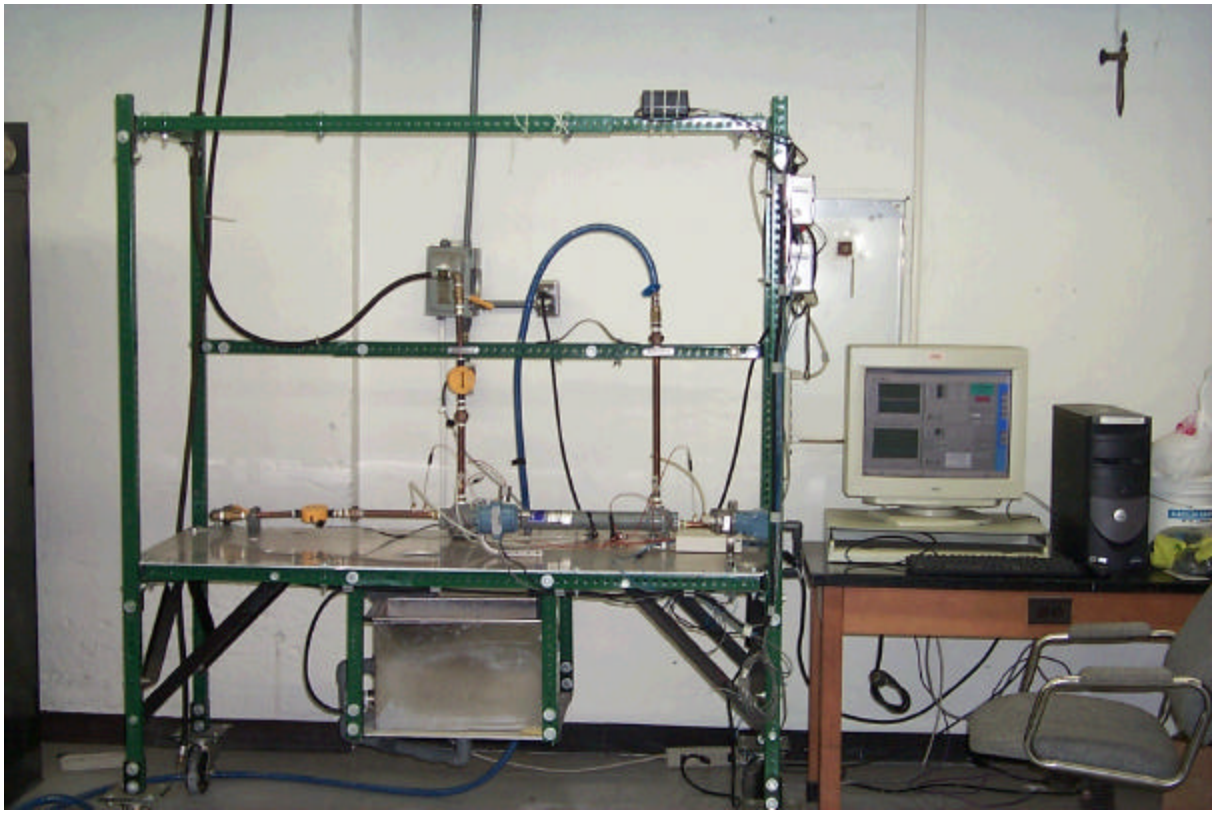

Figure 4.12. Experimental Setup showing the heat exchanger on the mobile table, water tank (underneath the table) connections to hot and cold water lines, and the data acquisition computer.

4.4. Calculation of Overall Thermal Resistance and Preliminary Experimental Results

The effect of the fouling progression can be monitored by continuously evaluating the overall heat transfer thermal resistance (1/UA). From energy balance, we have

$$\dot{Q} = UA\Delta T_{LMTD} = \dot{m}_h C_h \Delta T_h = \dot{m}_c C_c \Delta T_c \qquad (4.1)$$

ΔT_{LMTD} is the logrithmic mean temperature difference for the heat exchanger and is defined as

$$\Delta T_{LMTD} = \frac{\Delta t_1 - \Delta t_2}{\ln(\Delta t_1 / \Delta t_2)} \qquad (4.2)$$

For parallel or concurrent flow: $\Delta t_1 = t_{h,in} - t_{c,in}$; $\Delta t_2 = t_{h,out} - t_{c,out}$

For counter flow: $\Delta t_1 = t_{h,in} - t_{c,out}$; $\Delta t_2 = t_{h,out} - t_{c,in}$.

In the above equation, U is the overall heat transfer coefficient, and A is the heat transfer area, which may change with fouling pregression. However, the product UA can be calculated and be thought of as inseparable in terms of the effect of fouling on heat transfer. The inverse of UA is the overall thermal resistance, which increase as the fouling increases. This overall thermal resistance, 1/(UA), is continuously computed so as to monitor the particulate fouling behavior in the heat exchanger. To determine the overall thermal resistance, we continuously measure the mass flow rate of the cold side or/and the hot side, inlet and outlet temperatures of both the cold side and the hot side, as shown in Figure 4.11 and Figure 4.12. It should be noted that in our experimental design, we adapted the parallel or concurrent flow pattern in the heat exchanger.

In our experiment, 120 gm of KAOLIN particles were added to the water tank, which has a dimension of 18"×12"×12". This resulted in a fairly high concentration of about 2823 ppm. The experiment has been run for more than 150 hours. Figure 4.13 shows the preliminary experimental results of the changes in the overall thermal resistance with time. From this figure, we see that the overall fouling resistance first increases with time, then at after about 120 hours of running it tends to attain a steady state value. This proves that the overall thermal resistance also exhibits an asymptotic behavior even in a real small-scale heat exchanger.

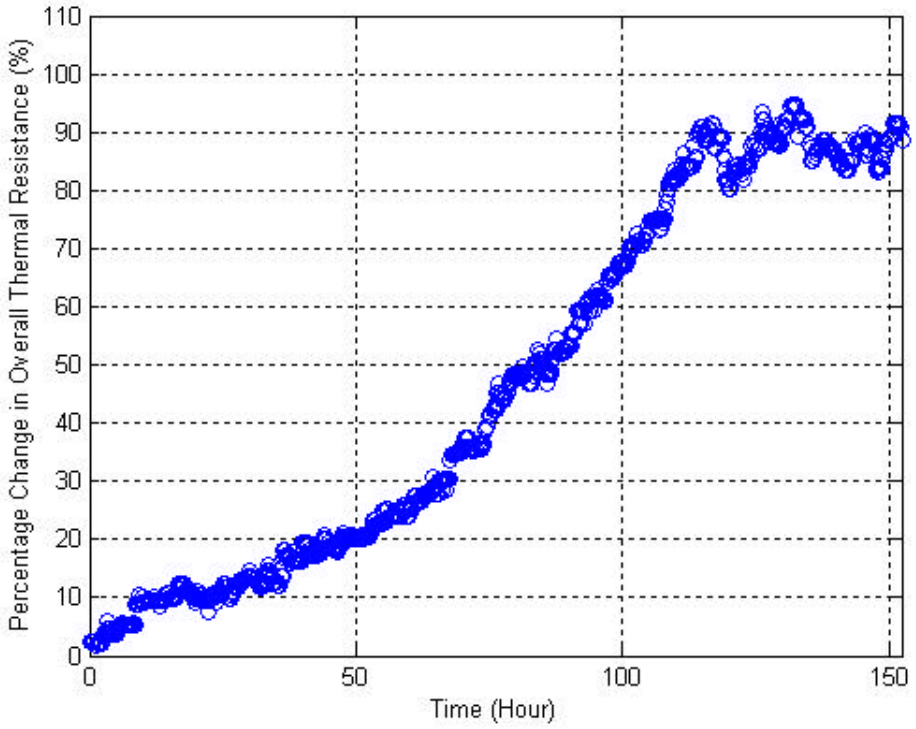

Figure 4.13. Preliminary Experimental Results—The Overall Thermal Resistance Variation vs. Experimental Running Time.

4.5. Remarks and Future Research

From the above preliminary experimental study on particulate fouling in a small-scale heat exchanger, we can temporarily reach the following conclusions:

- The particulate fouling in a small-scale heat exchanger still exhibits an asymptotic behavior.

- The experimental methodology and design of the setup for particulate fouling study are correct and effective.

However, to further verify the above conclusions and the particulate fouling model, more experiments and analysis are needed. The future research will include:

(1) Further experimental investigation of the fouling progression in a heat exchanger and verification of the particulate fouling model.
(2) Using the developed UTSG model to generate data and develop a GMDH data-driven model to monitor and diagnose the faults, especially fouling in a UTSG.

5. MONITORING AND DIAGNOSIS OF A HEAT EXCHANGER USING HYBRID SYSTEM MODELING

5.1. Introduction

Hybrid modeling integrates first principles models and data-based models, such as neural networks, to correctly model physical phenomena. This section presents the results of the development of hybrid model for monitoring and diagnostics of heat exchanger systems. The earlier study used simulated data for a heat exchanger to develop the hybrid modeling in both parallel and series architectures. In this report, experimental data from the heat exchanger setup, instead of simulation, are used to implement the data based model. The results show that the parallel hybrid system developed can be used to model the heat exchanger. The hybrid model performs better than the first principle model, within the normal operating regime.

The two most common groups of models used in Fault Detection and Isolation (FDI) systems are the first-principle models and the data-based models. The first-principle models may not always incorporate all of the functionality of the system and do not provide the sensitivity necessary to detect small changes in plant degradation; however, data-based models have been used to accurately perform sensitive FDI task [39]. First principle models also require substantial engineering time to develop; and in some instances, such as complex chemical reactions, accurate first principle models are not available.

Data based systems are applicable to operating plants and systems where operational data are recorded over the entire operating range. The data based systems are only accurate when applied to the same, or similar, operating conditions for which data are collected. When plant conditions or operations change significantly, the model must extrapolate outside the training space and the results should not be trusted. Unlike linear models, which extrapolate in a known linear fashion, non-linear models extrapolate in an unknown manner. These empirical (data-based) models must be trained on past plant data. Since automated data acquisition systems may not have acquired data on the system of interest, especially for new generation designs that have not been constructed, data may not be available and first principle models must be used. These models can be improved by appending them with data based models as data become available.

The combination of data-based and first-principle models are termed hybrid models. In these
designs, the first-principle models are developed and then appended with data based models as data become available. This method provides the robustness of first principle models with the sensitivity of data based models. This hybrid framework, although more complicated, has a very important advantage. Purely data based systems are not reliable when the system moves into new operating conditions which may result from configuration changes, new operating practices, or external factors such as unusual cold cooling water temperatures in condensers. By using the hybrid system, the predictions tend towards the first-principle model when new operating conditions are encountered and will additionally use the data-based models when in familiar operating conditions.

5.2. Methodology

In order to understand the application of hybrid modeling, we first present the methods of modeling a heat exchanger from first principles and then explain methods to integrate empirical models, such as neural networks, through parallel hybrid modeling.

5.2.1. Heat Exchanger Physical Modeling

A heat exchanger (HX) is a device used to transfer heat between two fluids that are at different temperatures and are separated by a solid wall. Heat exchangers are generally classified according to the type of construction and the flow arrangement. The simplest configuration, termed double pipe, consists of two concentric tubes containing the hot and cold fluids. The flow direction of the cold and hot fluids determines whether we have a double pipe parallel flow or a double pipe counter flow heat exchanger. The most common type of construction is the tube and shell arrangement that houses several internal tubes. The tube and shell HX provides a greater heat transfer area compared to the single tube version.

Other heat exchanger arrangements are described by Incropera [78].

For simplicity, the double pipe parallel flow concept, shown in Figure 5.1, is used in this work.

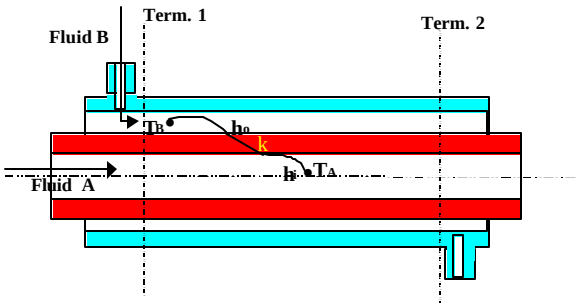

Figure 5.1. Double pipe parallel flow heat exchanger.

Two approaches to represent the heat exchanger by first principle model are commonly used: the Log Mean Temperature Difference (LMTD) method and the Effectiveness-NTU Method[58]. In this work, the NTU model was chosen. Both methods are based on energy balance equations, where the amount of heat given up by the hot fluid equals the amount of heat received by the cold fluid, as shown in Equation (5.1).

$$Q = \dot{m} c_p^h \Delta T^h = -\dot{m} c_p^c \Delta T^c \qquad (5.1)$$

where: Q = heat transfer

$\dot{m}$ = mass flow rate

cp = specific heat capacity

ΔT = temperature difference

h and c are superscripts designating hot and cold.

Additionally, the total heat transfer can also be expressed as

$$Q = U \cdot A \cdot \Delta T_m \tag{5.2}$$

where: U = overall heat-transfer coefficient
A = total surface area for heat transfer consistent with definition of U
ΔTm = suitable mean temperature difference across the heat exchanger

The Effectiveness-NTU Method is an alternative approach that can be used when the fluid output temperatures are unknown. The effectiveness-NTU method is based on the effectiveness of the heat exchanger in transferring a given amount of heat, with effectiveness defined as the ratio between the actual heat transfer and the maximum possible heat transfer:

$$e \equiv \frac{Q}{Q_{\max}} \tag{5.3}$$

The maximum heat transfer is given by:

$$Q_{\max} = \left(\dot{m} \times c_p\right)_{\min}\left(T_{h_{inlet}} - T_{c_{inlet}}\right) = C_{\min}\left(T_{h_{inlet}} - T_{c_{inlet}}\right) \tag{5.4}$$

Where C is the fluid capacity defined as $\dot{m}c_p$.

C_{min} is either the hot or the cold fluid that has the minimum fluid capacity. From Equations (5.2), (5.3) and (5.4), it follows that the effectiveness is given by:

$$e = \frac{C_h\left(T_{h_{inlet}} - T_{h_{outlet}}\right)}{C_{\min}\left(T_{h_{inlet}} - T_{c_{inlet}}\right)} \tag{5.5}$$

$$e = \frac{C_c\left(T_{c_{inlet}} - T_{c_{outlet}}\right)}{C_{\min}\left(T_{h_{inlet}} - T_{c_{inlet}}\right)} \tag{5.6}$$

The Number of Thermal Units (NTU) is defined as

$$NTU \equiv \frac{UA}{C_{\min}} \tag{5.7}$$

The effectiveness can be written as a function of NTU, C_{min}, and C_{max}. Holman [58] develops the effectiveness relationship for the double pipe parallel flow heat exchanger as

$$e = \frac{1 - \exp[-NTU(1 + C_{\min}/C_{\max})}{1 + C_{\min}/C_{\max}} \tag{5.8}$$

The NTU method has been chosen for use in this work to implement the heat exchanger physical model, as part of the hybrid modeling.

It is interesting to note that the overall heat-transfer coefficient (U) is a difficult parameter to be properly taken in account in the physical modeling due to its dependence on the fluid thermodynamics conditions, and on the heat exchanger geometrical parameters. This is where the data based modeling comes into play in compensating possible inaccuracies in the physical modeling.

5.2.2. Artificial Neural Networks

Neural networks are modeling techniques that learn system behavior through data acquired from that system. They are able to learn the relationship for operating regions that are presented to them during training. If the operation region moves outside the training region, the neural network model cannot be expected to give accurate predictions.

In this work neural networks are used for hybrid modeling. The neural network architecture is a Multi-Layer Perceptron (MLP) with four hidden neurons. In the hybrid parallel model, the neural network is trained to predict the error between the actual data, acquired from the heat exchanger, and the physical model, implemented through the NTU method. We now discuss the hybrid modeling.

5.2.3. Hybrid Modeling

Several useful overview papers on hybrid modeling include Thompson and Kramer (1994)[43], Wilson and Zorsetto (1997) [45], te Braake and van Can (1998) [42]. The hybrid approach has commonly been termed a "grey-box" modeling approach, as contrasted to "black box" modeling of Neural Networks or other data based approaches. The term grey-box comes from the idea that a portion of the internal model, the first principle model, is explainable. In other technical papers these approaches are termed semi-mechanistic models.

There are two major approaches to hybrid, grey-box, or semi-mechanistic modeling: the "series approach", and the "parallel approach". The series approach uses a data based model to construct missing inputs or parameter estimates to the first principle model, while the parallel approach uses a neural network to model non-linearities, disturbances, or other processes not accounted for in the first principles model. Both of these approaches have been used in the chemical industry and are being investigated for use in other industries to perform monitoring and diagnostic tasks. In this work the Parallel Approach will be implemented.

A. Parallel Approach: In the parallel hybrid modeling approach (see Figure 5.2), a neural network is trained to predict the residuals not explained by the first principles model. When in operation, the predicted residuals are added to the first principles model output, resulting in a total prediction that is much closer to the actual system. The parallel approach was first proposed by Kramer, Thompson, and Bhagat (1992) [40]. They applied radial basis function

neural networks to correct the output of a first principle model in a Continuous Stirred Tank Reactor (CSTR). In 1994 they published another paper applying the technique to a batch penicillin fermentation process (Thompson 1994) [5]. Both papers showed promising results.

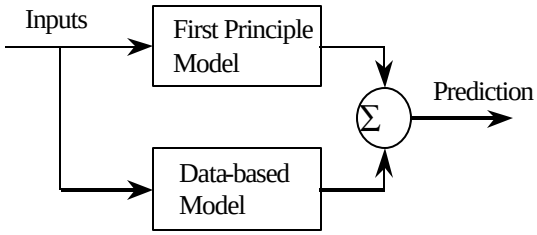

Figure 5.2. Parallel hybrid modeling approach.

B. Model Testing: The literature contains reports that compare the series parallel hybrid approaches. van Can et al. (1996) [44] reports that the serial approach is superior to the parallel approach and others have made similar reports. The work with simulated data reported at MARCON 2002 [79] also showed better results on hybrid series approach.

In this report, we compare the performance of a physical modeling, based on first principles equations, versus a hybrid parallel modeling. We assess the ability of each modeling technique in representing properly the behavior of the heat exchanger, considering several steady state conditions to which the HX was subjected. The hybrid series modeling will be developed and its performance compared to the hybrid parallel modeling now being discussed.

5.3. Heat Exchanger Experimental Loop and Test Results

To accomplish this comparison, a heat exchanger loop was assembled in the laboratory facility. The heat exchanger used in this experiment is a copper tube-and-shell structure, 24" long, with 31 internal tubes (1/4" diameter) that sit inside a 2.5" diameter shell. The HX is connected to the building hot and cold water supply in an open loop arrangement. The hot water goes through the tube side and the cold water through the shell side, in parallel flow directions. The HX is instrumented with temperature and flow rate sensors. Four type-J thermocouples allow monitoring the hot and cold water inlet and the hot and cold water outlet temperatures. Turbine type flow meters were installed in the hot and cold-water inlet piping. The temperature and flow rate signals are conditioned, and then sent to a digital data acquisition system that is based on National Instruments' hardware and LabView Virtual Instrument (VI) program. The data are acquired and stored for future use in developing the data based modeling, which will be part of the hybrid modeling. Figures 5.3 – 5.5 show the laboratory heat exchanger setup.

Figure 5.3. Laboratory heat exchanger loop.

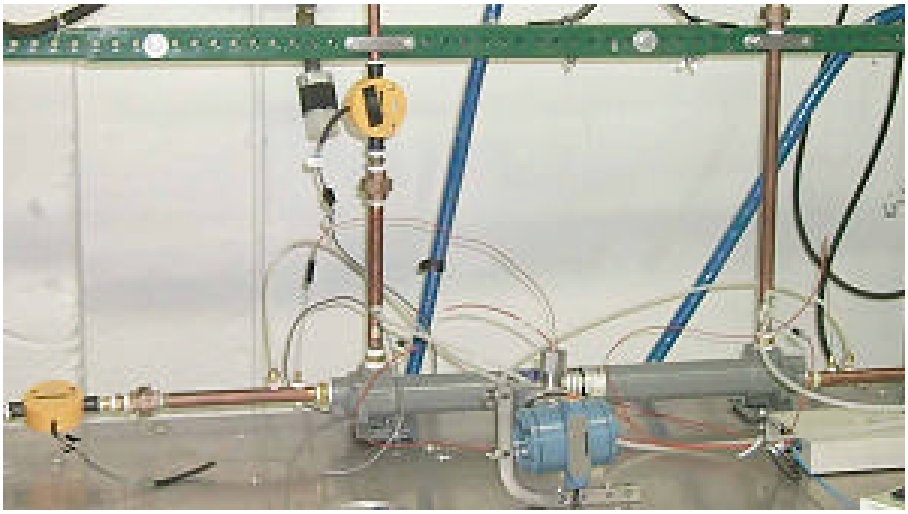

Figure 5.4. Laboratory heat exchanger close-up view.

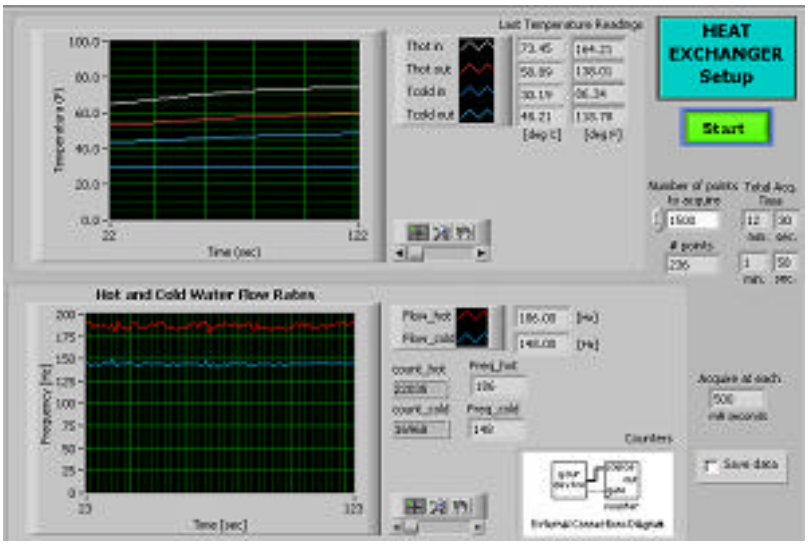

Figure 5.5. LabView based user interface.

5.3.1. Hybrid Parallel Model

The hybrid parallel model was developed using NTU method to implement the heat exchanger physical model and the MPL neural network architecture to implement the data based model. To achieve good results, when calculating the overall heat transfer coefficient (U), the physical model takes into consideration the different Nusselt and Prandtl numbers related to each different steady state thermodynamic conditions under which the data were acquired.

The MLP neural network architecture gave better results when implemented with one neural network to predict the error in the hot water temperature and another to predict the error in the cold water temperature, instead of using just one neural network model to predict both.

In the hybrid parallel approach, a neural network was trained to predict the residuals in the hot and cold temperatures on the output of heat exchanger that are not explained by the physical model. The inputs of the model are the hot and cold temperatures of the inlet water and the hot and cold mass flow rates. Figure 5.6 shows the hybrid parallel model schematic.

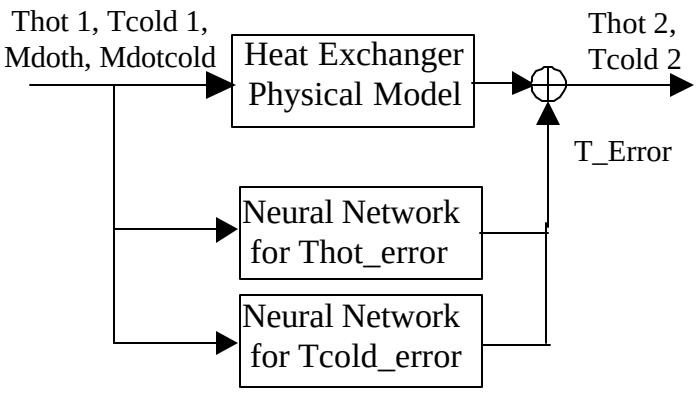

Figure 5.6. Heat exchanger parallel hybrid model.

5.3.2. Input Data

The heat exchanger was supplied with building water in an open loop arrangement. The different steady state conditions were established by varying the hot and cold water flow rates. By changing the water flow rates caused all the temperature measurements to change. For each steady state condition, the data were acquired and stored. Figures 5.7 – 5.9 show fourteen steady state levels, each one can be characterized roughly by a medium value for the hot and cold mass flow rate and the corresponding values for the inlet cold and hot temperatures.

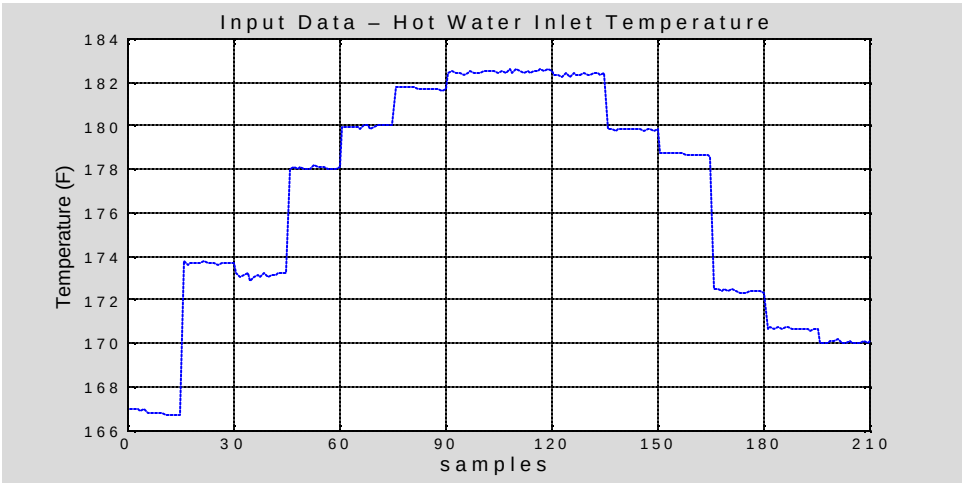

Figure 5.7. Input data: hot water inlet temperature.

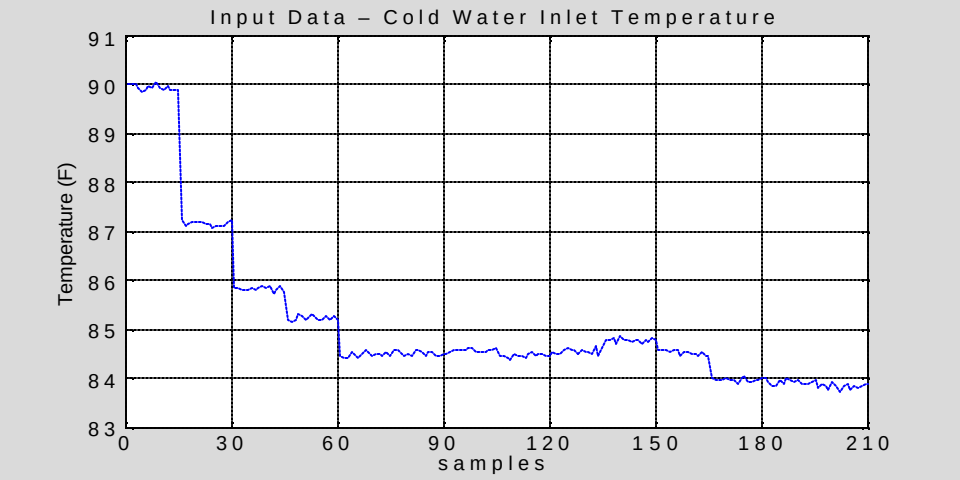

Figure 5.8. Input data: cold water inlet temperature.

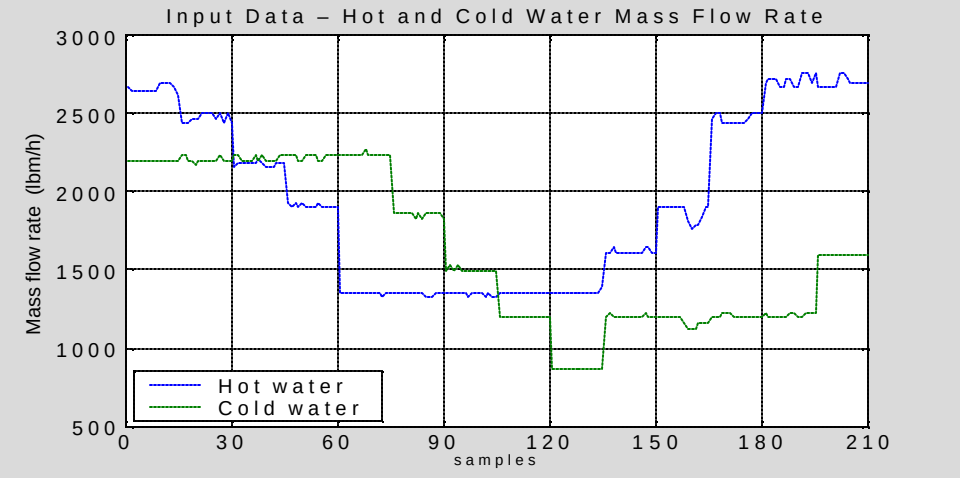

Figure 5.9. Input data: hot and cold water mass flow rate.

5.3.3. Results

Figure 5.10 shows the prediction of the physical and the parallel hybrid models for the hot water temperature output and its actual measurement.

The result (see Figure 5.10) shows that the physical model (blue line) is not able to exactly model the temperature at each steady state condition. This is due to the use of physical models that do not consider all inputs and disturbances such as heat loss to the room. On the other hand, the parallel hybrid model (red line) follows the actual data (green line) much better. The mean percent error is 0.10% for the hybrid model hot temperature predictions versus 0.53%

for the physical model: a performance increase of five times. The neural networks in the hybrid model attempt to explain or compensate for the residuals not taken in account by the physical model.

Figure 5.11 shows the predictions for the cold water temperature output, and similar performance can be observed. The hybrid model outperforms the physical model by a factor of about 5. The mean error, of the actual values is 0.26% for the hybrid model prediction versus 1.37% for the physical model. The remaining error is due to stochastic noise, unknown inputs, and other unmodeled disturbances.

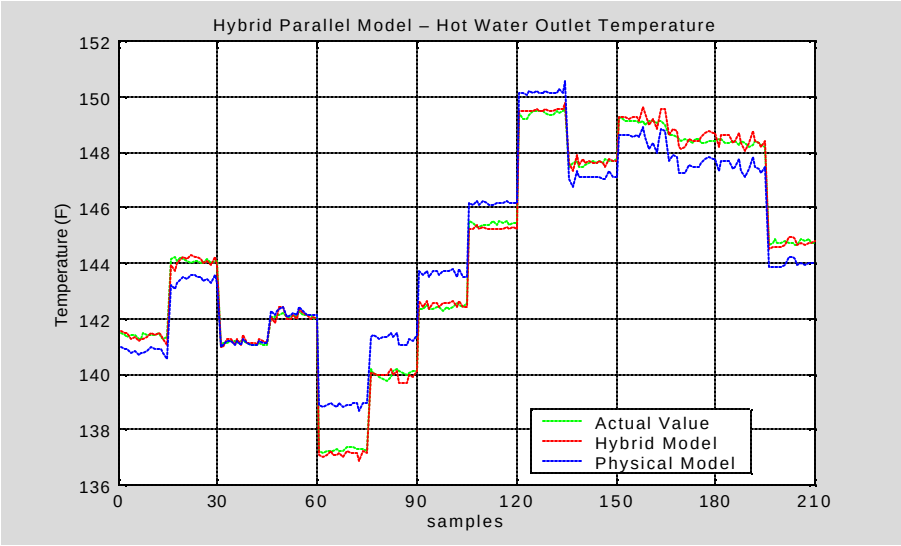

Figure 5.10. Hot temperature: hybrid and physical modeling predictions and measurements.

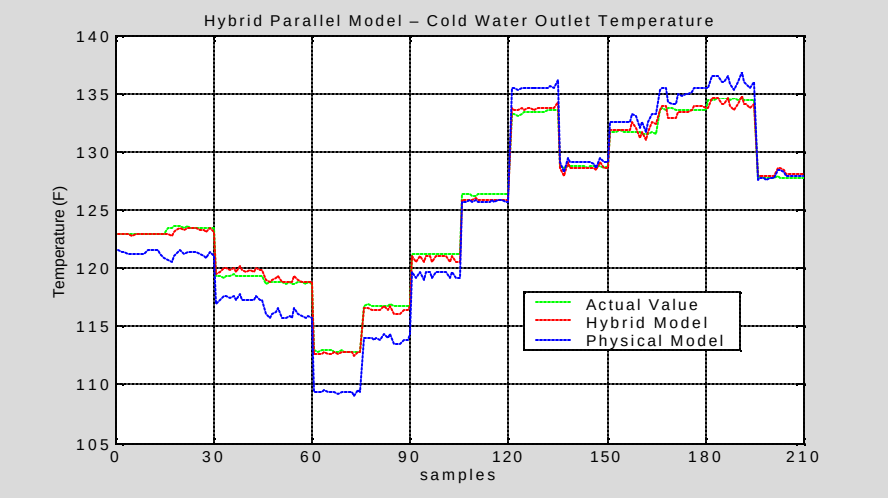

Figure 5.11. Cold temperature: hybrid and physical modeling predictions and measurements.

5.4. Remarks

The results show that the physical model and a parallel hybrid model architecture are capable of modeling a heat exchanger. The parallel hybrid approach has a small modeling error. The physical modeling did not perform well at all steady state conditions. The heat exchanger laboratory data have been very useful in demonstrating the effectiveness of the hybrid modeling technique.

5.5. New Data from Normal and Fault Condition Operations of the Heat Exchanger Loop

Data for the case of normal operation of the heat exchanger loop was acquired. This was followed by additional data acquisition for the conditions with faulty conditions. The faulty conditions included leakage and tube plugging. Several leakage conditions were imposed in the inlet hot water pipe (on the HX tube side) and in the inlet cold water pipe (on the HX shell side). HX tube faults were inserted by plugging various numbers of the interior HX tubes. This simulates a situation in which the system responds with a decrease in the flow rate and temperature changes due to actual tube plugging. Data were acquired at several steady state conditions.

Tube leakage conditions:

- Imposed to the cold water through a hole located just at the inlet pipe, right after the flow meter.
- Imposed to the hot water through a hole located just at the inlet pipe, right after the flow meter.

Tube plugging conditions:

- Imposed by plugging 1 to 5 tubes.
- Imposed by plugging 13 tubes.
- Imposed by plugging 17 tubes.
- Imposed by plugging 21 tubes.

Future Work: Analysis of the Faulty Data

Until now the data driven model used in the hybrid model in this research was implemented using multi-layer perceptron neural networks. We are currently investigating Locally Weighted Regression (LWR) for use in the hybrid model. LWR is a method that follows the lazy learning approach, in which a local, memory-based procedure is chosen to model the data as an alternative to the global, parametric approach used by MLP neural networks.

6. STRUCTURAL MONITORING OF STEAM GENERATORS AND HEAT EXCHANGERS USING PIEZOELECTRIC DEVICES

6.1. Introduction

The current industry practice for in-service inspection of steam generator (SG) tubing is the use of eddy current testing (and in some cases ultrasonic testing). This is performed when the system is shut down for either maintenance or refueling outages. Thus, the mechanical integrity of SG tubing and structure are not directly available at other times. In this project we propose to develop a sensor suite with sensor arrays that can be permanently embedded in the tubing and other structures and can be monitored continuously. The sensor arrays being developed use piezo-transducers, both as actuators and sensors. They can be either surface-bonded or embedded in the structure. Each of the piezo-transducers can generate and receive elastic waves propagating through the structure being monitored.

In the late 1800s Jacques and Pierre Curie discovered surface electric charges on tourmaline crystals, caused by mechanical stress. The phenomenon of electrical polarization of crystals caused by deformation in certain directions was later given the name piezoelectricity by Hankel. In 1881, using M.G. Lippmann's thermodynamic theories, the Curie brothers proved experimentally the reverse action of piezoelectric effect, that is, mechanical deformation of crystals due to an applied electric field.

Thus, when certain materials are subjected to stress an electric charge is produced, with its magnitude and direction being a function of the magnitude and direction of the stress being applied. Some of the recent developments in piezo-devices are due to the revolution in wireless and wire-line communications. Also, new developments in piezoelectric ceramics and ceramic/polymer composites have evolved into new markets. Even though piezoelectric quartz crystal still holds the largest market segment, several new piezoelectric ceramic and piezo-polymer materials are being developed. The principle of piezoelectric effect is widely used in Micro-Electro-Mechanical Systems (MEMS) with a multitude of applications.

6.1.1. Piezoelectric Material

A piezoelectric material generates an electric charge when mechanically deformed. Conversely, when an external electric field is applied to piezoelectric materials they deform mechanically. The piezoelectric effect is found only in crystals, which have no center of symmetry. Examples of piezoelectric materials are quartz, Rochelle salt and many synthetic polycrystalline ceramics.

Many polymers, ceramics, and molecules such as water are permanently polarized: some parts of the molecule are positively charged, while other parts of the molecule are negatively charged (Figure 6.1a). When an electric field is applied to these materials, the polarized molecules will align themselves with the electric field, resulting in induced dipoles within the molecular or crystal structure of the material (Figure 6.1b**)**.

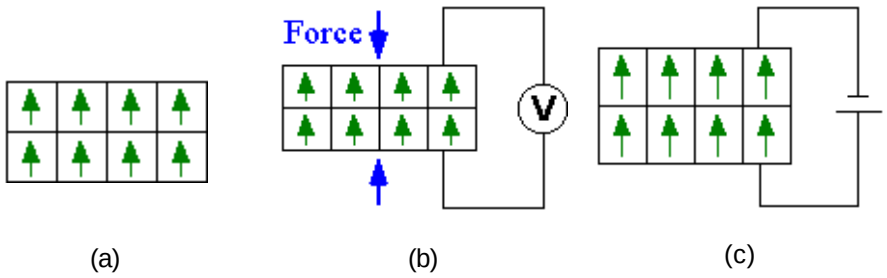

Figure 6.1. Piezoelectric effect.

Furthermore, a permanently polarized material such as quartz (SiO_2) or barium titanate ($BaTiO_3$) will produce an electric field when the material changes dimensions as a result of an imposed mechanical force. These materials are piezoelectric, and this phenomenon is known as the piezoelectric effect (Figure 6.1c). Conversely, an applied electric field can cause a piezoelectric material to change dimensions. This phenomenon is known as electrostriction in which the material density increases by excitation of transverse acoustic vibrational eigenmodes of the fiber in response to the intensity of an applied field or just the reverse piezoelectric effect.

Thus, a piezoelectric material can be used both as an actuator, which converts electrical energy to mechanical energy and as a sensor, which converts mechanical energy into electrical energy. In most cases, the same element can be used to perform both tasks.

6.1.2. Structure Guided Waves

The guided waves refer to the waves propagating along the immediate vicinity of material boundaries, where the boundaries have the effect of guiding acoustic waves along their surfaces. Two examples of guided wave are the thin plate and the long tube shown in Figure 6.1.2.

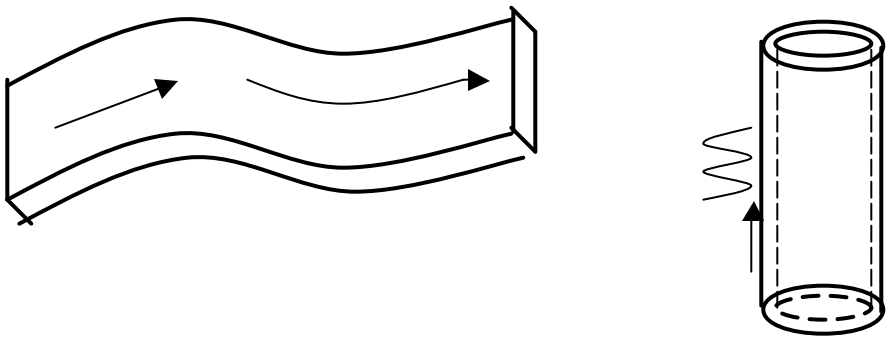

Figure 6.2. Examples of guided waves.

Ultrasonic testing has been used in nondestructive inspection of materials and in medical diagnosis. An ultrasonic pulse is usually transmitted and collected using special (commercially available) equipment. Although it has been wisely utilized, there are still many conditions where the traditional NDE technique is invalid. For example, the material change caused by corrosion is not easily detectable by traditional pulse-echo ultrasonic techniques. In addition, it is common that heat exchanger tubes have fouling deposits. Too much fouling may cause problems such as inefficient heat transfer. Furthermore, the traditional technique is still an offline inspection method. It is desirable in monitoring key equipments online without disturbing normal operation.

Guided waves have been studied and applied in non-destructive examination since (original studies by Rayleigh, Lamb, Stonely, and others). The displacement potentials and other methods have been used to derive general solutions. The Lamb wave propagating along a thin structure has more complicated solutions than the Raylegh wave propagation near the surface of a half infinite medium due to dual free boundaries. It is found that the wave properties are directly related to the stress distribution. Some researchers have studied the relationship between the stress change caused by additional loading and wave spectrum. The studies indicate the potential of the applications of guided waves in microstructure monitoring.

6.2. Laboratory Experimental System

The theory of reflection and scattering of guided acoustic waves has potential applications in non-destructive examination. The experimental setup used to generate acoustic waves and measure the output is described below.

6.2.1. Aluminum Beam and Piezoelectric Sensors

For this work, samples of aluminum beam (Al 6061) 305mm long, 25mm wide and 3mm thick, were cut then polished using sandpaper and degreased.

At each extremity one strip 30mm long, 10mm wide and 0.27mm thick piezoelectric material (PSI-5A-S4-ENH from Piezo Systems, Inc., Cambridge, MA) was bonded on the beam surface with ECCOBOND® 15LV Black (EMERSON & CUMMING Inc., Woburn, MA) and CATALYST 15LV Black. This combination resulted in a rigid layer. The capacitance of both strips were measured before and after bonding them to make sure the equivalent capacitance were the same on each strip. One piezo was then elected as active sensor, used to generate the elastic acoustic waves, while the other was used as a passive sensor. The resulting specimen is shown in Figure 6.3.

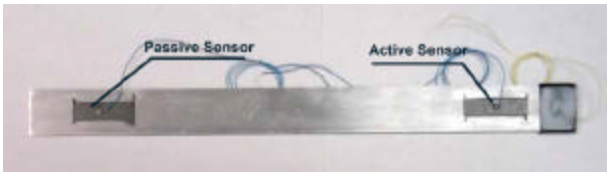

Figure 6.3. Aluminum Beam Specimen.

6.2.2. Acoustic Wave Generation and Signal Acquisition

A Data Acquisition Card from National Instruments together with a Labview® Virtual Instrument program user interface was used to generate an AC output with a profile appropriate for a given task (burst chirp or harmonic signal) which was first fed into an amplifier and then into the active piezo sensor. The signal was then picked up by the passive piezo and sent back to the data acquisition system and saved as an ASCII file for analysis to evaluate the effect of the damage on the character of transmitted acoustic waves. A schematic of the experimental setup is shown in Figure 6.4.

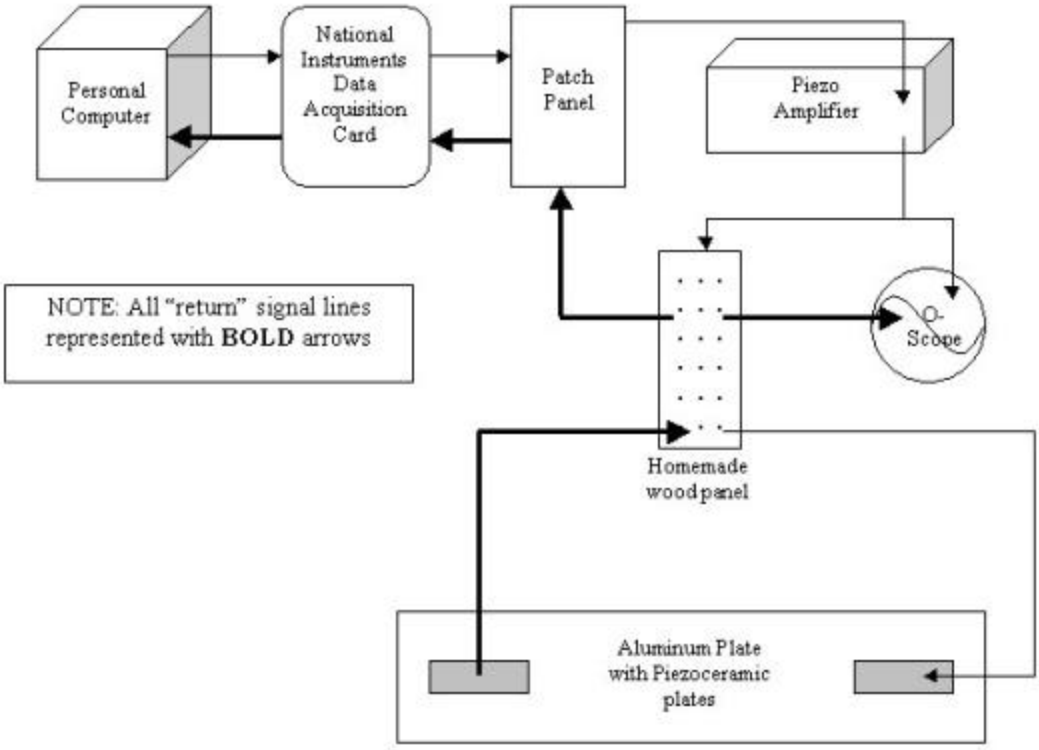

Figure 6.4. Schematic of the Experimental Setup.

6.3. Experimental Procedure

First, a no-defect database, using a plain (not damaged) aluminum beam was prepared using chirps and harmonic signals with different frequencies and amplitudes for later comparison, for the cases of controlled defects.

6.3.1. Defects

Two different defects were created on the same beam to evaluate its influence on the character of acoustic waves:

- First a partial hole 1.56mm in diameter and 50% of the beam thickness deep.
- The through hole was afterwards enlarged to a diameter of 2.4 mm.

It is important to note that the hole was made halfway between the piezoelectric sensors. Figure 6.5 shows the details of the hole.

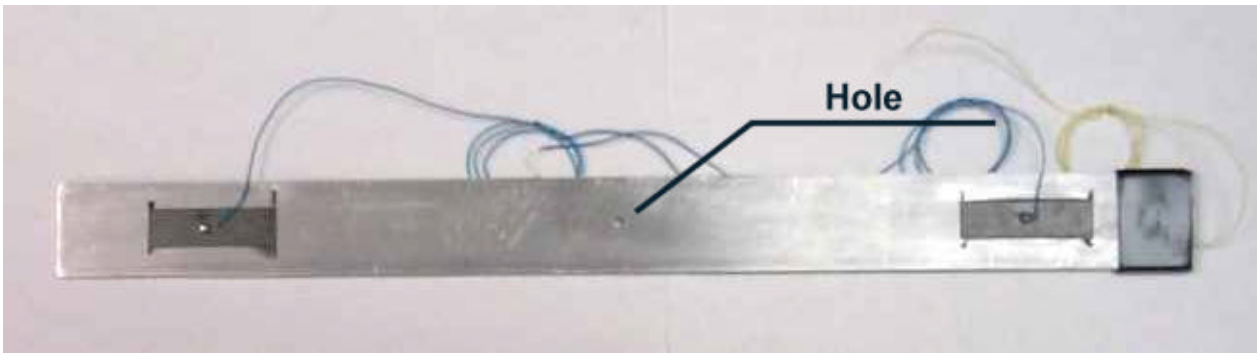

Figure 6.5. Details of the Hole Halfway between Piezoelectric Sensors.

6.3.2. Actuating Signals

Two different kinds of actuating signals were used:

- Burst chirps with different duration, frequency ranges and amplitudes.
- Single frequency sine waves with different frequencies and amplitude levels.

6.4. Summary of Intermediate Results

After generating the database with the plain beam a partial hole was drilled. Then the specimen was subjected to frequency chirps ranging from 1.1 kHz to 5.0 kHz with a duration of 10s and 10V amplitude level. The influence of this damage can be seen on the PSD plots in Figure 6.6 where one can notice a slight shift in the characteristic frequency peaks before and after the damage condition.

The hole was then enlarged to a diameter of 2.4 mm. Figure 6.7 shows similar shifts in the frequencies for the same chirp set up, but with a larger frequency shift.

This shift becomes even more significant as the chirp amplitude level is increased from 10V to 60V as shown in Figure 6.8**.** The spectral magnitude shows an increase with increased signal level.

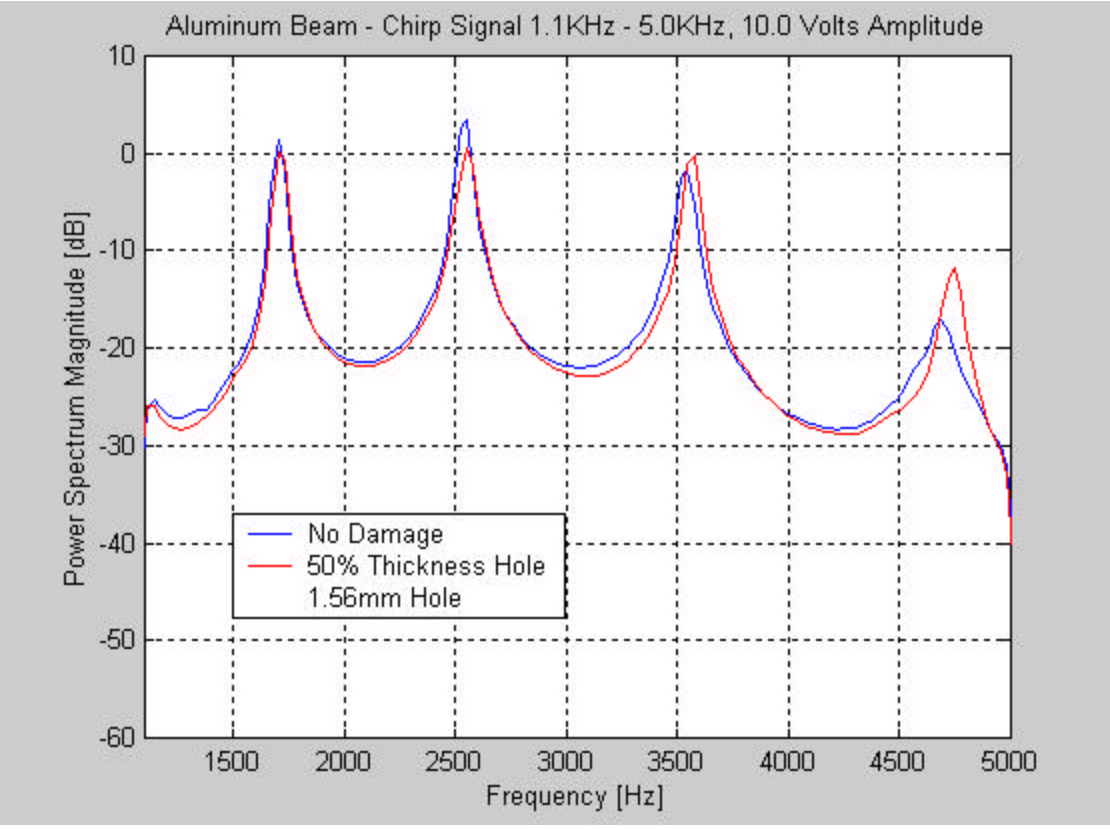

Figure 6.6. Influence of Partial Hole on the Acoustic Wave Output.

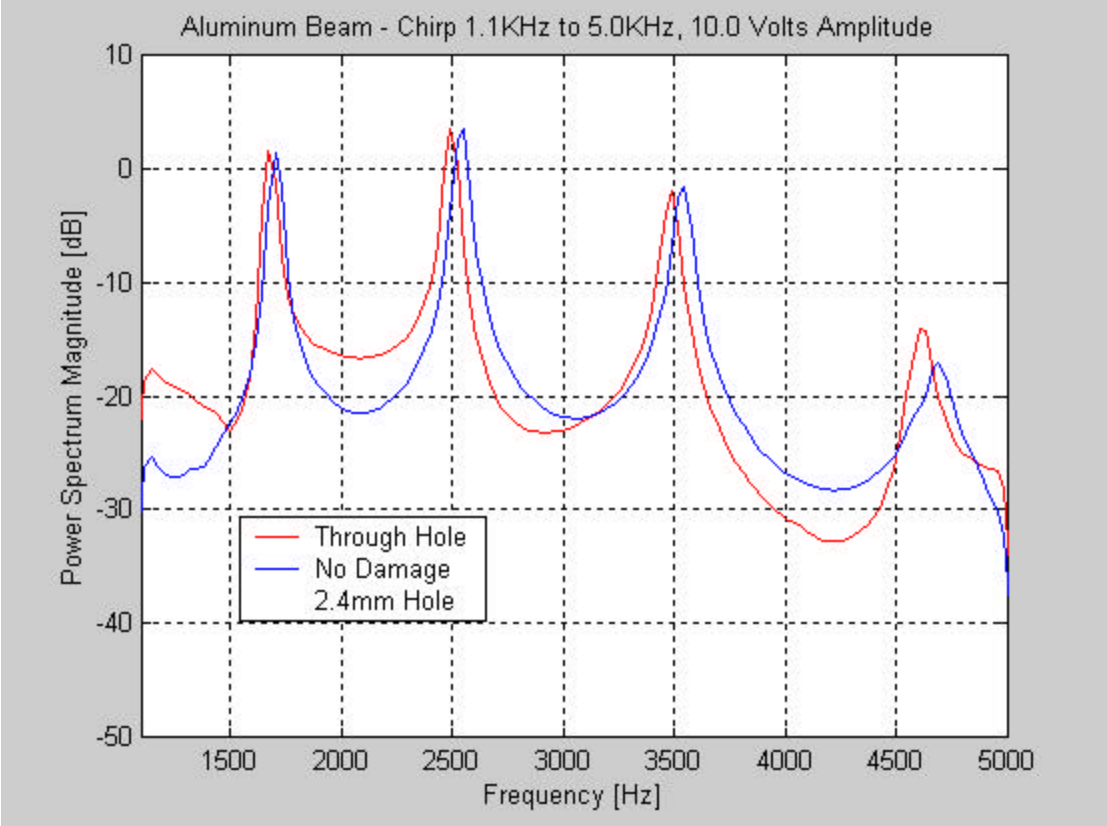

Figure 6.7. Influence of Through Hole on Acoustic Wave Output.

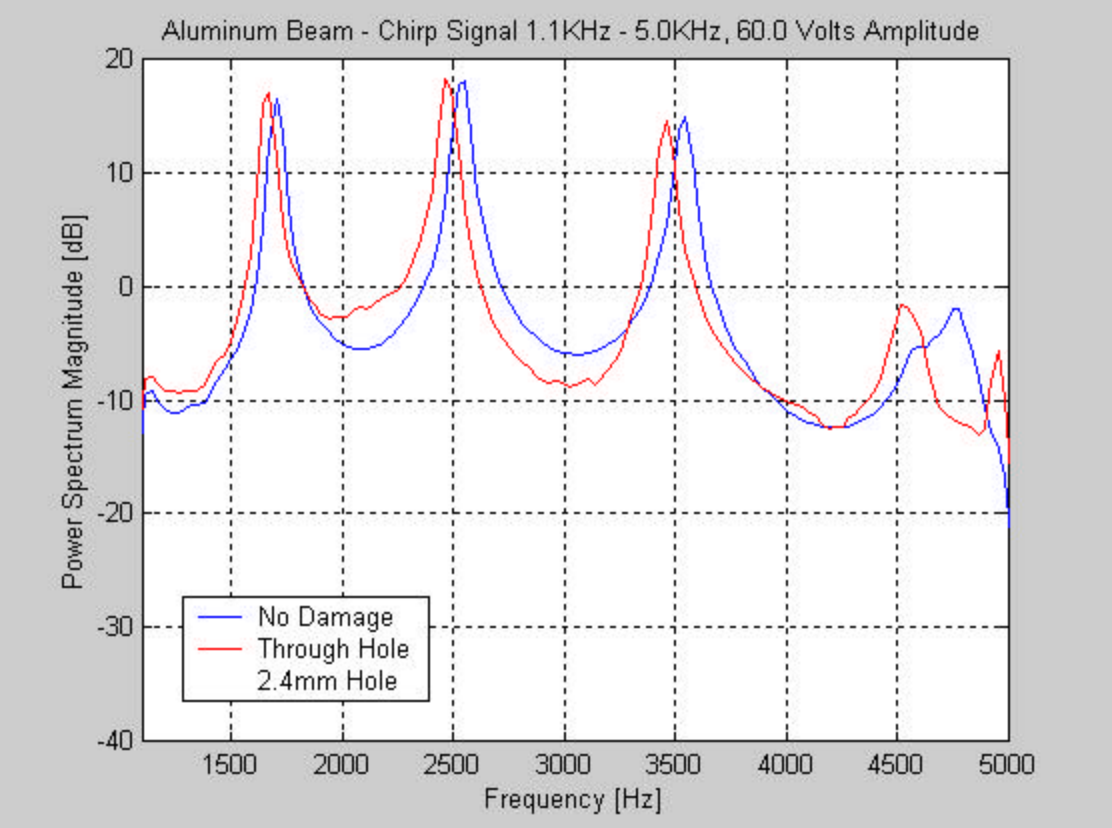

Figure 6.8. Influence of Amplitude Level on Acoustic Wave Output.

A new aluminum beam specimen was tested and in this particular one a small hole was drilled where each piezo is located so the ground wire can be soldered to the piezo negative pole and be slipped through the hole before gluing the piezo to the aluminum. This procedure eliminates the impedance-changing problem.

In this case high frequencies for input acoustic signal are tested to avoid the effect of resonance of aluminum plate and piezo-sensors. Figure 5.9 shows the PSD of the received signals under 50 kHz input sine wave. The sample for the 1st subplot has a 1.5-mm hole in the path of wave propagation, but there is no hole under piezo-sensors. The second subplot shows the signal for the aluminum beam with no flaws, but there are two small holes under the piezo-sensors attached on the sample for the purpose of creating good contact between the sensors and negative electrode. The third subplot gives the result of a plate with a partial hole (in depth) midway in wave propagation from active sensor to passive sensor. In the last subplot, the result comes from a sample beam with a through-hole (1.5-mm) in the way of wave transmission.

The power of acoustic signal received by the passive sensor changes due to the effect of wave scattering and reflection. The size of the flaw that stands in the way of wave propagation is directly related to the amplitude of PSD of the received signals. Hence, the main peaks in subplot two is the highest one, and the third subplot has a

higher main peak than subplot 1 and 4, whose sample plates get a through hole in the path of wave propagation. All the input signals have the same input amplitude, and we also assume that all these sample plates are similar enough such that the received wave depends only on the propagation path.

Another important change is also illustrated in Figure 6.9. Some extra sub peaks appear in the PSD of sample 3 and 4 compared with sample 2 where there is no flaw. This change is due to the scattering mechanism of flaw, which changes the propagation mode of incident acoustic wave from few modes to all modes. A further study of the acoustic mode change will be performed to identify the position and size of the flaw included in metal plates or tubes.

Figure 6.10 gives the results with 100 kHz incident sine signal of acoustic wave. The third subplot has two-volt amplitude sine wave signal, and the others have 1-volt amplitudes. This figure verifies the relationship between passive signal and the size of the included flaw as shown in Figure 6.9.

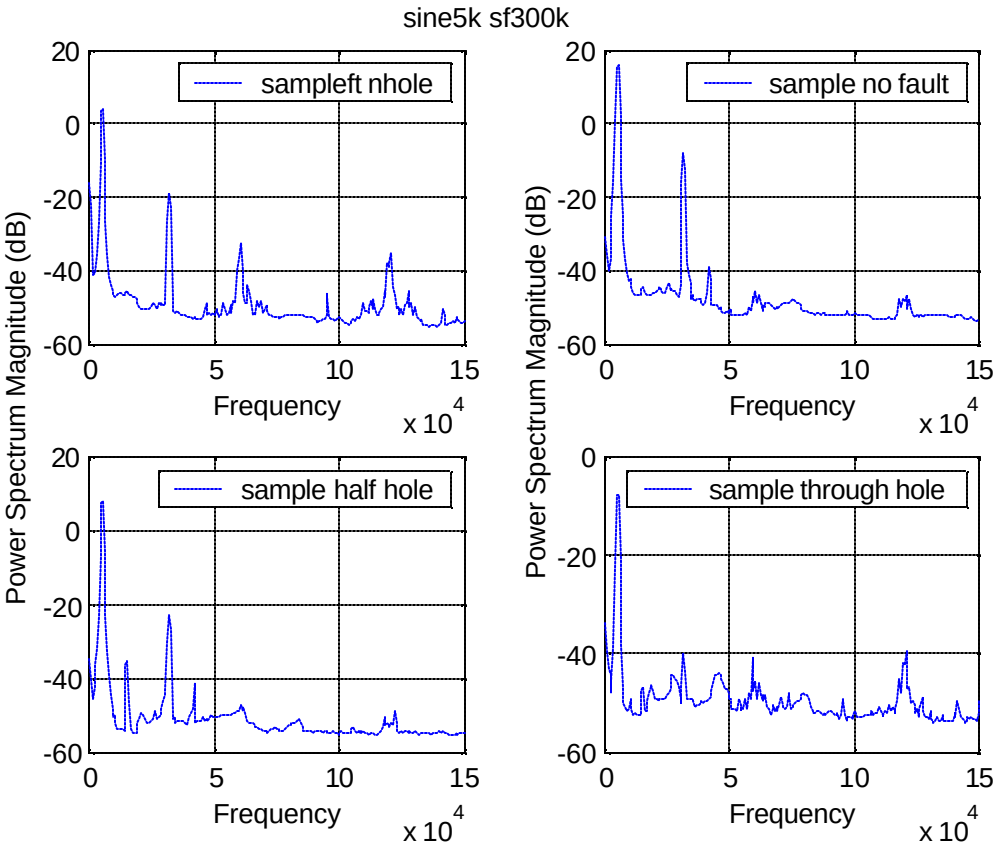

Figure 6.9. Power spectral density of receiving acoustic signal under 50 kHz input sine wave for four different aluminum plate samples.

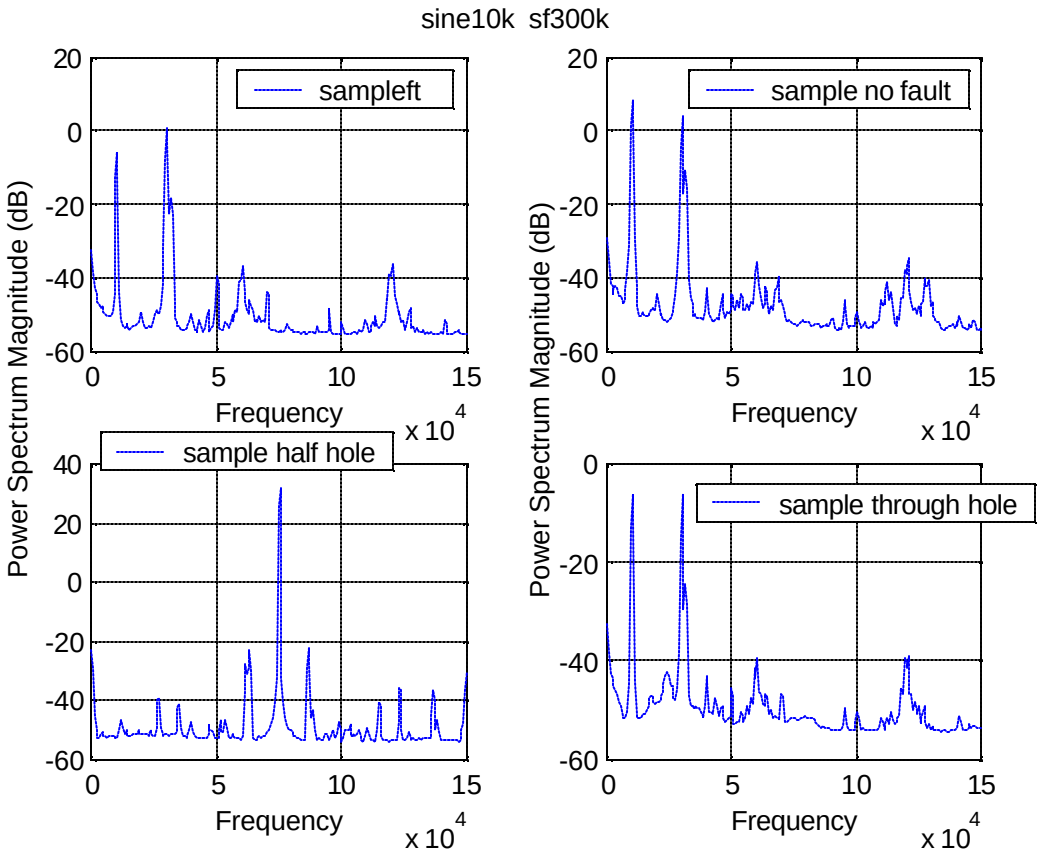

Figure 6.10. Power spectral density of receiving acoustic signal under 100 kHz input sine wave for four different aluminum plate samples.

6.5. Remarks

Results of this preliminary study indicate that acoustic waves transferred between piezoelectric sensors are affected by the presence of defects in the aluminum beam structure. Furthermore, the tests indicate that the signals have repeatable character and the piezo sensors were able to produce and receive signals with magnitudes of several volts.

The epoxy glue caused capacitance changes in some specimens (aluminum beam plus epoxy glue) that caused discrepancies in the piezo sensor behavior. New and improved experimental studies and data processing techniques are presented in Section 7 and contain test results using tubular specimens.

7. THEORY OF ELASTIC WAVE PROPAGATION AND NEW RESULTS OF DEFECT MONITORING IN FLAT PLATES AND TUBULAR SPECIMENS

7.1. Introduction

New tests have been performed on aluminum plates and brass tubes. Plate dimensions: $350 \times 25 \times 3$ (mm). The tubular specimens used for experiments are 613 mm long, 13mm diameter and 1.8mm wall thickness. Tests for plates include the half depth hole in the middle of the plate, a through hole in the middle of the plate, normal plate without flaw, and half width and full width v-notch at $1/3^{rd}$ the distance between the active and the passive sensor. For the tests performed on the tubes, the data consist of normal specimen and a tube with a through hole.

Figures 7.1 and 7.2 show the test set up for the aluminum plate and the brass tube, respectively.

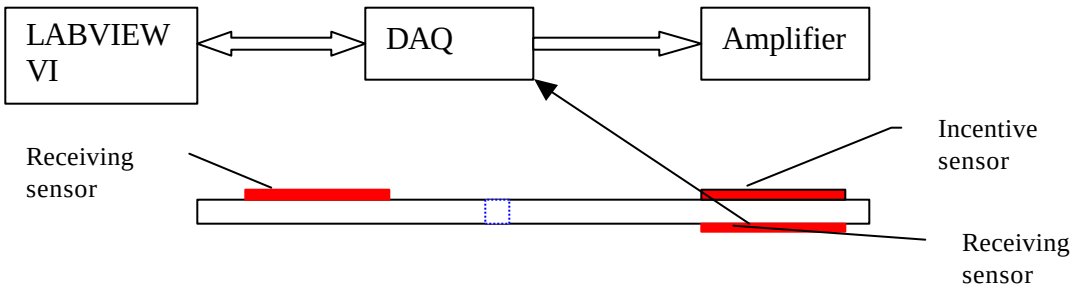

Figure 7.1.Experimental set up for tests on the aluminum plate.

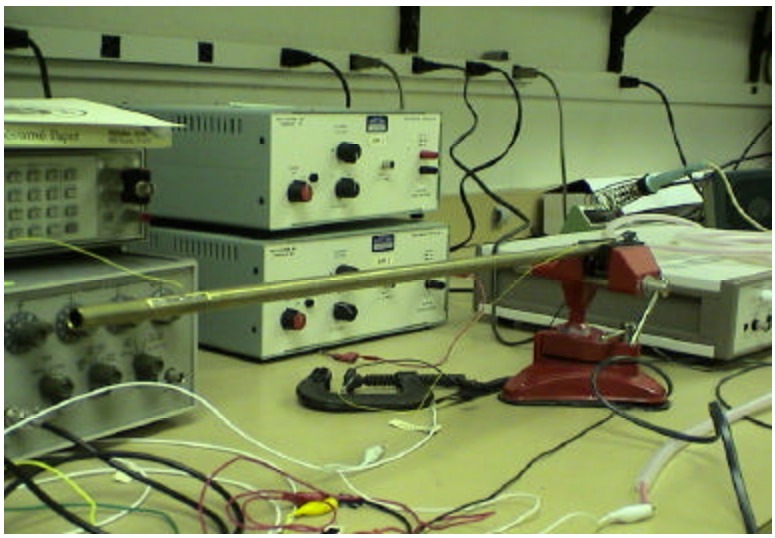

Figure 7.2. Experimental set up for tests on the brass tube.

7.2. Theory of Elastic Wave Propagation

7.2.1. Elastic Waves Along Thin Plates

Considering wave propagation along a thin plate, Lamb wave is a special type of surface wave, for which the displacements occur in the direction of both propagation and its normal direction with free boundaries. The stress components on the boundaries must be zero. The particle displacement equation is written as

$$\begin{aligned} &\bar{v} = \nabla f + \nabla \times (j) \\ &f : scalar\ \ potential\ of\ \ longitudal\ \ wave \\ &j\ : vector\ \ potential\ of\ \ transverse\ wave \end{aligned} \tag{7.1}$$

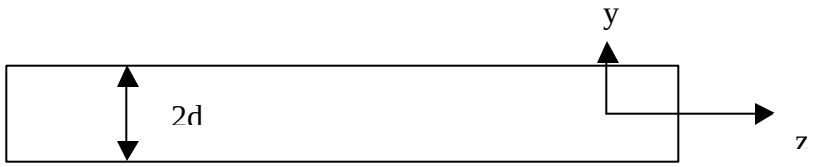

By assuming that the potentials along x-axis are zero, we can write the wave equations as follows:

$$\begin{aligned} &\frac{\partial^2 f}{\partial z^2} + \frac{\partial^2 f}{\partial y^2} + k_l^2 f = 0 \\ &\frac{\partial^2 j}{\partial z^2} + \frac{\partial^2 j}{\partial y^2} + k_t^2 j = 0 \end{aligned} \tag{7.2}$$

The solution takes the following form:

$$\begin{aligned} f &= A * ch(y\sqrt{k^2 - k_l^2})e^{i(kz-wt)} + B * sh(y\sqrt{k^2 - k_l^2})e^{i(kz-wt)} \\ j &= C * sh(y\sqrt{k^2 - k_t^2})e^{i(kz-wt)} + D * ch(y\sqrt{k^2 - k_t^2})e^{i(kz-wt)} \end{aligned} \tag{7.3}$$

Using the condition that stresses at the free boundaries must be zero, we are able to write two characteristic equations to determine the wave number k.

$$\begin{aligned} &(k^2 + s^2)^2 ch(d\sqrt{k^2 - k_l^2})sh(d\sqrt{k^2 - k_t^2}) - 4k^2\sqrt{k^2 - k_l^2}\sqrt{k^2 - k_t^2}\, sh(d\sqrt{k^2 - k_l^2})ch(d\sqrt{k^2 - k_t^2}) = 0 \\ &(k^2 + s^2)^2 sh(d\sqrt{k^2 - k_l^2})ch(d\sqrt{k^2 - k_t^2}) - 4k^2\sqrt{k^2 - k_l^2}\sqrt{k^2 - k_t^2}\, ch(d\sqrt{k^2 - k_l^2})sh(d\sqrt{k^2 - k_t^2}) = 0 \end{aligned} \tag{7.4}$$

These yield solutions of wave number k_s and k_a (symmetric and antisymmetric).

Finally, the potentials related to the Lamb waves are given by

$$f = A * ch(y\sqrt{k_s^{\,2} - k_l^2})e^{i(k_s z - wt)} + B * sh(y\sqrt{k_a^{\,2} - k_l^2})e^{i(k_a z - wt)}$$
$$j = C * sh(y\sqrt{k_s^{\,2} - k_t^2})e^{i(k_s z - wt)} + D * ch(y\sqrt{k_a^{\,2} - k_t^2})e^{i(k_a z - wt)} \qquad (7.5)$$

The constants C and D can be expressed using A and B, therefore two arbitrary constants A and B exist for the Lamb wave equation.

Since there are two types of wave modes for Lamb waves, symmetric and antisymmetric, it is very important to know how many different modes are there for a specific frequency. According to the acoustic analysis theory, there are at least two modes, 0-symmetric and 0-antisymmetric modes, for low frequencies. As the frequency increases, more symmetric and antisymmetric modes appear, the frequency at which a new mode appears is called the critical frequency and is given by the following relations.

$2d = \frac{l_l}{2}, \frac{3l_l}{2}, \frac{5l_l}{2} \cdots$ for symmetrical modes and $2d = l_l, 2l_l, 3l_l \cdots$ for $2d = l_t, 2l_t, 3l_t \cdots$ $2d = \frac{l_t}{2}, \frac{3l_t}{2}, \frac{5l_t}{2} \cdots$ antisymmetrical modes (? is wavelength).

Similarly, the more complicated Lamb wave properties in metal tubes have been derived. In summary, it is found that Lamb waves propagate in multiple modes. Hence the signals received by a transducer are affected by sensor position, wave frequency, and plate thickness. An important property related to the defect inspection is that a single input mode signal will be scattered forward and backward as a multimode wave. This flaw can be viewed as a new wave source that is emitting waves around. Its existence will definitely alter the signal spectrum, whose changes are useful for the nondestructive examination technique.

7.2.2 Elastic Waves in Metal Tubes

For a hollow cylinder, the circumferential wave equations in terms of the potentials ϕ and ψ are:

$$\left(\frac{\partial^2}{\partial r^2} + \frac{1}{r}\frac{\partial}{\partial r} + \frac{1}{r^2}\frac{\partial^2}{\partial q^2}\right)f + \frac{w^2}{c_L^2}f = 0$$
$$\left(\frac{\partial^2}{\partial r^2} + \frac{1}{r}\frac{\partial}{\partial r} + \frac{1}{r^2}\frac{\partial^2}{\partial q^2}\right)y + \frac{w^2}{c_T^2}y = 0 \qquad (7.6)$$

Where c_L and c_T are longitudinal and shear wave velocities, respectively. Using the boundary conditions, the general solution is given by

$$f(r) = A_1 J_{kb}(\frac{wr}{c_L}) + A_2 Y_{kb}(\frac{wr}{c_L})$$
$$f(r) = A_3 J_{kb}(\frac{wr}{c_T}) + A_4 Y_{kb}(\frac{wr}{c_T}) \quad (7.7)$$

Where $J_{kb}(z)$ and $Y_{kb}(z)$ are the first and second kinds of Bessel functions, respectively. A_1, A_2, A_3, and A_4 are constants.

The particle displacements can be represented using the potential functions as:

$$u_r = \frac{\partial f}{\partial r} + \frac{1}{r}\frac{\partial y}{\partial q}$$
$$u_q = \frac{1}{r}\frac{\partial f}{\partial r} - \frac{\partial y}{\partial r} \quad (7.8)$$

The solution of Lamb wave potential equations gives a complicated dispersion equation in the circumferential and the axial directions.

For the longitudinal wave propagation, three types of wave modes are studied, namely, longitudinal modes, torsional modes, and flexural modes. The particle displacements are assumed to have the following forms.

$$u_r = U(r)\cos(nq)e^{i(kz-wt)}$$
$$u_q = V(r)\cos(nq)e^{i(kz-wt)} \quad (7.9)$$
$$u_z = W(r)\cos(nq)e^{i(kz-wt)}$$

Where U, V, W are the displacement amplitudes composed of Bessel functions. Among them the longitude mode displacement equations are analyzed below.

$$(\frac{\partial^2}{\partial r^2} + \frac{1}{r}\frac{\partial}{\partial r} + \frac{\partial^2}{\partial z^2})f - \frac{1}{c_l^2}\frac{\partial^2 f}{\partial t^2} = 0$$
$$(\frac{\partial^2}{\partial r^2} + \frac{1}{r}\frac{\partial}{\partial r} + \frac{\partial^2}{\partial z^2})y - \frac{1}{c_t^2}\frac{\partial^2 y}{\partial t^2} = 0 \quad (7.10)$$

The analytical solutions for longitudinal mode potential equations have the following forms.

$$
\begin{aligned}
f &= \Phi(r)e^{i(wt-kz)} = (A_1 J_0(k_l r) + A_2 Y_0(k_l r))e^{i(wt-kz)} \\
y &= \Psi(r)e^{i(wt-kz)} = (A_3 J_1(k_t r) + A_4 Y_1(k_t r))e^{i(wt-kz)} \\
f &: scalar\ \ potential\ of\ \ longitudal\ \ wave \\
y &: vector\ \ potential\ of\ \ transverse\ wave \\
k_t^{\,2} &= \left(\frac{w}{c_t^2}\right) - k^2, k_l^{\,2} = \left(\frac{w}{c_l^2}\right) - k^2
\end{aligned}
\qquad (7.11)
$$

Where J and Y refer to the first and the second type of Bessel functions, respectively.

7.3. Short-Time Fourier Transform (STFT) and Wavelet Transform

Since the signal used for wave generation and the resulting received signals at other locations in the specimen are non-stationary, it is more effective to use time-frequency analysis. The excitation waveforms are either chirp signals or pulse signals. Two of the time-frequency techniques are the short-time Fourier transform and the wavelet transform. STFT uses fixed-window transform, whereas the wavelet analysis is more general in compressing a time signal. The multi-resolution property of the discrete wavelet transform (DWT) is found to be desirable in quantitative analysis for surface or sub-surface flaws in structures. The DWT decomposes the signal into various sub-band frequencies.

The properties of Lamb wave like propagation, such as speed and wave number in a guided structure, are decided by specimen dimensions, material densities, input wave frequency, etc. One of the objectives of the experimental study is to establish an optimal frequency band of the excitation frequency.

7.3.1. Short-Time Fourier Transform (STFT)

The STFT of a signal is defined as

$$
F_{STFT}\left(f(t,w)\right) = \frac{1}{\sqrt{2p}} \int f(t)h(t-t)e^{-jwt}\,dt \qquad (7.12)
$$

where f(t) is a time signal, and h(t) is the window function. One issue related to the STFT is the selection of the window width. Within the constraints of the uncertainty principle, STFT is not able to provide instantaneous frequency information. Optimal window size has been explored in many papers.

7.3.2. Wavelet Transform

The continuous wavelet transform (CWT) has the property of providing both frequency and time resolution by continuously varying the window size. The window function is defined by a mother wavelet, which is characterized by time and scale (inverse frequency). A significant difference between CWT and STFT is that the CWT

deals with a portion of signal using a shifted and scaled mother wavelet. Therefore, the CWT usually has better resolution than STFT, and reveals the information in the joint time and frequency plane.

One problem connected with CWT is the complexity of coefficient calculations. This problem is especially critical for online data processing. In addition, the display of CWT results has high requirements of computer memory and CPU speed, even for a two-dimensional case. The discrete wavelet transform (DWT) solves this problem by decreasing the data size in the order of two at each level compared with the higher level, without losing good resolution. The DWT filter theory is discussed in detail by Strang and Nguyen. In short, the DWT filter can be summarized as follows: the low frequency information needs less sampling data per unit time compared with the high frequency data, and the high frequency component is filtered out at each level. The sub-band signals may then be processed using the standard FFT to provide spectral information as patterns.

7.4. New Data Acquisition

The guided acoustic wave propagation along metal plates or tubes is a complex physical process. The boundary conditions and material structure play an important role in the transfer of energy along wave guide. The dimensions of the sample specimens, structural natural frequencies, and the properties of the excitation waveform frequency, influence the properties of the signals received at different locations in the specimens. Therefore, the experiments were designed to consider several issues.

1. Input signal selection. Usually, pulse signals such as sine pulse with several cycles is used in ultrasonic NDE. The pulse signal generation needs special equipment. The test pulse signals generated and received by piezoelectric transducers in our experiments have not revealed much useful information due to the frequency limit of piezoelectric transducers and the dimension of experimental samples. But the natural frequency information can be extracted from impulse response. Hence chirp signal instead of pulse wave is applied in this study due to the needs of optimal band selection. The chirp signal has constant amplitude and its frequency changes (increases) as a function of time.

$$Chirp(t) = A\sin(bf_0 t^2) \qquad (7.13)$$

Where f_0 is the initial frequency of the signal.

2. Optimal frequency band selection.
We have found in the experiments that a resonance band exists for the metal plates or tubes in the frequency band 0 – 50 kHz. The formation of resonance region will be discussed separately. The optimal frequency band of input signal for aluminum beam, with dimensions of 350mm × 25mm × 3mm, is 26 kHz to 37 kHz. For the brass tube used in our experiments, the important input signal band

is 16 kHz to 40 kHz. Figure 7.3 shows the received signal collected for an aluminum plate (#1) and for a brass tube (#2) with chirp signal input.

3. Exploration of the formation of resonance band.
The formation of resonance band is due to the modulation of input acoustic signals and reflected waves from the free boundary. The input signal is chirp and its frequency is changing linearly with time: f = bt. Therefore, the input and reflected waves at position 1 have a small frequency difference $\Delta f = a * \frac{2l}{V}$. Where, l is the distance from the transducer to the boundary and V is the Lamb wave velocity. If the input wave can be written as $s_{in} = \cos(wt - kx)$, then the reflected wave is $s_{ref} = \cos((w + \Delta w)t - (k + \Delta k)x)$, therefore the wave data collected by the passive transducer is:

$$s = s_{in} + s_{ref} = 2\cos(\frac{1}{2}(\Delta wt - \Delta kx) * \cos(wt - kx) = 2\cos(\frac{1}{2}\Delta w(t - \frac{2l}{V})) * \cos(wt - kx)$$

. The combinational effect of natural frequency, the Lamb wave leakage and the modulation decides the resonance band for the metal plates and tubes. Here we assume that the low frequency acoustic wave is more easily transmitted into the air or other fluid around the test samples, thus we get low reflected coefficient and high leakage rate for low frequency elastic waves compared to high-frequency components. The multiple peaks in the spectrum come from the natural frequencies of test specimens.

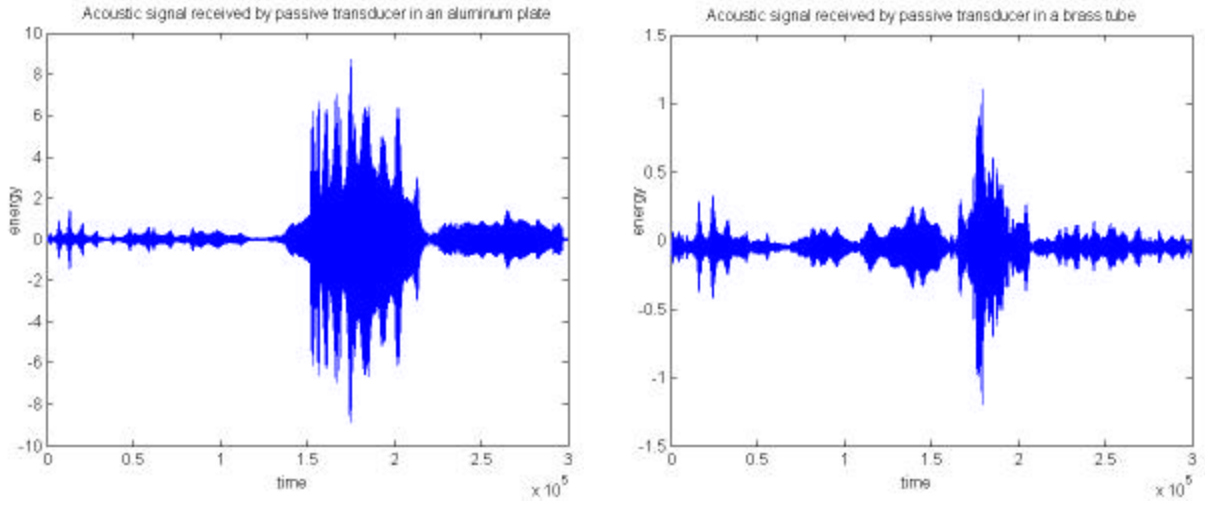

Figure 7.3. Typical acoustic signals from an aluminum plate and a brass tube.

7.5. Analysis of Lamb Wave Properties

7.5.1 Properties of Lamb waves

The Lamb wave is more complicated compared with the surface wave or acoustic wave in the air because of the multi-propagation mode. There are more than two types of particle distributions along the transverse cross section of the guided structure. Dispersion of phase velocity may happen due to the change of signal frequency or sample thickness. It is desirable to study the properties of Lamb waves both in metal plates and tubing structures. Many studies about the dispersion curves of lamb waves are available. As an example, the dispersion curve for an aluminum plate is illustrated in Figure 7.4. The x-axis represents the product of signal frequency and the thickness of aluminum plate. Since our input chirp signal has the range from 1 kHz up to 50 kHz and the experimental plat has a thickness of 3 mm, the corresponding x-axis coordinate should be from 0.003 to 0.15 (MHz-mm).

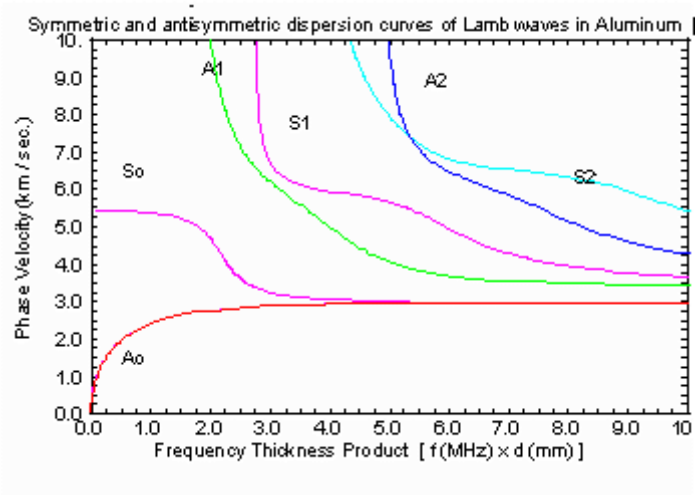

Figure 7.4. Lamb wave dispersion curves for the aluminum plate.

7.5.2. Experimental Lamb wave property analysis using cross-spectrum

We are able to perform property analysis using the cross-spectrum technique due to the arrangement of multi-sensor on each aluminum beam. It is noticed that the coherence between these two receiving signals are really high between 10 kHz and 20 kHz, the phase velocity related with the gradient can be estimated as 0.18m/(1/5000Hz)= 0.9 km/s (see Figure 7.5). We also notice that the gradient of the phase curve is decreasing from 1 kHz to 30 kHz, therefore the phase speed of Lamb wave is increasing with frequency. Therefore, we can relate our experimental results with anti-symmetric mode of theoretical curves in Figure 7.4. The effect of the defect on the aluminum sample on coherence and phase is obvious as shown Figure 7.6.

7.5.3. Lamb wave properties in brass tubes

Cross spectrum and coherence are calculated for the input and output Lamb wave signals in brass tube experiments. High coherence is found between 8 kHz and 17kHz. The wave propagation speed along the brass tube can be estimated using the gradient of phase plot shown in Figures 7.7 and 7.8 as 0.315m/(1/2500Hz)= 787.5m/s (approximately). Obvious changes are generated due to the existence of the through hole, in both the phase and the coherence.

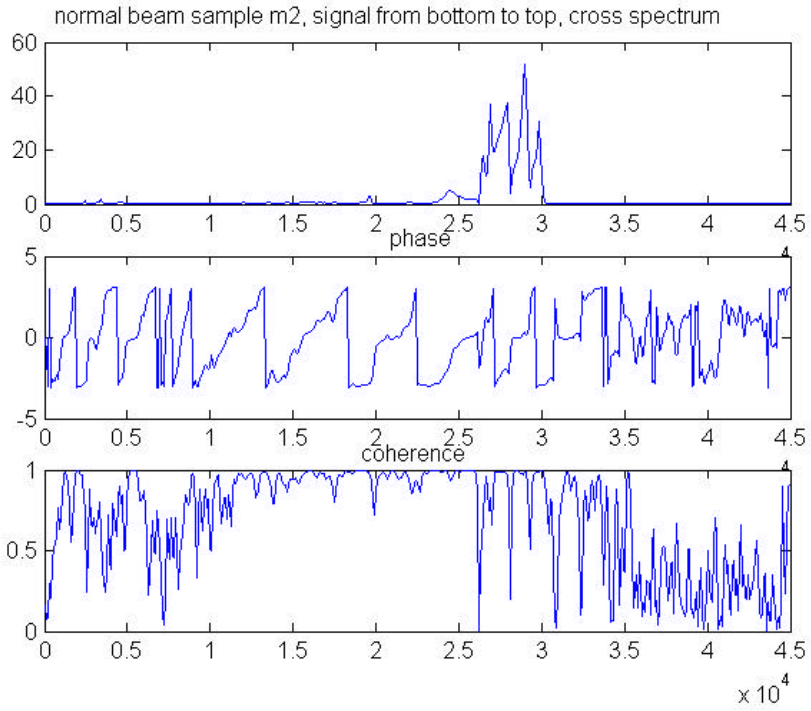

Figure 7.5. Cross spectrum analysis for elastic signals from the aluminum plate sample 2 without defect.

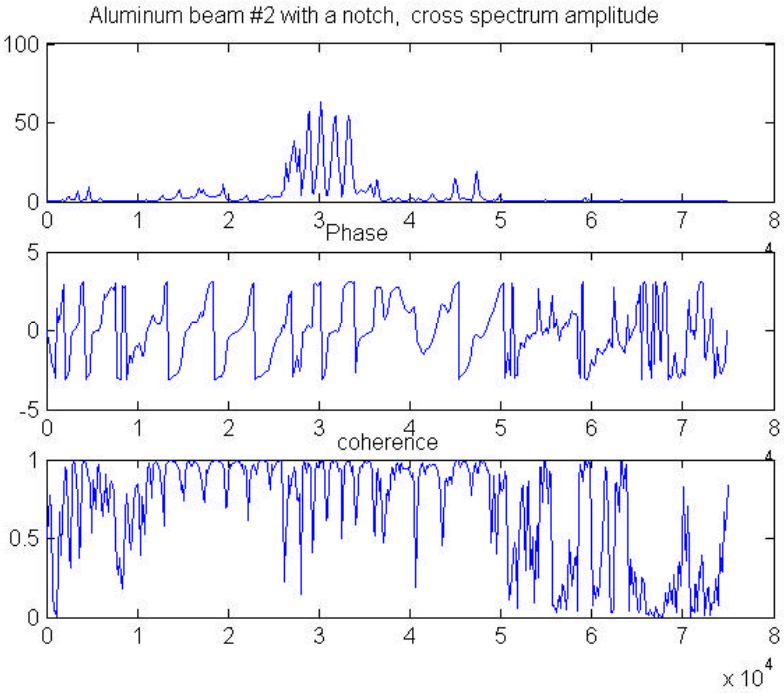

Figure 7.6. Cross spectrum analysis for elastic signals from the aluminum plate sample 2 with a notch-type defect.

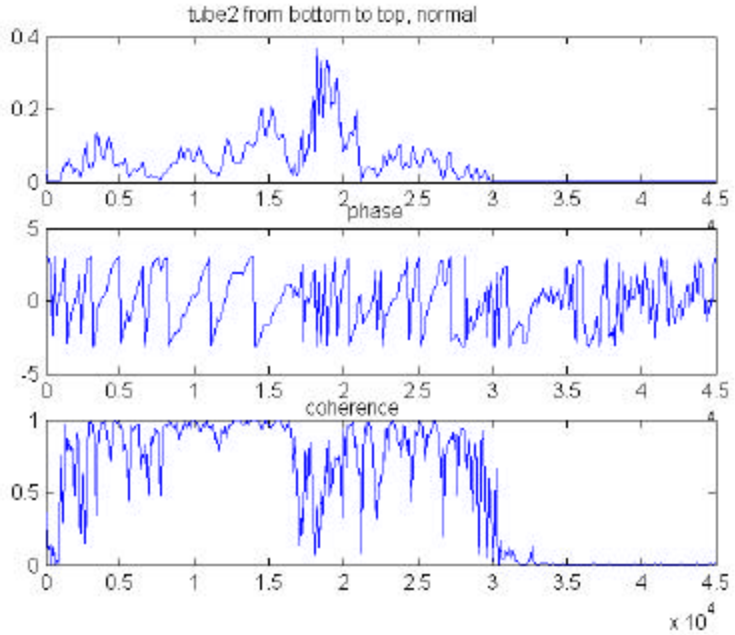

Figure 7.7. Cross spectrum analysis for elastic signals from the brass tube 2 without defect.

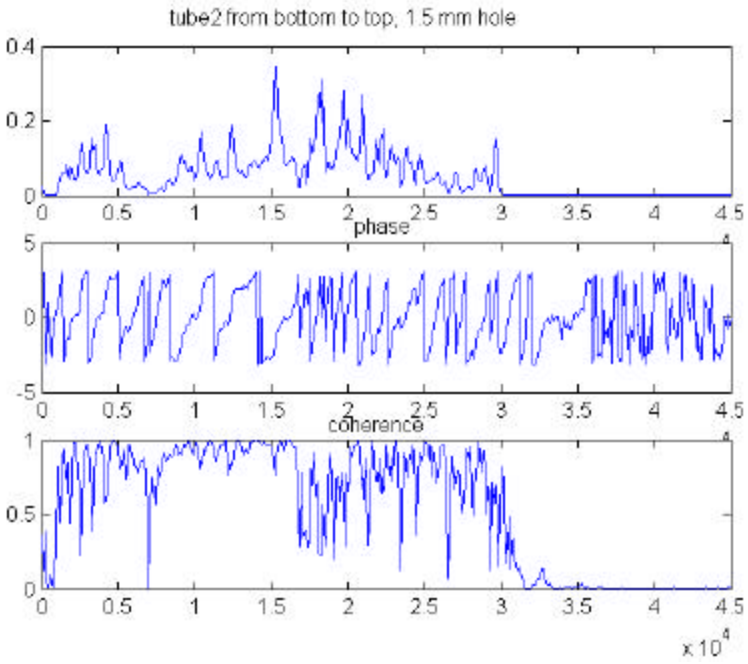

Figure 7.8. Cross spectrum analysis of elastic signals from the brass tube 2 with a 1.5mm through hole.

7.6 Acoustic Signal Analysis for Flaw Detection

7.6.1. Aluminum plate experimental results and analysis

Three aluminum plates with multiple sensors attached near two terminals are tested. The input signals are in the range 1-5 kHz or 1-30 kHz. Elastic wave signals are collected using the piezoelectric transducers before and after a half width v-notch is added onto the beam plate sample #1. Signals are collected for sample 2 before and after a v-notch is added as well. The third sample consists of an irregular notch produced using a punch. Acoustic signals were analyzed though traditional FFT and short time Fourier analysis. It is found that STFT provides better resolutions than the FFT in determining the signal characteristic changes in time and frequency domains due to the existence of different flaws.

A detailed comparison of the signatures of received acoustic signals for aluminum plates #1 and #2 are demonstrated in the Table 7.1.

Table 7.1. Acoustic signal features from the aluminum plates

Features	Aluminum plate #1		Aluminum plate #2	
	Half-width notch	Normal	With Notch	Normal
Energy	4.75×10^5	3.76×10^5	8.43×10^5	7.72×10^5
Time projection Mean	2.58	2.62	2.61	2.62
Frequency projection Mean	2.38×10^4	2.46×10^4	2.42×10^4	2.45×10^4
Time position of Maximum	3.03	3.055	3.025	3.195
Frequency position of Maximum	27540	27720	27540	28980
Time projection variance	0.769	0.746	0.712	0.733
Frequency projection variance	7.28×10^7	6.42×10^7	6.99×10^7	6.66×10^7

The projected spectrum means STFT spectrums are projected onto time domain and frequency domain, respectively. We find that mean value of time weighted by the energy $t_m = \frac{\sum_i t_i e_i}{\sum_i e_i}$ decreases due to the existence of defect on the surface of aluminum plates, for both the half width notch on sample 1 or the transverse notch on sample 2. The ratio of decrease is 1.63% and 0.52%, respectively. The mean value of frequency weighted by the energy $f_m = \frac{\sum_i f_i e_i}{\sum_i e_i}$ also decreases due to the existence of defect on the surface of aluminum plate. The ratio of decrease is 2.91% and 1.24%, respectively.

The time variance of projected spectrum onto time domain is defined as $t_v^2 = \frac{\sum_i t_i^2 e_i}{\sum_i e_i}$, and the frequency variance of projected spectrum onto frequency domain is defined as $f_v^2 = \frac{\sum_i f_i^2 e_i}{\sum_i e_i}$. We find that the variance of frequency weighted by the energy increases due to the existence of defect on the surface of both aluminum plates. The ratio of increase is 13.27% and 4.93%, respectively.

The projections of STFT spectrogram of elastic signals onto time domain are illustrated in Figures 7.9 – 7.12, where we can observe both the peak shift and amplitude change of the spectra.

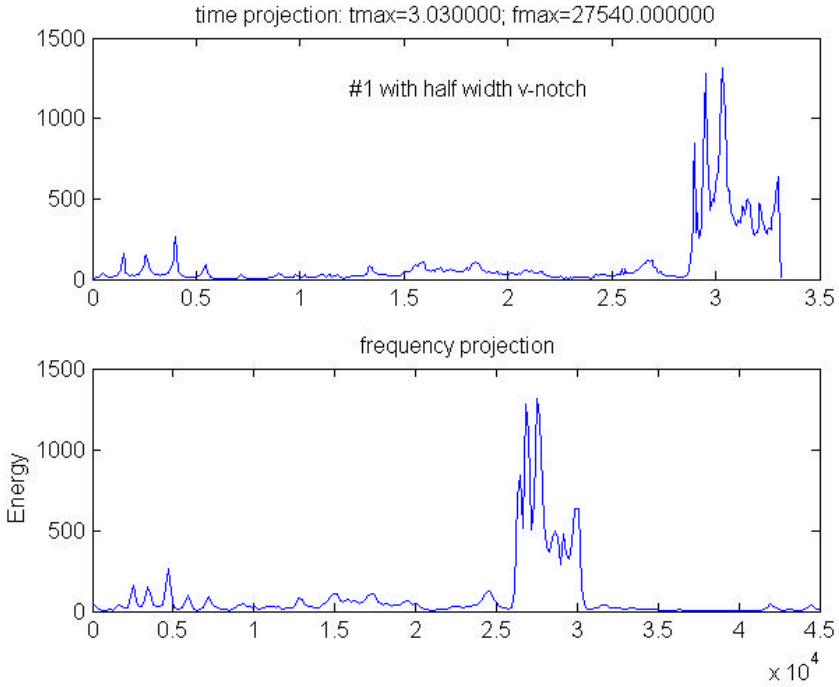

Figure 7.9. Elastic wave received by piezoelectric transducer from aluminum plate sample #1, with a half-width notch (time and frequency projections).

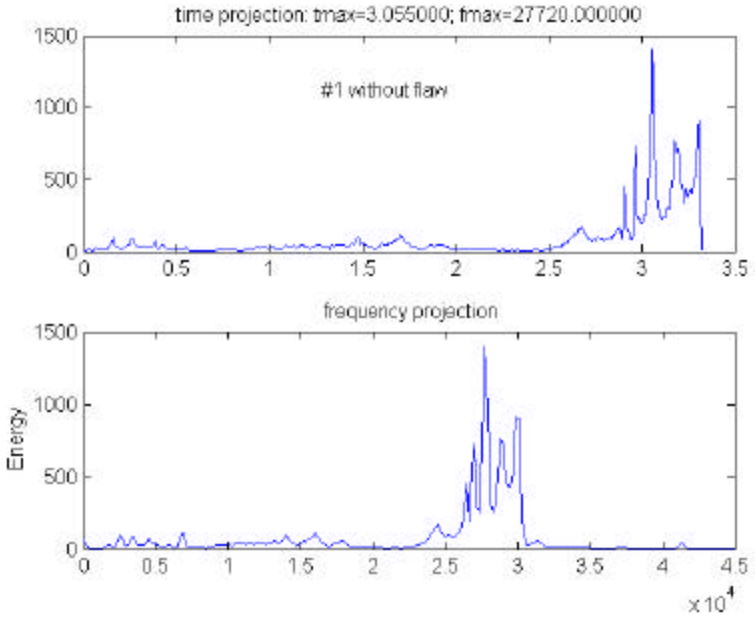

Figure 7.10. Elastic wave received by piezoelectric transducer from aluminum plate sample #1 without flaw (time and frequency projections).

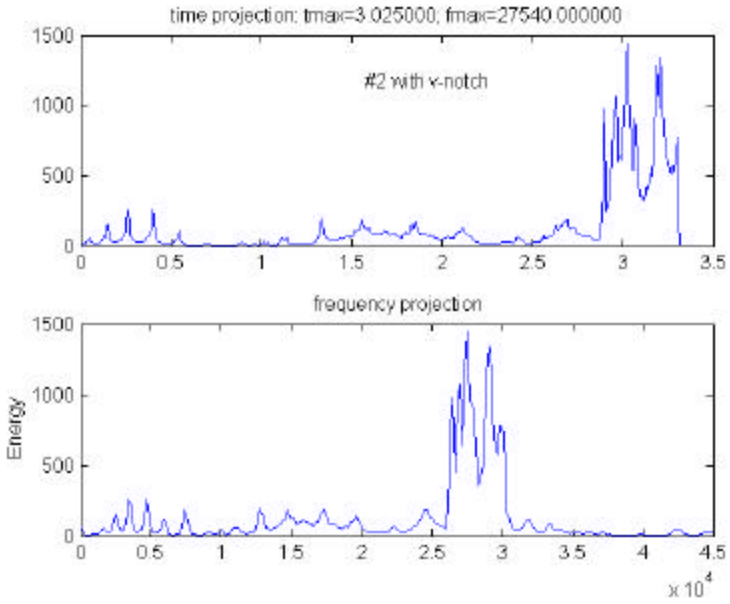

Figure 7.11. Elastic wave received by piezoelectric transducer from aluminum plate sample #2, with a v-notch (time and frequency projections).

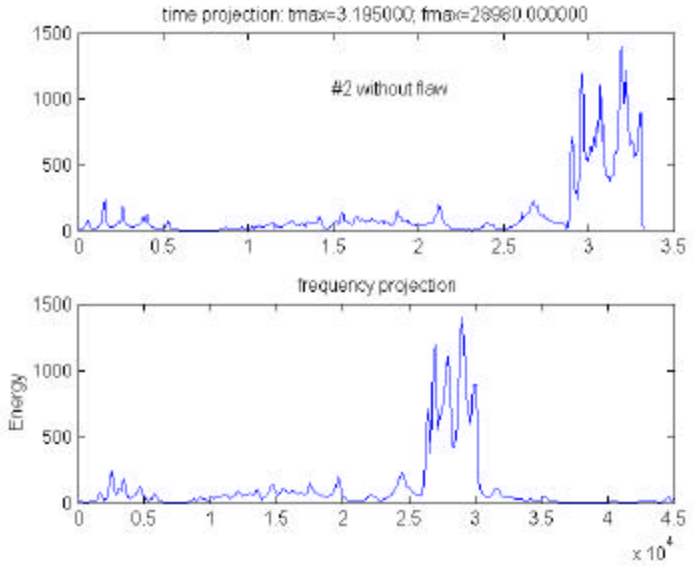

Figure 7.12. Elastic wave received by piezoelectric transducer from aluminum plate sample #2, without flaw (time and frequency projections).

7.6.2. Experiments on brass tube specimens

Signals from brass tubes were acquired before and after a defect. Their FFTs are shown in Figure 7.13, where the energy (sum square of signal) for the normal case is 4860 compared with 4000 for the flaw case. Variance with respect to frequency is $3.7x10^7$ for normal case compared with $4.43x10^7$ for the flaw condition. The mean frequency is 16198 Hz for normal condition compared with 16174 Hz for the flaw condition. The CWT plot for the same signal is shown in Figure 7.14, where a more obvious peak change can be found. The only problem with CWT is the heavy computational load due to the large data size in our experiments. By contrast, STFT and DWT can be performed quickly without much delay, which is very important for online monitoring purposes.

Table 7.2 gives the results from the STFT analysis of signals from the brass tube. We can find obvious changes in the energy, projection mean, and projection variance. Table 7.3 illustrates the change of energy in each DWT decomposition level. We can find a significant decrease of the energy in detail signal of level four, and some variations of energy in other DWT levels.

The frequency decompositions using DWT are illustrated in Figures 7.15 – 7.20. These indicate that the energy is concentrated more in level 4. The flaw in the way of acoustic wave propagation causes the increase of energy in low levels and the decrease of energy in level four. The amplitude and frequency distribution provides some potential features in defect monitoring. Figures 7.21 and 7.22 are the plots of time and frequency projections of the STFT spectra for the brass tube with and without defect, respectively. These show the shift in the peak energy value towards low frequencies and an overall broadening of the spectral frequencies for the case of with a defect in the brass tube.

Table 7.2. Acoustic signal features for brass tubes

Features	Brass tube #2		Brass tube #1	
	Normal	With 1.5mm hole	Normal	
Energy	0.0486×10^{5}	0.0400×10^{5}	0.0693×10^{5}	
Time projection Mean	1.7121	1.7054	1.8487	
Frequency projection Mean	1.6650×10^{4}	1.6731×10^{4}	1.8070×10^{4}	
Time position of Maximum	1.99	1.96	1.945	
Frequency position of Maximum	18360	18180	18000	
Time projection variance	0.7324	0.7450	0.5785	
Frequency projection variance	6.5211×10^{7}	7.2900×10^{7}	5.9863×10^{7}	

Table 7.3. Acoustic signal features for brass tubes

Energy	Brass tube #2		Brass tube #1	
	With 2mm hole	Normal	Normal	
Level 1, approximation	343.878773	721.192418	24.880754	
Level 1, details	124.664969	66.078126	108.845406	
Level 2, details	262.996571	204.816084	170.634731	
Level 3, details	202.342457	144.041699	157.340776	
Level 4, details	2558.641194	3373.427379	5462.706192	
Level 5, details	507.742552	354.440824	1008.673444	

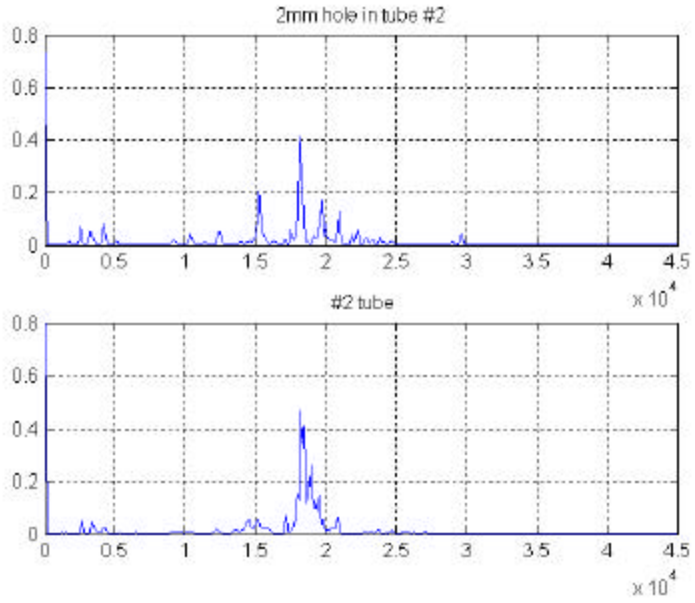

Figure 7.13. FFT plot of the acoustic signal before and after flaw.

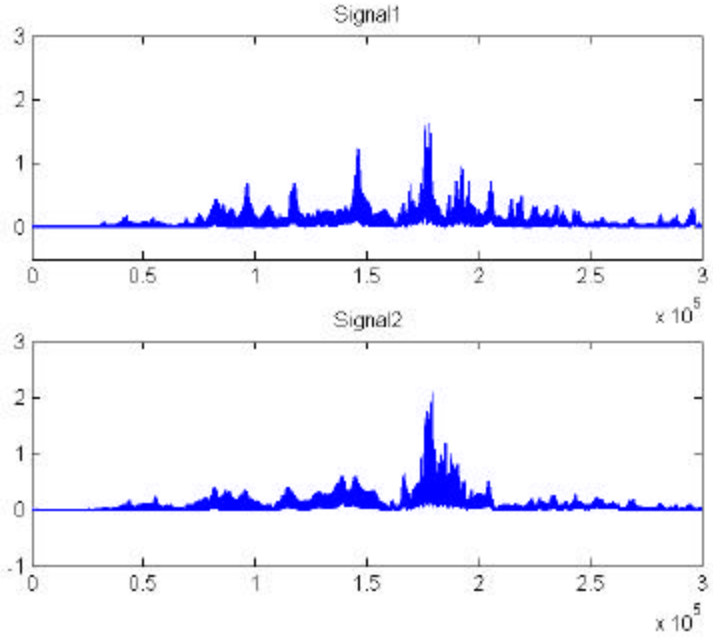

Figure 7.14. The projection of CWT on to time domain.

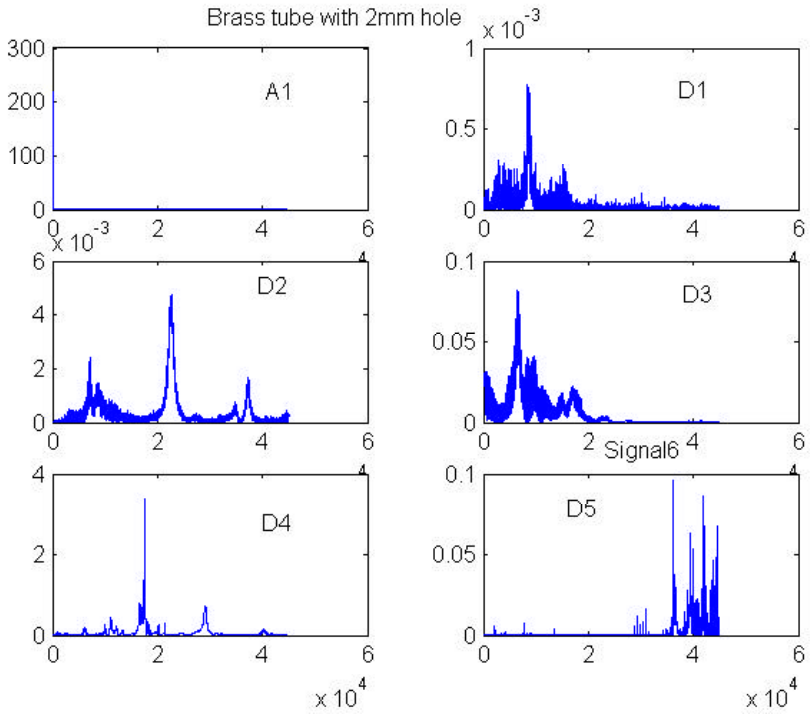

Figure 7.15. DWT decomposition of elastic wave received by the passive transducer from the brass tube sample #2, with a 2mm hole.

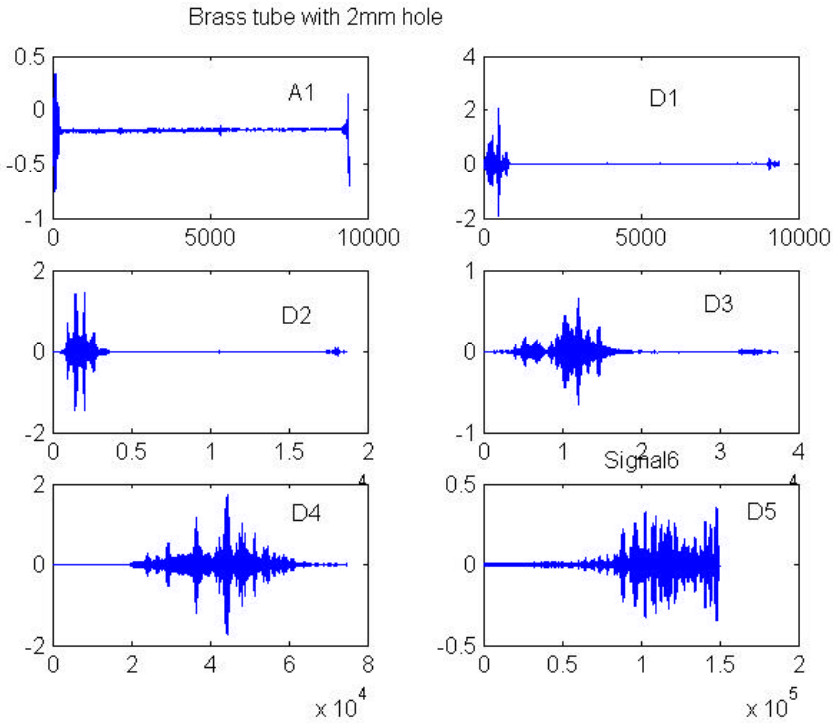

Figure 7.16. DWT decomposition of elastic wave received by the passive transducer from brass tube #2, with a 2mm hole

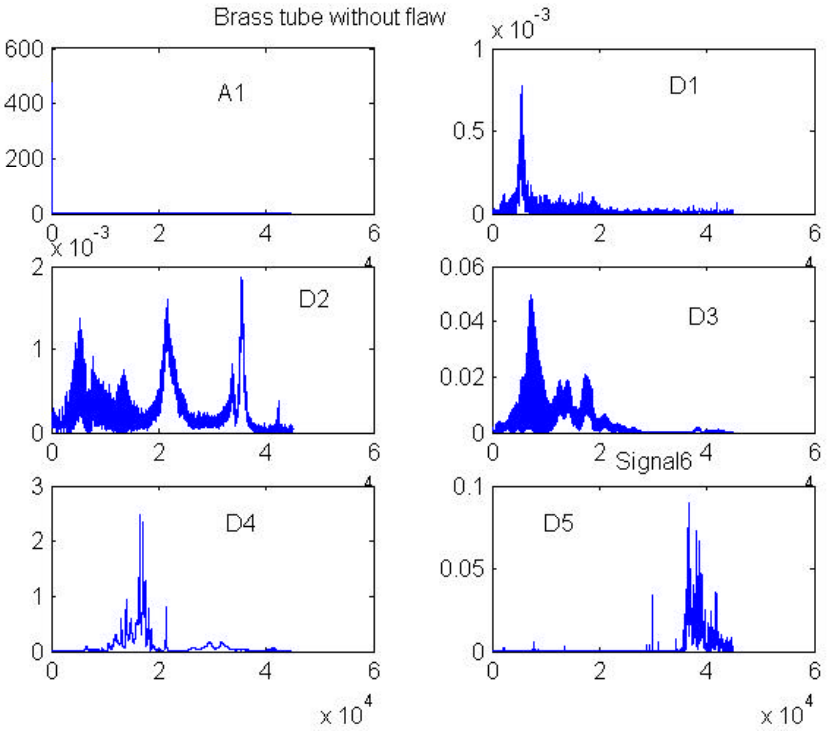

Figure 7.17. DWT decomposition of elastic wave received by the passive transducer from brass tube #2, without flaw

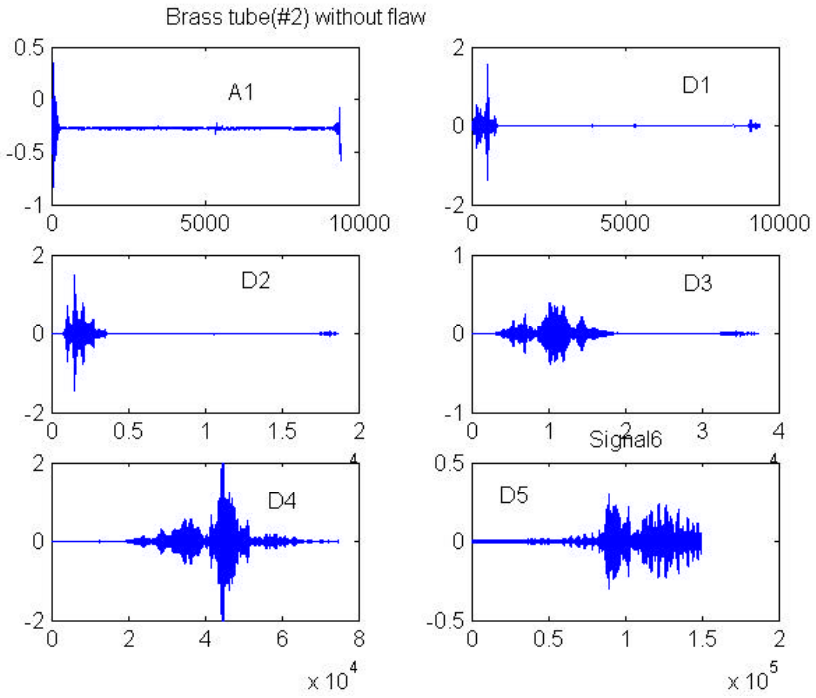

Figure 7.18. DWT decomposition of elastic wave received by the passive transducer from brass tube #2, without defect

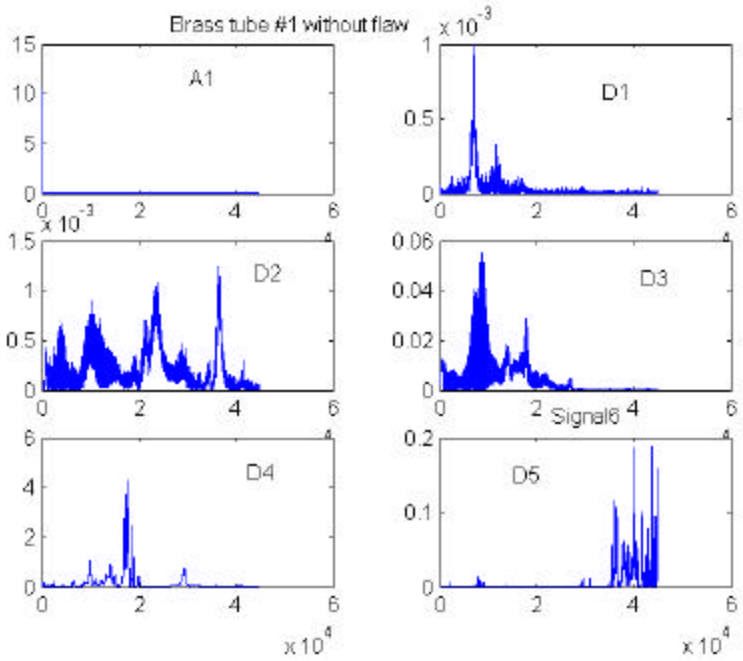

Figure 7.19. DWT of acoustic signals from normal brass tube #1.

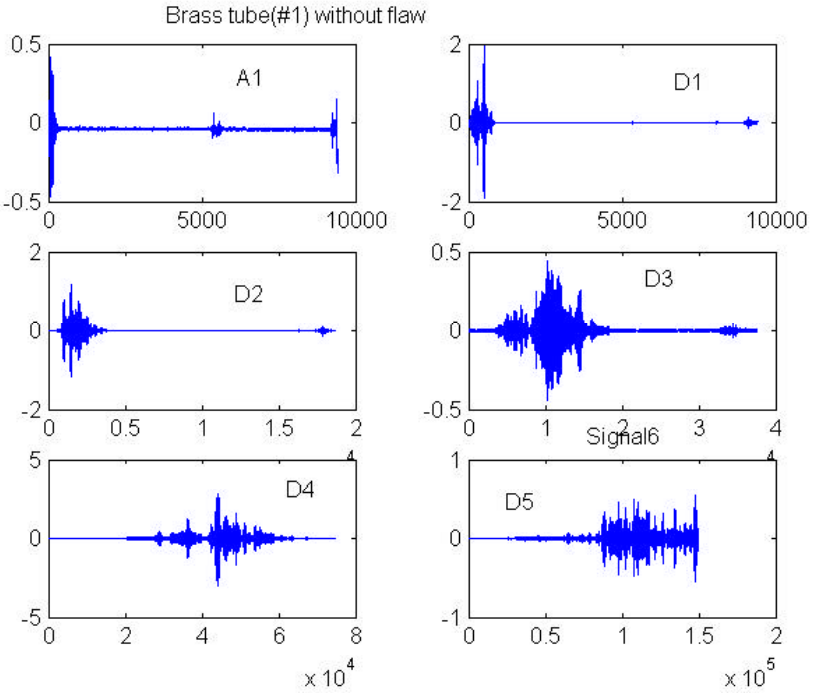

Figure 7.20. DWT of acoustic signals from normal brass tube #1.

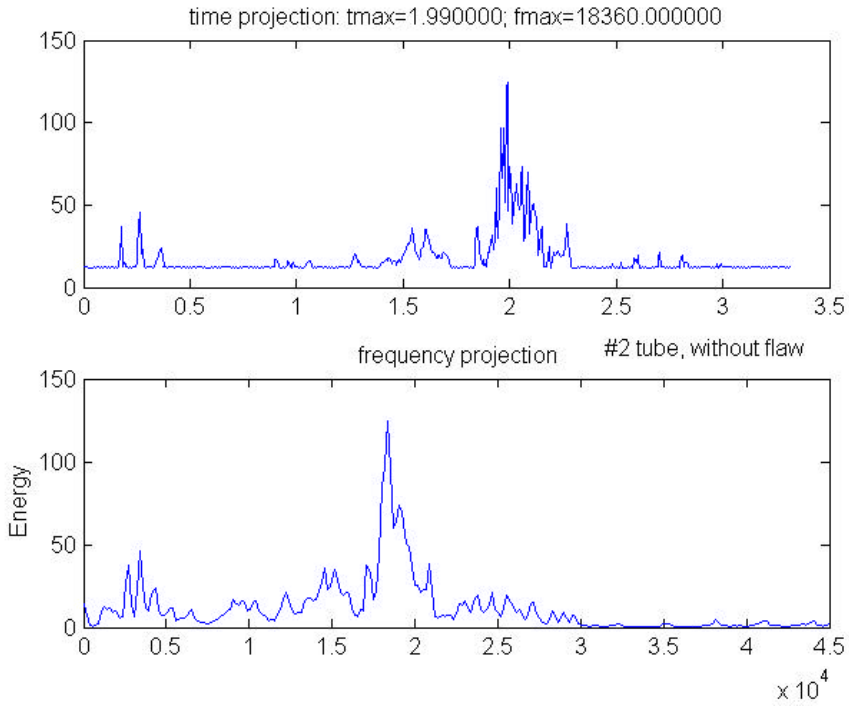

Figure 7.21. Time and frequency projections of STFT spectrum for the brass tube without flaw.

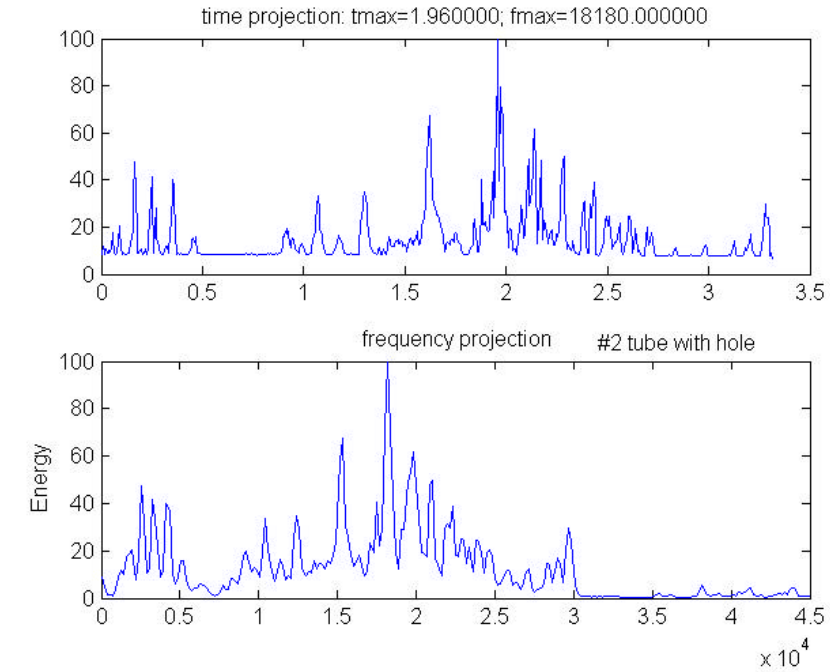

Figure 7.22. Time and frequency projections of STFT spectrum for a brass tube with defect.

7.6.3. Optimal level selection for DWT analysis

We are interested in establishing the number of decomposition levels in signal filtering. From the theoretical point, the decomposition process can continue until there are only two data points, but obviously too many decomposition levels are not necessary to reveal the most useful information included in the signals. Entropy provides a potential criterion in selecting DWT decomposition level. There are several different definitions for DWT entropy, the most frequently used ones are Shannon entropy and the log energy entropy. These are given by

$$E(s) = s_i^2 \sum \log(s_i^2) \text{ and } E(s) = \sum \log(s_i^2).$$

The log-energy entropy calculated under different decomposition levels for a brass tube is shown in Figure 7.23, which suggests an optimal level number of five. However, the results from Shannon entropy gives two levels, which indicates that the different entropy may indicate different optimal DWT level number.

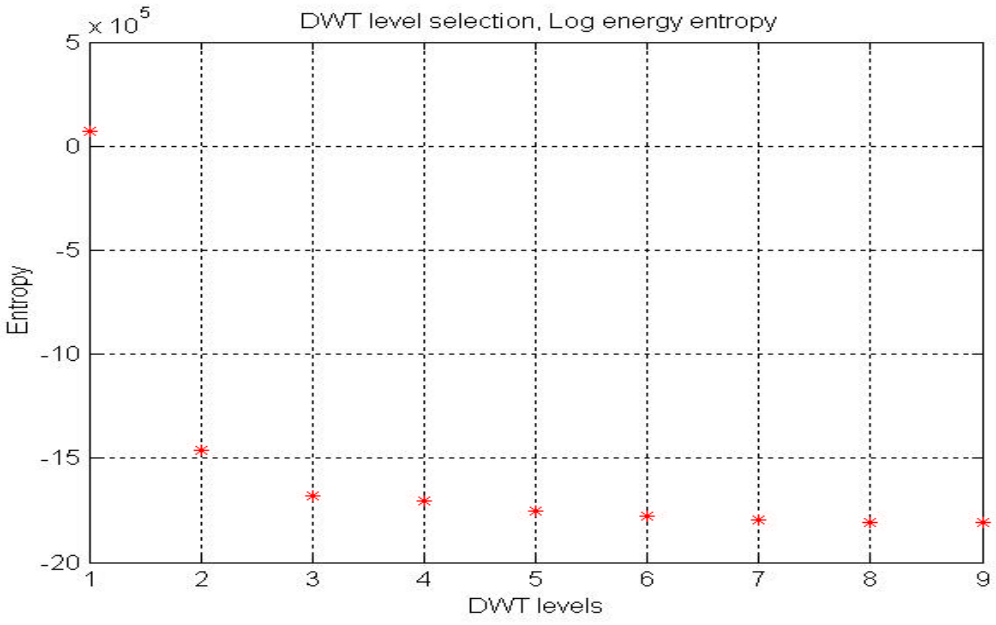

Figure 7.23. DWT level selection using Log-Energy entropy for a brass tube.

7.7. Remarks

The results of analysis to-date indicate that the presence of a defect in the structure reduces the energy of the propagated elastic wave, increases the frequency spread of the signal, and shifts the peak energy level to a lower frequency. This property has been observed in both aluminum plate and brass tube specimens.

There are optimal resonant frequency bands for both aluminum plates and brass tubes. Modulation, leakage, natural frequencies, and piezo-sensor position influence the characteristics of the Lamb waves received, and increase the complexity of signal spectra. There are less wave modes due to the low frequency of the input signal. The Lamb wave characteristics are changed by the defects along the wave-guide. Changes in statistical properties include mean value, and variance in both time and frequency domain. The received signal energy provides another feature due to its sensitivity to the structural discontinuity. Hence the Lamb waves provide a potential technique for online monitoring of the integrity of SG structure in nuclear power plants. The time-frequency analysis is important in this research because of the transient elastic signals generated in the experiments. Among them are STFT that has higher resolutions through multi-dimension (time and frequency) information and multi-resolution of DWT that can be used for collecting representative features for defect classification.

8. CONCLUDING REMARKS AND FUTURE WORK

8.1. Summary

The Phase-2 research and development during 2002-2003 has resulted in the following accomplishments.

1. Completion of the MATLAB-Simulink™ code to simulate the dynamic performance of a U-tube steam generator (UTSG) in a typical 1,140 MWe PWR. This multi-nodal model is being used to simulate the effects of tube fouling and tube plugging. The nodal structure has been expanded to account for spatial variations in the physical parameters. For example, the effect of fouling in the sub-cooled region has a higher influence on the steam pressure compared to a similar effect in the boiling region. A detailed model of particulate fouling, with time-dependent variations in the heat transfer coefficient, has been developed.

2. Completion of an experimental evaluation of particulate fouling in a tube-and-shell heat exchanger. The results of laboratory tests verify the time-dependent nature of fouling as seen by the changes in the thermal resistance, and its eventual asymptotic behavior.

3. Completion of a hybrid first principle and data-based model that will be used to update and fine-tune the model using process data. Predictive artificial neural network and local regression techniques are used for process monitoring and diagnostics. The hybrid models are classified into serial hybrid and parallel hybrid models. Our studies show that the serial modeling exhibits a better performance in predicting process variables compared to parallel modeling. A simple heat exchanger model is used for this study.

4. This model study is being complimented by the development of a laboratory heat exchanger system that is being used to generate normal operation data and data under faulty device operation. This portable test rig is being equipped with flow and pressure transmitters, flow meters, and thermocouples to measure fluid temperatures. An extensive database has been generated for testing the hybrid model approach. Additional data were acquired for the cases of faults in the heat exchanger loop.

5. Development of a laboratory piezo-device sensor suite for structural monitoring and a data acquisition system for measuring both the input excitation signal and the response signal. Both flat metal plates and tubing specimen are used for this study. The comparison of the input excitation signal (transmitted signal) and the signal received at another location in the plate show excellent frequency response characteristics. The frequency characteristics change when there is a flaw in the plate (or tubing) such as a crack, indentation, or a through hole. This task includes the review of elastic wave propagation in plates under normal and fault

conditions. The results to date indicate that the frequency characteristics of the signals change with the presence of a defect in the specimen. These include (a) shift in the energy peaks to lower frequencies, (b) decrease in the overall signal energy, and (c) an increase in the frequency and time spread of signal features.

6. Publications/Presentations of the following papers at the 2002 Americas Nuclear Energy Symposium (ANES 2002), Miami, Florida, October 2002:

   (a) Structural Monitoring of Steam Generators and Heat Exchangers Using Piezoelectric Devices.
   (b) Application of Hybrid Modeling for Monitoring Heat Exchangers.

Presentations at MARCON 2003, Knoxville, TN, May 2003.

(a) Particulate Fouling and its Effects on U-Tube Steam Generator Thermal Performance.
(b) Time-Frequency Analysis of Acoustic Signals for Flaw Monitoring in Steam Generator Structures.

Presentation at the American Nuclear Society Annual Meeting, San Diego, CA, June 2003.

Defect Monitoring in Steam Generator Structures Using Piezoelectric Transducers and Time-Frequency Analysis.

8.2. Future Work During Phase-3

The following are the continuing tasks under this project:

1. A comprehensive simulation of the UTSG responses to defects, e.g. fouling, should be performed to generate data for UTSG process monitoring.

2. Based on the generated data, a mathematical equation will be established using the Group Method of Data Handling (GMDH). This will relate UTSG performance parameters (thermal resistance, heat transfer) to the characteristic defect parameters, and is important especially for UTSG residual life prediction and maintenance planning.

3. The experimental fouling data will be used to evaluate the effectiveness of condition monitoring models.

4. The neural network architectures used in this research are standard multi-layer perceptrons (MLP), but future work will use generalized regression neural network (GRNN), developed by Specht (1991), which can be made to produce zero outputs when operating in new conditions. This will allow the hybrid models to revert back to the first principle models when new conditions are encountered.

5. The Local Weighted Regression [119,120] technique will be used in this research as an alternative to the neural network, for the data based model.

6. Theoretical study of the propagation of elastic waves due to defects in flat plate and tubular specimens. This task would help verify the experimental observations.

7. The research related to the piezo-transducer suite development will continue using aluminum beams and tubular specimens. Experiments will be performed in air, under water, and with two-phase flow conditions. Several different types of defects will be considered. In the near future a test setup using steam generator tubes will be used to study the feasibility of using piezo-generated acoustic waves to detect damages.

8. Preparation of conference and journal manuscripts.

BIBLIOGRAPHY related to the NEER Project

(neer01ref)

1. G. Kawiecki and A Seagle, "Feasibility of Applying Distributed Piezotransducers to Structural Damage Detection," Proceedings of MARCON 98, Vol. 2, pp. 69.01-69.11, May 1998.

2. A.A. de Castro and D.K.S. Ting, "Sub-cooled Boiling Detection Using Spectral Analysis of Pressure Transducer Signals," Proceedings of MARCON 98, Vol. 2, pp. 68.01-68.15, May 1998.

3. M. Sakuma, S. Kanemoto, M. Ochiai, K. Higuma and M. Kobayashi, "Leakage Detection in Nuclear Power plants Using Ultrasonic Microphone Array System," Proceedings of MARCON 98, Vol. 2, pp. 67.01-67.09, May 1998.

4. F.-K. Chang, "Structural Health Monitoring: A Summary Report on the First International Workshop on Structural Health Monitoring, September 18-20, 1997," Proceedings of Structural Health Monitoring 2000, Stanford University, September 8-10, 1999.

5. A.V. Gribok, A.M. Urmanov and A.N. Volov, "Independent Component Analysis of Acoustic Signals Recorded During PFR End-of-Life Experiments," Proceedings of MARCON 97, Vol. 1, pp. 20.01-20.09, May 1997.

6. A.V. Gribok, I. Attieh, J.W. Hines and R.E. Uhrig, "Regularization of Feedwater Flow Rate Evaluation for Venturi Meter Fouling Problem in Nuclear Power Plants," Proceedings of Ninth International Topical Meeting on Nuclear Reactor Thermal Hydraulics, San Francisco, October 3-8, 1999.

7. V.I. Frankfurt and D.S. Kupperman, "Review of Electromagnetic NDT Methods for Monitoring the Degradation of Nuclear Reactor Components," Materials Evaluation, Vol. 50, No. 9, pp. 1053-1057, September 2001.

8. P.E. MacDonald, V.N. Shah, L.W. Ward and P.G. Ellison, *Steam generator Tube Failures*, NUREG/CR-6365, INEL-95/0383, April 1996.

9. D.R. Diercks, S. Bakhtiari, K.E. Kasza and D.S. Kupperman, *Steam Generator Tube Integrity Program*, NUREG/CR-6511, Vol. 7, ANL-00/4, September 2000.

10. S. Yokell, *A Working Guide to Shell-and-Tube Heat Exchangers*, McGraw-Hill, New York, 1990.

11. G. Walker, *Industrial Heat Exchangers*, McGraw-Hill, New York, 1982.

12. M. Naghedolfeizi and B.R. Upadhyaya, *Dynamic Modeling of a Pressurized Water Reactor Plant for Diagnsotics and Control*, Research Report, DOE/NE/88ER12824-02, June 1991.

13. F.-K. Chang, *A Summary Report of the 2nd Workshop on Structural Health Monitoring*, Stanford University, 2000. http://structure.stanford.edu/workshop

14. Piezo Systems, Inc., Cambridge, Massachusetts, *Introduction to Piezo Transducers*, June 2001. www.piezo.com

15. IAEA Report, *Advanced Signal Processing Techniques for Acoustic Detection of Sodium/Water Reaction*, IAEA-TECDOC-946, May 1997.

16. *Smart Structures and Materials*, Proceedings of Industrial and Commercial Applications of Smart Structures Technologies, SPIE Vol. 2721, San Diego, February 1996.

17. *Smart Structures and Materials*, Proceedings of Smart Structures and Integrated Systems, SPIE Vol. 2717, San Diego, February 1996.

18. S. Majumdar et al., *Failure Behavior of Internally Pressurized Flawed and Unflawed Steam Generator Tubing at High Temperature – Experiments and Comparison with Model Predictions*, NUREG/CR-6575, ANL-97/17, March 1998.

19. B.E. Morgan and C.L. Foster, *Acoustic Emission Monitoring of High-Energy Steam Piping*, Volume 1: Acoustic Emission Guidelines for Hot Reheat Piping, EPRI Report, TR-105265-V1, 1995.

20. B.C. Morgan and J.M. Rodgers, *Acoustic Emission Monitoring of High-Energy Headers*, Volume 1: Acoustic Emission Guidelines for Superheater Outlet Headers, EPRI Report, TR 107893-V1, 1997.

21. D.R. Diercks, J. Muscara and W.J. Shack, "Steam Generator Steam Integrity Program," Nuclear Engineering and Design, Vol. 165, pp. 143-149, 1996.

22. R. Comby, "Secondary Side Corrosion in Steam Generator Tubes: Lessons Learned in France from the In-service Inspection Results," Nuclear Engineering and Design, Vol. 168, pp. 255-259, 1997.

23. F. Cattant, "Lessons Learned from the Examination of Tubes Pulled from Electricite de France Steam Generators," Nuclear Engineering and Design, Vol. 168, pp. 241-253, 1997.

24. P. Calmon et al., "Models for the Computation of Ultrasonic Fields and Their Interaction with Defects in Realistic NDT Configurations, Nuclear Engineering and Design, Vol. 180, pp. 271-283, 1998.

25. R. Masini, E. Padovani, M.E. Ricotti and E. Zio, "Dynamic Simulation of a Steam Generator by Neural Networks," Nuclear Engineering and Design, Vol. 187, pp. 197-213, 1999.

26. D.R. Diercks, W.J. Shack and J. Muscara, "Overview of Steam Generator Tube Degradation and Integrity Issues," Nuclear Engineering Design, Vol. 194, pp. 19-30, 1999.

27. S. Majumdar, "Prediction of Structural Integrity of Steam Generator Tubes Under Severe Accident Conditions," Nuclear Engineering and Design, Vol. 194, pp. 31-55, 1999.

28. G. Srikantiah and P.R. Chappidi, "Particle Deposition and Fouling in PWR Steam Generators," Nuclear Engineering and Design, Vol. 200, pp. 285-294, 2000.

29. D.S. Kupperman, S. Bakhtiari and J. Muscara, "Steam generator Mock-up for Assessment of In-service Inspection Technology," Nuclear Engineering and Design, Vol. 207, pp. 299-305, 2001.

30. P.H. Hutton et al., *Acoustic Emission/Flaw Relationships for In-service Monitoring of LWRs*, NUREG/CR-5645, PNL-7479, October 1991.

31. K. Krishnamurthy, F. Lalande and C.A. Rogers, "Effects of Temperature on the Electrical Impedance of Piezoelectric Sensors," Proceedings of Smart Structures and Integrated Systems, SPIE Vol. 2717, pp. 302-310, February 1996.

32. G. Kawiecki, "Bending-Torsion Response of Open-Section Beams Actuated by Skewed Piezoelements," Proceedings of Smart Structures and Integrated Systems, SPIE Vol. 2717, pp. 494-508, February 1996.

33. IAEA-TECDOC-946, *Acoustic Signal Processing for the Detection of Sodium Boiling or Sodium-Water Reaction in LMFBRs*, Final Report of a Coordinated Research Program (1990-1995), IAEA, Vienna, 1997.

34. R. Whiteley and Y. Hu, "Integration of First-Principles Models with Neural Networks and Historical Data," MCEC Literature Review, August 1999.

35. B. Kohler, "Sound Fields of Ultrasonic Circumferential Arrays – Case of an Array for Steam generator Heat Exchanger Tubes," Proceedings of the 21st International Symposium on Acoustical Imaging, Laguna Beach, CA, March 2000.

36. F. Fellinger and K.J. Langenberg, “Numerical Techniques for Elastic Wave Propagation and Scattering,” in *Waves and Ultrasonic Nondestructive Evaluation,* Edited by S.K. Datta et al, pp. 81-86, North Holland, 1990.

37. A. Alessandri and T. Parisini, "Non-Linear Modeling of Complex Large-Scale Plants Using Neural Networks and Stochastic-Approximation", IEEE Transactions on Systems, Man and Cybernetics, Part A- Systems and Humans, 27(6), pp. 750-757, 1997.

38. P.B. Ferreira and B.R. Upadhyaya, “On-line Fault Monitoring and Isolation of Field Devices Using the Group Method of Data Handling,” Proceedings of MARCON 99, Vol. 2, pp. 79.01-79.15, May 1999.

39. A.V. Gribok, I. Attieh, J.W. Hines and R.E. Uhrig, "Stochastic Regularization of Feedwater Flow Rate Evaluation for the Venturi Meter Fouling Problem in Nuclear Power Plants," *Inverse Problems in Engineering*, Vol. 00, 1-26, 2001.

40. M.A. Kramer, M.L. Thompson and P.M. Bhagat, "Embedding Theoretical Models in Neural Networks," *Proc. Amer. Control Conference*, 1992.

41. D.C. Psichogios and L.H. Ungar, "A Hybrid Neural Networks First Principles Approach to Process Modeling," *AIChE Journal* 38(10), pp. 1499-1511, 1992.

42. H.A.B. te Braake, H.J.L.V. van Can and H.B. Verbruggen, "Semi-mechanistic Modeling of Chemical Processes with Neural Networks," *Engineering Applications of Artificial Intelligence*, 11(4), pp. 507-515, 1998.

43. M.L. Thompson, and M.A. Kramer, "Modeling Chemical Processes Using Prior Knowledge and Neural Networks," *AIChE Journal*, 4 (8), pp. 1328-1340, 1994.

44. H.J.L. van Can, C. Hellinga, K.C.A.M. Luyben, J.J. Heijnen and H.A.B. te Braake, "Strategy for Dynamic Process Modeling Based on Neural Networks in Macroscopic Balances," *AIChE Journal*, 42(12), pp. 3403-3418, 1996.

45. J.A. Wilson and L.F.M. Zorsetto, "A Generalized Approach to Process State Estimation Using Hybrid Artificial Neural Network Mechanistic Models," *Computer & Chemical Engineering*, 21(9), pp. 951-963, 1997.

46. K. Choi and F.-K. Chang, “Identification of Impact Force and Location Using Distributed Sensors,” AIAA Journal, Vol. 34, No. 1, pp. 136-142, January 1996.

47. G. Hearn and R.B. Testa, “Modal Analysis for Damage Detection in Structures,” Journal of Structural Engineering, Vol. 117, No. 10, pp. 3042-3063, October 1991.

48. J.-S. Lew, “Using Transfer Function Parameter Changes for Damage Detection of Structures,” AIAA Journal, Vol. 33, No. 11, pp. 2189-2193, November 1995.

49. R.Y. Liang, J. Hu and F. Choy, “Quantitative NDE Technique for Assessing Damages in Beam Structures,” Journal of Engineering Mechanics, Vol. 118, No. 7, 1468-1487, July 1992.

50. R.A. Manning, “Structural Damage Detection Using Active Members and Neural Networks,” AIAA Journal, Vol. 32, No. 6, pp. 1331-1333, 1994.

51. M.A. Moetakef, S.P. Joshi and K.L. Lawrence, “ Elastic Wave Generation by Piezoceramic Patches,” AIAA Journal, Vol. 34, No. 10, pp. 2110-2117, October 1996.

52. N. Stubbs and J.-T. Kim, “Damage Localization in Structures Without Baseline Modal Parameters,” AIAA Journal, Vol. 34, No. 8, pp. 1645-1649, August 1996.

53. G. Kawiecki and A. Seagle, "Feasibility of Applying Distributed Piezo-transducers to Structural Damage Detection", Journal of Intelligent Material Systems and Structures, Vol. 9, pp. 189-197, March 1998.

54. Sandia Laboratory Homepage: http://www.sandia.gov

55. P.A. Meyer and J.L. Rose, “Guided Wave Applications of Piezo-composite Transducers,” ASNT Fall Conference Seattle, Washington, October 1996.

56. P. Meyer, “Improved Sound Field Penetration Using Piezo-composite Transducers,” ASNT Fall Conference Seattle, Washington, October 1996.

57. M.A. Hamstad, “An Illustrated Overview of the Use and Value of a Wavelet Transformation to Acoustic Emission Technology,” AGU-Vallen Wavelet, 2002.

58. J.P. Holman, *Heat Transfer*, McGraw-Hill, Ninth Edition, New York, 2002.

59. M.A. Heckl, "Sound Propagation in Bundles of Periodically Arranged Cylindrical Tubes," Acustica, Vol. 77, pp. 143-152, 1992.

60. X.Y. Huang and M.A. Heckl, "Transmission and Dissipation of Sound Waves in Tube Bundles," Acustica, Vol. 78, pp. 191-200, 1993.

61. D. Firth, M.A. Heckl, J.A. McKnight, L.S. Mulholland, and R. Rowley, "Sound Propagation in a Steam generator: Experimental and Theoretical Results," Nuclear Energy, Vol. 32, No. 6, pp. 369-378, December 1993.

62. B.A.T. Petersson, "Structural Acoustic Power Transmission by Point Moment and Force Excitation, Part II: Plate-Like Structures," Journal of Sound and Vibration, Vol. 160, No. 1, pp. 67-91, 1993.

63. P.A. Meyer, "Piezocomposites Improve Ultrasonic Testing," Advanced Materials & Processes, pp. 37-38, 1997.

64. P. E. MacDonald, V. N. Shah, L. W. Ward, and P. G. Ellison, "Steam Generator Tube Failures," NUREG/CR-6365, 1996.

65. K. C. Wade, "Steam Generator Degradation and its Impact on Continued Operation of Pressurized Water Reactors in the United States," Energy Information Administration/ Electric Power Monthly, August 1995.

66. http://domino.pall.com/www/weblib.nsf/pub/80EC605D2451474E852567EF0053F173?opendocument

67. http://www.cpe.surrey.ac.uk/dptri/hms/fouling.htm

68. C.I. Hussain, I.H. Newson, and T.R. Bott, "Diffusion Controlled Deposition of Particulate Matter from Flowing Slurries," Proceeding of the Eighth International Heat Transfer Conference, San Francisco, 1986.

69. S.K. Beal, "Particulate Fouling of Heat Exchangers," Proceeding of the Engineering Foundation Conference, White Harie, PA, Oct.-Nov. 1982.

70. H. Muller-Stehinhagen, F. Reif, N. Epstein, and A.P. Watkinson, "Influence of Operating Conditions on Particulate Fouling," *Canadian Journal of Chemical Engineering*, Vol. 66, pp. 42-50, February 1988.

71. Y. Mussalli et al, "Effects of Fouling and Corrosion on Heat Transfer," American Society of Mechanical Engineers, 1985.

72. R.L. Watts and L.O. Levine, "Monitoring Technology Trends with Patent Data: Fouling of Heat Exchangers - A Case Study," Presented at the 22nd National Heat Transfer Conference and Exhibition, Niagara Falls, New York, August 1984.

73. J. Taborek, T. Aoku, R.B. Ritter, J.W. Paeln, and J.G. Knudsen, "Fouling: the Major Unresolved Problem in Heat Transfer," *Chemical Engineering Progress*, Vol. 68, No. 2, February 1972.

74. H. Muller-Steinhagen, and R. Bloch, "Particulate Fouling in Heat Exchangers," Transcripts of Institute of Professional Engineers, New Zealand, EMC Eng-Sec., Vol. 15, No. 3, pp. 109-118, November 1988.

75. A.K. Gupta and T.W. Jackson, “On the Mechanism of Particle Deposition through Boundary Layers in a Heat Exchanger System,” Presented at the American Institute of Aeronautic and Astronautics, 24th Aerospace Sciences Meeting, Reno, Nevada, January 1986.

76. J.G. Knudsen, “Coping with Cooling Water Fouling in Tubular Heat Exchangers,” AIChE Symposium Series, Vol. 85, No. 269, pp. 1-12, 1989.

77. P.G. Papavergos and A.B. Hadley, “Particle Deposition Behavior from Turbulent Flows,” *Chemical Engineering Research*, Vol. 62, September 1984.

78. F.B. Incropera and D.P. DeWitt, Fundamentals of Heat and Mass Transfer", 4th Edition, John Wiley, New York, 1996.

79. R.L. Penha and J.W. Hines, "Hybrid System Modeling for Process Diagnostics," Proceedings of MARCON 2002, Knoxville, TN, May 2002.

80. S.R. Perillo and B.R. Upadhyaya, "Applications of Piezoelectric Devices in Engineering Systems," Proceedings of MARCON 2002, Knoxville, TN, May 2002.

81. B.R. Upadhyaya, J.W. Hines, X. Huang, N.A. Johansen, A.V. Gribok, and S.R. Perillo, "Automated Monitoring and Diagnostics of the Integrity of Nuclear Plant Steam generators, Transactions of the American Nuclear Society Annual Meeting, June 2002.

82. C.W. Turner, "Modeling Magnetite Particle Deposition in Nuclear Steam Generators and Comparisons with Plant Data," AECL Report, No. 1112, pp. 1-14, December 1994.

83. A. Stutzmann, L. Viricel, M. Dijoux, and P. Lemaire, "French Experience on o.d. IGA/SCC and Fouling of SG Tubes," Nuclear Energy, Vol. 41, No. 2, pp. 137-144, 2002.

84. H. Muller-Steinhagen, "Mitigation of Process Heat Exchanger Fouling: An Integral Approach," Transactions of IchemE, Vol. 76, 1988.

85. K.I. Shin, J.H. Park, H.D. Kim, and H.S. Chung, "Simulation of Stress Corrosion Crack Growth in Steam Generator Tubes," Nuclear Engineering and Design, Vol. 214, pp. 91-101, 2002.

86. S. Kakac and H. Liu, *Heat Exchangers: Selection, Rating, and Thermal Design*, Second Edition, CRC Press, 2002.

87. A.D. Dimarogonas, "Vibration For Engineers," 2nd Ed., 1996 Prentice-Hall.

88. A.D. Dimarogonas, "Vibration Engineering," West Publishing, 1976.

89. S. Timoshenko, D.H. Young, and W. Weaver Jr, "Vibration Problems in Engineering," 4th Edition, John Wiley, 1974.

90. J.W.S. Rayleigh and J.W. Strut, "The Theory of Sound", Vol. 1, 2nd Edition, Dover Publications, 1945.

91. J.W.S. Rayleigh, and J.W. Strut, "The Theory of Sound", Vol. 2, 2nd Edition, Dover Publications, 1945.

92. P.W. Smith, "Validation of Torsional - Bending Piezoelectric Actuator Concept," MS Thesis, The University of Tennessee, December 1993.

93. J. Zelenka, "Piezoelectric Resonators and their Applications", Elsevier Science, October 1986. (We have a hard copy of this book taken by the UT Dept. of Mechanical and Aerospace Engineering).

94. A. Hyvarinen, J. Karhunen, and E. Oja, *Independent Component Analysis*, Wley Interscience, New York, 2001.

95. T.-W. Lee, *Independent Component Analysis: Theory and Applications*, Kluwer Academic Publishers, Boston, 1998.

96. S. Roberts and R. Everson (Ed), *Independent Component Analysis: Principles and Practice*, Camridge University Press, UK, 2001.

97. M. Girolami (Ed), *Advances in Independent Component Analysis*, Springer, New York, 2000.

98. M.G. Fontana and N.D. Greene, " Corrosion Engineering," 2nd ed., McGraw-Hill, New York, 1978.

99. A. Stutzmann, et al, "French Experience on OD-IGA/SCC and Fouling of SG Tubes," Nuclear Energy, Vol. 41, No. 2, April 2002.

100. J. R. Davis et al, "Corrosion—Understanding the Basics," ASM International, 2000.

101. P. Marcus et al, "Corrosion Mechanisms in Theory and Practice," Marcel Dekker, 1995.

102. T. Kuppan, "Heat Exchanger Design Handbook," Marcel Dekker, New York, 2000.

103. C.F. Britton et al, "Effective Corrosion Monitoring," NACE, Material

Performance, April 1988.

104. C. Wood, “On Chemistry and Corrosion at Nuclear Power Plants,” Nuclear News, October 2002.

105. J. Gorman, “Survey of PWR Water Chemistry,” NUREG/CR-5116, 1989.

106. “Water Chemistry and Corrosion Problems in Nuclear Power Plants,” Proceedings of an International Symposium on Water Chemistry and Corrosion Problems of Nuclear Reactor Systems and Components Organized by IAEA, 1982.

107. NEI 97-06 (Rev 1) “Steam Generator Program Guidelines,” January 2001.

108. PWR Steam Generator Examination Guidelines, EPRI Report TR-107569.

109. PWR Primary-to-Secondary Leak Guidelines, EPRI Report TR-104788.

110. PWR Secondary Water Chemistry Guidelines, EPRI Report TR-102134.

111. PWR Primary Water Chemistry Guidelines, EPRI Report TR-105714.

112. Steam Generator Integrity Assessment Guideline, EPRI Report TR-107621.

113. PWR Steam Generator Tube Plug Assessment Document, EPRI Report TR-109495.

114. EPRI PWR Sleeving Assessment Document, EPRI Report TR-105962.

115. EPRI NP-7552 “Heat Exchanger Performance Monitoring Guidelines,” December 1991.

116. Y. Liner et al, “Simulation of Magnetite Particulate Fouling in Nuclear Steam Generators,” Chalk River Laboratories, AECL Research, Ontario, Canada, 1992.

117. C.W. Turner et al, "Modeling Magnetite Particle Deposition in Nuclear Steam Generators and Comparisons with Plant Data," Presented at the Second International Steam Generator and Heat Exchanger Conference, Toronto, Canada, 1994.

118. Cleaver J.W. et al, “The Effect of Re-entrainment on Particle Deposition,” Chemical Engineering and Science, Vol. 31, 1976.

119. G. Bontempi, M. Birattari, and H. Bersini, "Lazy Learning: a Local Method for

Supervised Learning in New Learning Paradigms in Soft Computing," L.C. Jain and J. Kacprzyk (eds.) Physica-Verlag (Springer-Verlag), Heidelberg and New York, 97 - 137. (http://iridia.ulb.ac.be/~gbonte/Papers.html), 2001.

120. M. Birattari and G. Bontempi. (1999) The Lazy Learning Toolbox, for use with Matlab, Technical Report TR/IRIDIA/99-7, 1999. Iridia, Université Libre de Bruxelles, Brussels, Belgium.(http://iridia.ulb.ac.be/~mbiro/paperi.html)

121. T. Ikeda, *Fundamentals of Piezoelectricity,* Oxford University Press, 1997.

122. C.Z. Rosen et al., *Piezoelectricy,* Springer-Verlag New York, 1995.

123. G.W. Taylor et al., *Piezoelectricity,* Gordon & Breach Publishing, 1985.

124. N.N. Rogacheva, *Theory of Piezoelectric Plates and Shells,* CRC Press, 1994.

125. G. Gautschi, *Piezoelectric Sensorics: Force, Strain, Pressure, Acceleration and Acoustic Emission Sensors, Materials and Amplifiers,* Springer-Verlag New York, 2002.

126. K.-H. Hoffmann, *"1st Caesarium - Smart Materials: Proceedings of the 1st Caesarium,"* Bonn, Nov. 17-19, 1999.

127. C. Lu and A.W. Czanderna, *Applications of Piezoelectric Quartz Crystal Microbalances,* Elsevier Science, February 1984.

128. J.M.M. Herbert, *Ferroelectric Transducers and Sensors, Vol. 3,* Gordon & Breach Publishing, January 1982.

129. H.F. Tiersten, *Linear Piezoelectric Plate Vibrations: Elements of the Linear Theory of Piezoelectricity and the Vibrations of Piezoelectric Plates,* Kluwer Academic Publishers, February 1969.

130. K. Uchino, *Piezoelectric Actuators and Ultrasonic Motors,* Kluwer Academic Publishers, November 1996.

131. M.E. Regelbrugge, *"Smart Structures and Integrated Systems", Vol. 332,* SPIE-International Society for Optical Engineering, July 1998.

132. C.S. Lynch, *"Smart Structures and Materials 2000 Active Materials: Behavior and Mechanics,"* SPIE Optical Engineering Press, January 2000.

133. J. Holnicki-Szulc et al., *"Smart Structures : Requirements and Potential Applications in Mechanical and Civil Engineering,"* Kluwer Academic Publishers, May 1999.

134. *"Specifications and Tests for Piezoelectric Pressure and Sound-Pressure Transducers: ISA Standard S37.10,"* Instrument Society of America, 1982.

135. Y. Yuan and F.F. Ling, *Vibrations of Elastic Plates : Linear and Nonlinear Dynamical Modeling of Sandwiches, Laminated Composites, and Piezoelectric Layers*, Springer-Verlag New York, January 1995.

136. K. Choi. and F.-K. Chang, *"Identification of Impact Force and Location Using Distributed Sensors,"* AIAA Journal, Vol. 34, No. 1, pp. 136-142, January 1996.

137. G. Hearn.and R.B. Testa, *"Modal Analysis for Damage Detection in Structures,"* J. of Structural Engineering, Vol. 117, No. 10, pp. 3042-3063, October 1991.

138. J.-S. Lew, *"Using Transfer Function Parameter Changes for Damage Detection of Structures,"* AIAA Journal, Vol. 33, No. 11, , pp. 2189-2193, November 1991.

139. R.Y. Liang, J. Hu, and F. Choy, *"Quantitative NDE Technique for Assessing Damages in Beam Structures,"* Journal of Engineering Mechanics, Vol. 118, No. 7, 1468-1487, July 1992.

140. R.A. Manning, *"Structural Damage Detection Using Active Members and Neural Networks,"* AIAA Journal, Vol. 32, No. 6, pp 1331-1333, 1994.

141. M.A. Moetakef, S.P. Joshi, and K.L. Lawrence, *"Elastic Wave Generation by Piezoceramic Patches,"* AIAA Journal, Vol. 34, No. 10, pp. 2110-2117, October 1996.

142. N. Stubbs and J.-T. Kim, *"Damage Localization in Structures Without Baseline Modal Parameters,"* AIAA Journal, Vol. 34, No. 8, , pp. 1645-1649, August 1996.

143. Z. Ounaies, *"Piezoelectric Materials for Sensor and Actuator Applications at NASA LaRC,"* ICASE Research Quarterly.
http://www.icase.edu/RQ/archive/v8n2/art1.html
http://www.icase.edu/

144. American Institute of Physics Website, http://www.aip.org

145. Materials Engineering, University of Purdue's Website
http://www.ecn.purdue.edu/Engr/

146. G. Kawiecki, *"Feasibility of Applying Distributed Piezotransducers to Structural Damage Detection,"* Journal of Intelligent Material Systems and Structures, Vol. 9, pp. 189-197, March 1998.

147. P.W. Smith, "Validation of Torsional - Bending Piezoelectric Actuator Concept," MS Thesis, The University of Tennessee, December 1993.

148. J. Zelenka, "Piezoelectric Resonators and their Applications," Elsevier Science, October 1986.

149. B.R. Upadhyaya, J.W. Hines et al, *On-Line Monitoring and Diagnostics of the Integrity of Nuclear Plant Steam Generators and Heat Exchangers*, Annual Report prepared for the U.S. Department of Energy, Report No. DE-FG07-01ID14114/UTNE-03, The University of Tennessee, June 2002.

150. L.F. Melo et al, "Particle Transport in Fouling Caused by KAOLIN-Water Suspensions on Copper Tubes," Canadian Journal of Chemical Engineering, Volume 66, February 1988.

151. J. Middis et al, "Particulate Fouling in Heat Exchangers with Enhanced Surfaces," 18th Australasian Chemical Engineering Conference, Auckland, New Zealand, 1990.

152. L. M. Chamra et al, "Effect of Particle Size and Size Distribution on Particulate Fouling in Enhanced Tubes," Enhanced Heat Transfer, Vol. 1, No. 1, 1993.

153. H. Muller-Steinhagen et al, "Particulate Fouling in Heat Exchangers," Transactions of EMCh, Vol. 15, No. 3, November 1988.

154. M. Basset et al, "The Fouling of Alloy-800 Heat Exchange Surfaces by Magnetite Particles," Canadian Journal of Chemical Engineering, Vol. 78, February 2000.

155. T. Sugioto et al, "Formation of Uniform Spherical Magnetite Particles by Crystallization from Ferrous Hydroxide Gels," Journal of Colloid and Interface Science, Vol. 74, No. 1, March 1980.

156. C.W. Turner et al, "Deposition of Magnetite Particles from Flowing Suspensions under Flow-Boiling and Single-Phase Forced-Convective Heat Transfer," Canadian Journal of Chemical Engineering, Vol. 78, December 2000.

157. H. Muller-Steinhagen et al, "Influence of Operating Conditions on Particulate Fouling," Canadian Journal of Chemical Engineering, Vol. 66, February 1988.

158. G. Bontempi, M. Birattari and H. Bersini, "Lazy Learning: A Logical Method for Supervised Learning," http://iridia.ulb.ac.be/~lazy.

159. J.L. Rose, *Ultrasonic Waves in Solid Media*, Cambridege University Press, 1999.

160. I.A. Viktorov, *Raleigh and Lamb Waves*, Plenum Press, New York, 1967.

161. B.A. Auld, *Acoustic Fields and Waves in Solids*, 2nd Edition, Robert E. Krieger Publishing Company, 1990.

162. J. Miklowitz, *The Theory of Elastic Waves and Waveguides*, North-Holland Publishing Company, New York, 1978.

163. C.K. Chui, *An Introduction to Wavelets*, Academic Press, New York, 1992.

164. G. Strang and T. Nguyen, *Wavelets and Filter Banks*, Wellesley-Cambridge Press, 1997.

165. D.N. Alleyne, M.J.S. Lowe and P. Cawley, "The Reflection of Guided Waves From Circumferential Notches in Pipes," J. of Applied Mechanics, Vol. 65, pp. 635-641, September 1998.

166. J.J. Ditri, "Utilization of Guided Elastic Waves for the Characterization of Circumferential Cracks in Hollow Cylinders," J. Acoust. Soc. Am., Vol. 96, No. 6, pp. 3769-3775, December 1994.

167. D. Alleyne and P. Cawley, "A Two-dimensional Fourier Transform Method for the Measurement of Propagating Multimode Signals," J. Acoust. Soc. Am., Vol. 89, No. 3, pp. 1159-1167, March 1991.

168. S.K. Goumas, M.E. Zervakis, and G.S. Stavrakakis, "Classification of Washing Machines Vibration Signals Using Discrete Wavelet Analysis for Feature Extraction, IEEE Transactions on Instrumentation and Measurement, Vol. 51, No. 3, June 2002.

169. P. Maass, G. Teschke, W. Willmann, and G. Wollmann, "Detection and Classification of Material Attributes – A Practical Application of Wavelet Analysis, IEEE Transactions on Signal Processing, Vol. 48, No. 8, August 2000.

170. L.R. Dragonette, D.M. Drumheller, C.F. Gaumond, D.H. Hughes, B.T. O'Connor, N. Yen, and T.J. Yoder, "The application of Two –Dimensional Transformations to the Analysis and Synthesis of Structural Excitations Observed in Acoustical Scattering," Proceedings of the IEEE, Special Issue on Time Frequency Analysis, Vol. 84, No. 9, pp. 1249-1263, September 1996.

171. N. Yen, "Wave Packet Decomposition," J. Acoust. Soc. Am., Vol. 95, No. 2, pp. 889-896, February 1994.

172. T.W. Wu, "On Computational Aspects of the Boundary Element Method for Acoustic Radiation and Scattering in a Perfect Waveguide, J. Acoust. Soc. Am., Vol. 96, No. 6, pp. 3733-3743, December 1994.

173. G.V. Frisk, J.W. Dickey, and H. Uberall, "Surface Wave Modes on Elastic

Cylinders," J. Acoust. Soc. Am., Vol.58, No. 6, pp. 996-1008, November 1975.

174. G.C. Gaunaurd, "Elastic and Acoustic Resonance Wave Scattering," Applied Mechanics Review, Vol. 42, No. 6, pp. 143-192, June 1989.

175. M. Tohyama and T. Koike, *Fundamentals of Acoustic Signal Processing*, Academic Press, 1998.

176. L.E. Kinsler and A.R. Frey, *Fundamentals of Acoustics*, 2nd Edition, John Wiley, 1962.

177. O.V. Rudenko and S.I. Soluyan (Translated by R. T. Beyer), *Theoretical Foundations of Nonlinear Acoustics*, Consultants Bureau, New York, 1977.

178. L.B. Felsen et al., *Transient Electromagnetic Fields*, Springer-Verlag, New York, 1976.

179. D.F. Parker and G.A. Maugin (Eds), *Recent Developments in Surface Acoustic Waves*, Springer-Verlag, New York, 1987.

180. C. Campbell, *Surface Acoustic Wave Devices and Their Signal Processing Applications*, Academic Press, New York, 1989.

181. F.B. Stumpf, *Analytical Acoustics*, Ann Arbor Science Publishers, Michigan, 1980.

182. A.A. Oliner et al., *Acoustic Surface Waves*, Springer-Verlag, Berlin, 1978.

183. S. Nettel, *Wave Physics*, 2nd Edition, Springer, New York, 1995.

184. D.S. Ballantine et al., *Acoustic Wave Sensors Theory, Design and Physico-Chemical Applications*, Academic Press, San Diego, 1997.

185. K.F. Graff, *Wave Motion in Elastic Solids*, Ohio State University Press, 1975.

186. C.H. Chen, *Issues in Acoustic Signal Image Processing and Recognition*, Springer-Verlag, Berlin, 1983.

187. V.P. Gilbert, *Surface Acoustic Wave Device Designed to Monitor Frequency Shifts due to Adsorption of Mass on to a Piezoelectric Crystal*, M.S. Thesis, University of Tennessee, May 1992.

188. A. Hyvarinen, J. Karhunen, and E. Oja, *Independent Component Analysis*, John Wiley, New York, 2001.

189. P.J. Oonincx, *Mathematical Signal Analysis: Wavelets, Wigner Distribution, and a seismic Application*, Stichting Mathematisch Centrum, Amsterdam, 2000.

190. J. Miklowitz, *Elastic Waves and Waveguides*, North-Holland Publishing Company, New York, 1978.

191. J.L. Davis, *Wave Propagation in Solids and Fluids*, Springer-Verlag, New York, 1988.

192. L. Cohen, *Time-Frequency Analysis*, Prentice Hall, 1995.

193. U.B. Halabe and R. Franklin, "Fatigue Crack Detection in Metallic Members Using Ultrasonic Rayleigh Waves with Time and Frequency Analysis," Materials Evaluation, Vol. 59, No. 3, pp. 424-431, March 2001.

194. R. Carmona, W. Hwang, and B. Torresani, *Practical Time-Frequency Analysis*, Academic Press, New York, 1998.

195. J. Barshinger, J.L. Rose, and M.J. Avioli, "Guided Wave Resonance Tuning for Pipe Inspection," J. of Pressure Vessel Technology, Vol. 124, pp. 303-310, August 2002.

196. J. L. Rose, "A Baseline and Vision of Ultrasonic Guided Wave Inspection Potential," J. of Pressure Vessel Technology, Vol. 124, pp. 273-282, August 2002.

197. E.V. Malyarenko and M.K. Hinders, "Fan Beam and Double Cross-hole Lamb Wave Tomography for Mapping Flaws in Aging Aircraft Structures," J. of Acoust. Soc. Am., Vol. 108, No. 4, pp. 1631-1639, October 2000.

198. K. Motegi, "Ultrasound Radiation into Water by a Lamb Wave Device Using a Piezoelectric Ceramic Plate with Spatially Varying Thickness," Ultrasonics, Vol. 37, pp. 505-510, 1999.

199. M. Deng, "Cumulative Second-harmonic Generation of Generalized Lamb-wave Propagation in a Solid Wave-guide, J. Appl. Physics, Vol. 33, pp. 207-215, 2000.

(updated: 06/27/2003)